CONTINUOUS REACTOR NETWORK DESIGN FOR RIGID POLYOL PRODUCTIONS

Submitted in partial fulfillment of the requirements for

the degree of

Doctor of Philosophy

in

Department of Chemical Engineering

Yunhan Wen

B.S., CHEMICAL ENGINEERING, THE OHIO STATE UNIVERSITY

Carnegie Mellon University

Pittsburgh, PA

August 2021

Abstract

This thesis focuses on the development of continuous reactor networks that consist of continuous stirred tank reactors (CSTR) and plug flow reactors (PFR) with multiple injection points for the rigid polyol productions. To meet the product specifications of this polymerization process and to minimize the capital cost of the reactor configuration, four major topics are studied: 1. model development for rigid polyol production, 2. optimization formulations and solution strategies, 3. kinetic parameter estimation, 4. reactor network design under uncertainties in kinetic parameters. First, a detailed mathematical model is developed to capture the dynamic behavior of the polymerization process. This model includes mass balance, and energy balance. Then, this model is utilized to estimate the values of kinetic parameters involved in this process. Next, production and safety specifications are incorporated into the model to find the optimal continuous reactor network design and corresponding operation recipes that would lead to a minimum capital cost. The results show that a single PFR with multiple monomer injection points is the best design. However, the performance can deteriorate in the presence of parameter uncertainties. Compact problem formulations with modifications on the constraint (back-off constraints) and multi-scenario formulation with each scenario corresponding to one discretized uncertainty level are adopted to develop the reactor network and operation recipe. Back off terms that are obtained from Monte Carlo simulations tighten the constraint and shrink the feasible region of the optimization problem to such a level that variations of the constraints in the worst case can still be handled and thus feasibility is ensured. The multi-scenario formulation is also tolerant to the uncertainties and has better performance than the back off method, since it allows different operation recipes (recourse variables) for different scenarios. On the other hand, multi-scenario approach increases the problem size dramatically. In this work, we demonstrate the effectiveness of both uncertainty approaches and compare the results on the multi-product reactor network.

For dynamic optimization, simultaneous collocation strategy is applied to discretize the continu-

ous time/volume horizon into finite element mesh and to covert the differential-algebraic equation (DAE) optimization problems into nonlinear programming problems (NLP). These NLPs are further solved by NLP solvers IPOPTH or CONOPT.

Acknowledgments

First, I would like to express my appreciation to the Carnegie Mellon University. Thanks for providing all the opportunities that allow me to pursue my Ph.D. study at here. I would also like to express my deepest gratitude to my advisor Prof. Lorenz T. Biegler, who has been a tremendous mentor for me in academic and many other aspects. I really respect his enthusiasm, devotion and love towards research. And his wisdom, patience and advice have tremendously helped me with my research and led me to the right direction. It would be impossible for me to develop those invaluable skills and knowledge to complete this thesis work in the last five years without him.

I would like to express my sincere thanks to Dr. Maria Ochoa, Dr. John Weston, Dr. Nima Nikbin and Dr. Jeff Ferrio from the Dow Chemical Company for their strong support, generous help and valuable feedback. The collaboration with them in the last five years is a great and enjoyable learning experience. I am also grateful to the financial support from The Dow Chemical Company for my Ph.D. program in the past few years.

I would also like to express my grateful thanks to my committee members: Prof. Chrysanthos Gounaris, Prof. Javier Pena and Prof. Nikolas Sahinidis, for their careful reading of my thesis and valuable advice on the dissertation.

Finally, I would like to express my particular thanks to my parents for their endless amounts of love and support. There are not enough words to describe how thankful I am to both of you. You both have taught me so much. Going abroad and being apart from you has made me more independent, but also made me realize how much you both mean to me. In the end, I would like to express my thanks to my friends for always being there for me. They have enlightened my life and made it an enjoyable journey.

Table of Contents

List of Tables

List of Figures

Chapter 1 Introduction

1.1 Rigid Polyols

Rigid polyols are defined as polyether polyols that are formed by alkoxylation of initiators with three to eight active sites to form polyethers. These polyethers usually have a chain length less than 10, and are used with isocyanates to manufacture closed cell foams, which are utilized in the production of refrigerators, construction insulation and related products as shown in Fig. 1.1. Demand for these products has recently doubled, and is expected to grow with the energy efficiency market in the next 10 years [1].

Figure 1.1. Application of Rigid Polyols

In most current processes, semi-batch reactors are used to produce rigid polyols, with a few examples of continuous reactors in the patent literature [2]. As polymer product demand increases, more and larger semi-batch reactors must be built to meet the demand, and the capital cost per production capacity is reduced as expected. However, this capital cost may still be too high for

re-investment, and alternative lower capital cost solutions, such as switching the production from semi-batch reactor to continuous processes, could help sustained growth. Continuous processes can reduce capital & operating costs and improve productivity. Since in a continuous process, reactors do not need to be stopped at the end of a run, or be emptied and refilled with initiator to start over. Continuous processes can also reduce the cost required for the heat transfer equipment, since the heat load is more evenly distributed over time. In addition, continuous reactors are easier to optimize at a steady state to maximize the overall production rate. However, continuous reactors are not as flexible regarding multiple products, product transition can be difficult and scale-up of the products requires additional investment. The motivation of this project is to analyze the effect of switching the production from semi-batch reactors to continuous reactors, by exploring different network configurations that consist of plug flow reactor (PFR) and/or continuous stirred tank reactor (CSTR) models as shown in Fig. 1.2.

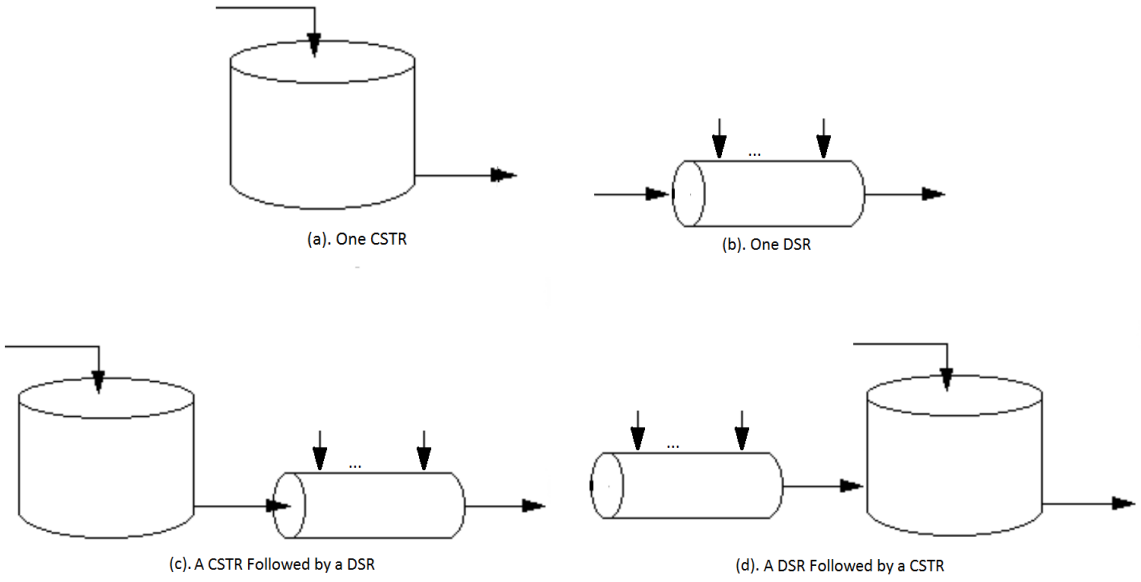

Figure 1.2. Potential Reactor Configurations

1.2 Reactor Network Design

The reactor plays an important role in chemical process; it affects unit operation and more importantly the product quality. Moreover, the character of a flowsheet is determined by reaction systems and reactor design. However, research in reactor network synthesis has met with limited success because of the non-linearity in the reaction models, the uncertainty in kinetic parameters, and the existence of numerous possible reactor types and networks. In this section, we first introduce the two main methods that are usually used to obtain the optimal reactor network: superstructure based approach [3], and attainable region [6]. Then, we cover the approach we applied in this work.

1.2.1 Superstructure

In 1994, Kokossis and Floudas [4] proposed a reactor network that included both CSTRs and PFRs, as shown in Fig. 1.3. The key advantage of the approach is that the objective value, optimal reactor network and operating conditions can be determined simultaneously. One of the limitations of this superstructure approach is that the model formulations typically are nonconvex, and subspaces of the response surface are often ”flat”, leading to many near-optimal solutions. In addition, the optimal solution is only as rich as the initial superstructure; therefore, the global optimal reactor network cannot be found if it is not contained within the superstructure. However, there is a trade off between the richness of the superstructure and the size and complexity of the model. In addition, some optimal reactor configurations are rather complex (contain multiple recycle streams) and are hard to validate.

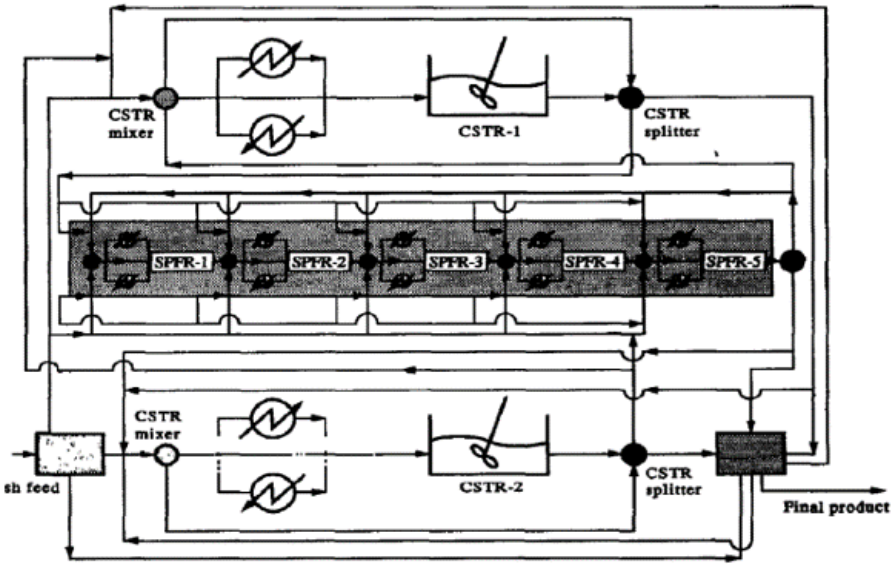

Figure 1.3. Superstructure Proposed by Kokossis and Floudas

Simple flowsheet configurations with two CSTRs in series and in parallel are frequently used in practice. However, due to the limitations of these conventional reactor network structures, many polymer grades, especially high-quality ones, may not be achievable even under a wide range of operating conditions. Hence, a more flexible process flowsheet configuration was constructed. In 2016, Zhang et al. [5] developed the optimization of continuous reactor networks for a polymerization process. The superstructure (Fig. 1.4) is constructed to incorporate all possible structural alternatives of interest. The basic idea is to place splitters at the exit of each CSTR, and then allow all CSTRs to be fully connected with each other. In Zhang's work, the configurations with one to four CSTRs were carried out to meet the target molecular weight distribution. The proposed superstructure is very flexible and allows recycles to occur, but it does not contain other types of continuous reactors, such as PFR and DSR.

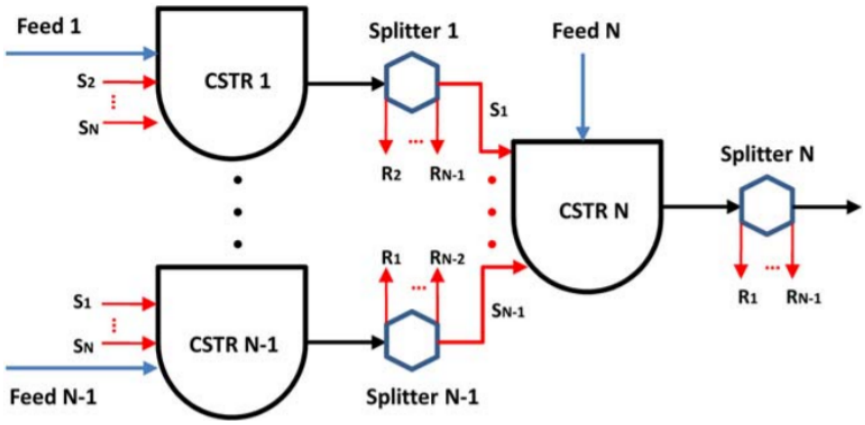

Figure 1.4. Superstructure Proposed by Chen

1.2.2 Attainable Region

Another way to formulate the reactor network is through the attainable region (AR) in concentration space, which finds the set of all possible outputs for all possible reactor configurations [6]. Every point in or on the AR is an output of a reactor combination. Once we have the region, we are assured that it contains the optimal solution. A picture that illustates the attainable region is shown in Fig. 1.5. However, for this polymerization problem, attainable regions with more than two dimensions would be required, since there are more than two independent reactants in the process. And such AR is hard to construct.

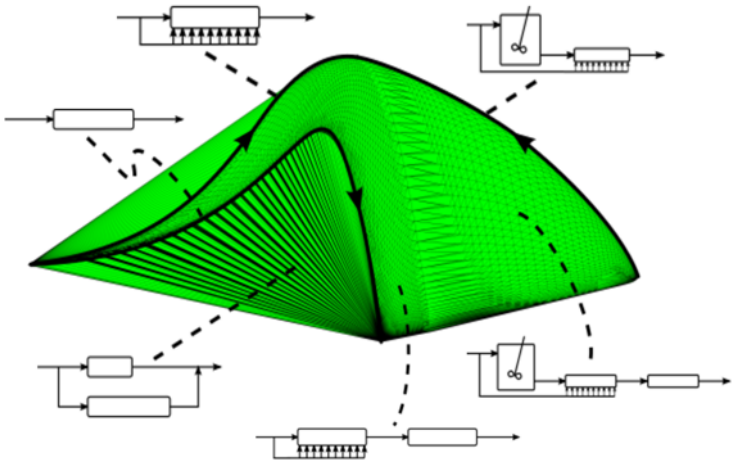

Figure 1.5. Attainable Region Proposed by Ming

In 2000, Feinberg analyzed the optimal reactor design from a geometric viewpoint [7], [8]. The first work focused on critical differential sidestream reactors (DSR), while the second one analyzed critical CSTRs. Critical reactors are the ones whose products lie entirely on the attainable region's boundary. Both critical DSR and CSTR play important roles in shaping the attainable region's boundary. In these studies, Feinberg determined the necessary conditions for a DSR/CSTR to be critical. These properties apply regardless of the problem dimension, although computational cost increases dramatically with the problem dimension. In addition, Feinberg did not discuss if these conditions would hold true when path constraints were considered. Nevertheless, these AR studies inspired our study to focus on the reactor networks that contain DSRs (i.e., a PFR with multiple monomer injection points) and/or CSTRs.

Lakshmanan and Biegler [9] proposed a superstructure framework as a sequence of modules, each consisting of a CSTR and DSR in parallel. These reactor modules are solved as a sequence of optimization problems with additional degrees of freedom. Because of this, the sequence leads to a monotonically decreasing objective function. An optimal network is assumed to have been found, when there are no further improvements within tolerance. This approach combines AR properties with superstructure techniques. From a geometric property that shows that network recycles and recycle reactors are unlikely to lie on the AR, Lakshmanan and Biegler [9] argued that the modular network is sufficiently rich to yield the optimum network. In addition, higher dimensional problems are addressed directly through the MINLP formulation.

Our approach combines the ideas in Feinberg's work [7],[8] (CSTR and DSR play important roles in shaping the AR boundary) and Lakshmanan and Biegler [9] papers (solving reactor modules in an increasing manner). First, we examine the reactor network with one CSTR or a PFR with multiple sidestreams. Then, we enrich the reactor design by adding one more CSTR/DSR in series, and we continue this procedure, until no improvement (within a tolerance of $1e^{-3}$) in the objective function is found.

1.2.3 Model Based Optimization

Besides reactor network design, model based optimization can be applied in all layers of the decision hierarchy, which includes regulatory control [10], model predictive control [11], [12], [13], [14],real time optimization [15], [16], [17], [18], [19], scheduling and planning [20], [21], [22], [23], [24], [25], [26] (from bottom to the top). Model based optimization allows us to translate an optimization task to a mathematical programming problem, from which optimal solutions can be obtained from a mathematical point of view with the help of efficient optimization algorithms. Hence, model based optimization has been extensively studied in academia. And it becomes the core of process system engineering (PSE). As these systematic problem solving tools become more and more mature, there is a stronger trend in process industry to implement these tools to replace the traditional methods that rely heavily on personal domain knowledge, expertise and trial and error lab experiment.

1.3 Uncertainty

The success of model-based optimization is highly based on model accuracy. In order to obtain reliable and meaningful optimal solutions, models used in the optimization problems need to be accurate and representative of the real chemical process. Even a small model mismatch or parameter uncertainty may result in infeasible solutions, and even leads to unsafe control actions in an actual plant. Although the off-line dynamic optimization is capable of handling reactor network design problem and generating operating recipes, its performance can be deteriorated in the presence of uncertainties. Uncertainties can come from many different sources, such as noises, disturbances, measurement errors, and uncertain kinetic parameters. In this work we will focus on the last type of uncertainty. In order to assess the impact of uncertainty in kinetic parameters and construct continuous reactor networks that work in different scenarios, robust optimization methods for reactor network design need to be considered. A bunch of methods have been proposed to deal with the uncertainties in dynamic optimization problem. Based on the utilization of measurements, these

approaches can be classified into two major categories: robust optimization [27], [28], [29], and stochastic programming [30], [31], [32], [33].

The robust optimization approach aims to obtain optimal solutions that give the best performance without using any additional measurements. Therefore, robust optimization does not react to measurements and its optimal solutions are more conservative. A typical formulation of robust optimization is bilevel minmax. In the lower level, we search for the worst case. In the upper level, we optimizes over the worst scenario. Since the occurrence probability of the worst case is usually small, the robust solution is often conservative and its performance is largely sacrificed when the nominal or the most probable uncertainty level is realized.

Stochastic programming first assumes that the probability distribution of the uncertain parameter can be estimated. Then, it takes advantage of the probability information to optimize the best expected performance. Moreover, this method utilizes measurements and introduces recourse variables into the model to improve the solution. Once the uncertainty is known in the first stage, its effect is observed and evaluated. In this way, different uncertainty levels can apply different reactive actions. The optimal solution results from the stochastic programming is less conservative compared to those of the robust optimization. However, its problem size is much larger and requires more computational cost, since it needs to cover multiple scenarios.

1.4 Research Statement and Thesis Outline

The goal of this study is to build model-based optimization problem to figure out the optimal reactor network design and the corresponding operating recipes for rigid polyol productions. To achieve this goal, four topics are carried out:

1. Kinetic parameter estimation
2. Reactor network design for a single rigid polyol
3. Reactor network design for multiple rigid polyols
4. Optimization under uncertainty

A detailed model that is representative of the process is a solid base for all the subsequent tasks. Once the model is ready, we focus on the reactor network design under uncertainty. The motivation, the background, the methodology as well as the results of each topic will be discussed in the remainder of the thesis.

Chapter 2 first introduces the dynamic optimization problem formulation. Then, it gives a brief overview of the optimization algorithms for dynamic optimization. In this work, simultaneous collocation method is widely applied to solve the dynamic optimization problems. Because this approach converts DAE problem into NLP, and enables efficient solution to the large-scale optimization problem. We also discuss three main nonlinear programming algorithms that are applied in the current NLP solvers.

Starting from Chapter 3, we focus on industrial applications of rigid polyol polymerization processes. First, we construct model that describes the polymerization process from scratch. Then, we utilize the model to estimate kinetic parameters present in the process with data provided by the Dow Chemical Company and a BASF patent.

Chapter 4 starts reactor network design for a single rigid polyol production. We focus on two types of continuous reactors: continuous stirred tank reactor (CSTR) and plug flow reactor (PFR) with multiple injection points. To this end, we examine five different reactor configurations: a single CSTR, two CSTRs in series, a single DSR, a CSTR followed by a DSR, and a DSR followed by a CSTR.

In order to remain competitive, companies are required to operate their systems at nearby optimal conditions for multiple products. Furthermore, multiproduct processes are widely used in different sectors due to their versatility and convenience. Therefore, in Chapter 5, we aim to find the optimal reactor network that is capable of producing multiple rigid polyols. We explore three main reactor configurations: CSTRs in series, a single DSR and a DSR followed by a CSTR.

Chapter 6 aims at obtaining robust optimal solutions in the presence of uncertainty in kinetic parameters. The motivation of considering uncertainty, as well as the background information on related research topics, will be introduced at the beginning of the chapter. Next, we formulate the

back-off and multi-scenario problems, and demonstrate and compare their effectiveness using a case study.

Chapter 7 concludes the dissertation, discusses the contributions of our work, and points out some open questions and future research directions.

Chapter 2 Optimization Methodology

2.1 Dynamic Optimization

Dynamic optimization [34], [35], [36] has been widely applied in chemical processes, including off-line problems [38], [39], [40], such as recipe and reactor network optimization, as well as on-line applications [41], [42] including predictive control, state estimation and online process identification. In most of the cases, a dynamic optimization problem with embedded differential algebraic equations (DAEs) is couched in the continuous time or volume horizon. The general form of a dynamic optimization problem can be summarised in Eqn. 2.1.

$$
\begin{aligned}
min \quad & CC = f(q, \beta_V) \\
s.t. \quad & \dot{z}(V) = f(z(V), y(V), u(V), q) = 0 \\
& g(z(V), y(V), u(V), q,) = 0 \\
& h(z(V), y(V), u(V), q, \beta_V) \leq 0 \\
& z(V)^L \leq z(V) \leq z(V)^U \\
& y(V)^L \leq y(V) \leq y(V)^U \\
& q^L \leq q \leq q^U \\
& u(V)^L \leq u(V) \leq u(V)^U \\
& \beta_V \in \{0, 1\}
\end{aligned}
\tag{2.1}
$$

The objective function of the dynamic optimization problem ($f(q, \beta_V)$) is to minimize the capital cost (CC), which is a function of decision variables (q) including reactor volume, heat exchanger capacity and monomer separation unit capacity. Binary variable β_V is also a decision variable, which represents the monomer injection points. It equals to 1 when monomers are added to the reactor at the reactor volume of V. If no monomer is fed to reactor at the volume of V, β_V equals to 0. z and y are differential and algebraic state variables, respectively, and u denotes the operation variables, which is also a type of decision variables that is a function of reactor volume V. It consists of the reactor temperature, feeding rates of monomer, catalyst and initiator. Also, the derivatives in differential equations are denoted by $\dot{z}$, which result from the material balance as well as the energy balance. In addition, $g(\cdot)$ and $h(\cdot)$ denote the algebraic equality and inequality constraints, respectively. The next four equations represent the upper and lower bounds for the differential, algebraic and decision, operation variables, respectively.

2.2 Solution Approaches for Dynamic Optimization

Numerical solution techniques are favored to obtain the approximated optimal solutions of dynamic optimization problem, because analytical solution is difficult for realistic problems and cannot handle inequality constraints in the dynamic optimization problem. There are two common numerical solution methods for solving the dynamic optimization problem: the sequential approach [43], [44], [45], [46] and the simultaneous approach [47], [48]. In both approaches, the decision variable is parameterized by applying an appropriate function approximation, such as piecewise constant parameterization. The major difference between these two methods is the way to treat the embedding DAEs. We are going to explore these two methods in the next two subsections.

2.2.1 Sequential Approach

The idea behind the sequential approach is to separate the DAE simulation problem from the optimization objective. At the meanwhile, the sequential approach links these two parts together through sensitivity calculations. In order to converge to a local optimal point, three functional blocks: DAE solver, sensitivity calculation and NLP solver are executed repeatedly [49], as shown in Fig. 2.1.

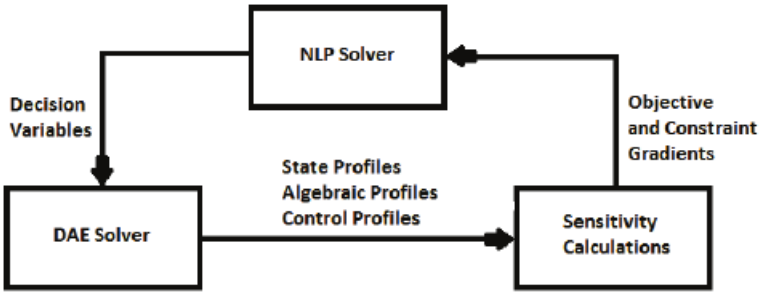

Figure 2.1. Sequential Approach for Dynamic Optimization

At each iteration, decision variables are fixed based on the DAE solver from the previous iteration. When the decision variables are specified, the DAE problem can be treated as an initial value problem and one can integrate the differential and the equality constraints forward in time or volume to obtain the differential state profile, algebraic state profile and control function profile. These profiles are used in the next component to evaluate the gradients of the objective and constraint functions with respect to the decision variables. Then, these function and gradient information are passed to the NLP solver, and the decision variables. One of the disadvantages of the sequential approach is that it cannot directly handle path constraints and inequality constraints in the sensitivity analysis. Further reformulation is required to convert those constraints to either end-point constraints or penalty terms in the objective function.

2.2.2 Simultaneous Dynamic Optimization

Both multiple shooting [50] and simultaneous collocation [51] methods can be considered as simultaneous approaches. The basic idea of multiple shooting is to divide the continuous time or volume horizon into several segments. Then, the sequential approach is applied to each time or volume slot. This approach performs better than the sequential approach when dealing with unstable systems. Moreover, not only the control variables but also the initial conditions of the states in each slot are considered in the sensitivity calculation, and thus more state variable information can be utilized by the NLP solver. Therefore, multiple shooting approach increases the problem size. The simultaneous collocation method follows a full discretization methodology, in which orthogonal collocation on a fixed/moving finite element mesh is introduced to represent the continuous time or volume horizon. By discretizing the continous time or volume horizon into a finite element mesh, the DAE problem is converted into NLP. State and decision variables are represented by a family of polynomials on the finite elements. In addition, the decision profiles are usually parametrized within finite elements using piecewise constant or linear profiles. More specifically, for the differential and algebraic state variables, a Runge-Kutta basis representation is introduced:

$$z(V) = z_{i-1} + h_i \sum_{j=1}^{K} \Omega_j(\tau) \dot{z}_{i,j} \tag{2.2}$$

$$y(V) = \sum_{j=1}^{K} l_j(\tau) y_{i,j} \tag{2.3}$$

where i corresponds to the index of finite elements, j is the index of collocation points up to K. h_i is the length of each element. $\tau \in [0, 1]$ represents the normalized time or volume in an element with $V = V_{i-1} + h_i\tau$. Moreover, z_{i-1} is the value of the differential variable at the beginning of the element, $\dot{z}_{i,j}$ is the value of the derivatives at the collocation point j in element i, and Ω_j is a polynomial of degree K, defined in Eqn. 2.4, where $l_j(\tau)$ denotes the Lagrange interpolation

polynomial basis function (Eqn. 2.5).

$$\Omega_j = \int_0^{\tau} l_j(\tau')d\tau' \tag{2.4}$$

$$l_j(\tau) = \prod_{k=1,\neq j}^{K} \frac{(\tau - \tau_k)}{(\tau_j - \tau_k)} \tag{2.5}$$

In addition, to ensure the continuity condition across the element boundary, Eqn. 2.6 is introduced. It requires the value of the differential variables at the beginning of each element to equal the value of the differential variables at the end of the previous element.

$$z_i = z_{i-1} + h_i \sum_{j=1}^{K} \Omega_j(1)\dot{z}_{i,j} \tag{2.6}$$

The algebraic state variables y are treated as K^{th} order Lagrange polynomials, but without the continuity condition across finite elements. By applying the collocation method, a dynamic optimization problem (Eqn. 2.1) is transformed into an MINLP problem with algebraic constraints (Eqn. 2.7). The binary variables $\beta_{i,j}$ can be manually fixed to convert the MINLP to a NLP, which

can later be solved by NLP solvers, such as IPOPT [52] and CONOPT [53], [54].

$$
\begin{aligned}
min \quad & CC = f(q, \beta_{i,j}) \\
s.t. \quad & z_{i,j} = z_{i-1} + h_i \sum_{j=1}^{K} \Omega_j(\tau_j) \dot{z}_{i,j} \\
& z_i = z_{i-1} + h_i \sum_{j=1}^{K} \Omega_j(1) \dot{z}_{i,j} \\
& \dot{z}_{i,j} = f(z_{i,j}, y_{i,j}, u_{i,j}, q), z_{1,0} = z_0 \\
& g(z_{i,j}, y_{i,j}, u_{i,j}, q) = 0 \\
& h(z_{i,j}, y_{i,j}, u_{i,j}, q, \beta_{i,j}) \leq 0 \\
& z_{i,j}^L \leq z_{i,j} \leq z_{i,j}^U \\
& y_{i,j}^L \leq y_{i,j} \leq y_{i,j}^U \\
& q^L \leq q \leq q^U \\
& u_{i,j}^L \leq u_{i,j} \leq u_{i,j}^U \\
& \beta_{i,j} \in \{0, 1\} \\
& i = 1...N, \quad j = 1...K
\end{aligned}
\tag{2.7}
$$

2.3 Nonlinear Programming Solvers

No matter whether one chooses to adopt the sequential or the simultaneous approach, an NLP solver is required to solve the dynamic optimization problem by conducting optimization searches on the decision variables. Newton type solvers [55], [56], [57] are generally preferred due to their fast convergence properties. The current NLP solvers usually apply three types of nonlinear programming algorithms: 1. sequential quadratic programming (SQP) method, 2. generalized reduced gradient (GRG) method, 3. interior point method.

SQP method [58], [59], [60], [61] is one of the most successful methods for generating the numerical solution of the constrained NLPs. SQP is an iterative procedure which models the NLP for a

given iteration by a Quadratic Programming (QP) subproblem. Then, it solves the QP subproblem and uses the solution to construct a new iteration. The QPs are constructed by using the variable value and derivative information at each iteration. SQP solvers are widely applied in the sequential method for dynamic optimization. First, the NLP problem size is relatively small in the sequential approach. Second, SQP methods generally perform well with approximated derivatives although second order derivatives are very expensive to compute via sensitivity analysis. SQP is adopted in solvers like SNOPT [62], [63], and NPSOL [64].

The main idea behind the GRG method [65], [66], [67] is to partition the variables in a NLP into basic, nonbasic, and superbasic variables. The basic variables are used to solve equality constraints, nonbasic variables are fixed at either their upper or lower bounds, and superbasic variables are used to drive the optimization search. CONOPT and MINOS [68], [69] are representative solvers implementing the GRG method.

The basic idea behind the interior point method is to reformulate the inequality constraints as barrier (penalty) terms to the objective function. Then, a series of NLP problems are solved with decreasing barrier parameters to recover the optimal solution of the original problem. The method has advantages dealing with large-scale problems with many degrees of freedom. Therefore, it is often used to solve the NLP problems resulting from the simultaneous collocation method. NLP solvers that apply the interior point method include IPOPT, and KNITRO [70], [71].

Chapter 3 Kinetic Parameter Estimation

3.1 Introduction

As mentioned in the previous chapters, the motivation of this project is switching the rigid polyol production from the existing semi-batch reactors to continuous reactors to lower the capital cost, and to increase the production rate. Before jumping into the continuous reactor network design, we first need to figure out and understand the reaction mechanism and the values of the kinetic parameters involved in the polymerization process. Rational design, simulation and optimization of an industrial process has to be built on an accurate basis, reliable data for mass, energy and momentum balance as well as chemical kinetics. In addition, scaling up from laboratory to industrial level requires predictive models with accurate parameter values. The aim of any kinetic parameter analysis in reaction engineering is to find adequate reaction model equations and to arrive at reliable parameter estimates dependent on the operating variables of the reactor, such as pressure, temperature, flow conditions and so on. These parameters then will be used to construct a reactor model, which consists of a set of equations that describe the behavior of a reactor with sufficient accuracy. Nowadays, model-based or equation-oriented kinetic parameter estimation [72], [73], [74], [75] is widely applied in chemical, biological and pharmaceutical process to deeper the understanding. Moreover, an open-source toolkit KIPET has been developed for kinetic parameter estimation.

3.2 Reaction Mechanism

The rigid polyols are initiated from base initiators like sucrose, glycerin, sorbitol, ethylene diamine, ortho-toluene diamine. These initiators often require special equipment to handle them due to their different physical and chemical nature. Typically, catalysts are used during the polymerization process to accelerate the desired reaction although there are some initiators that are autocatalytic for the first oxide addition. Typical catalysts that are used are divided into two categories – deactivating catalysts, such as amines, imidazoles and non-deactivating catalysts, like KOH. The deactivating catalysts have a side reaction with the oxides that accelerates with the increasing temperature. The oxides are typically propylene oxide and ethylene oxide.

In this kinetic parameter estimation case study:

Initiator: o-toluenediamine

Catalyst: none

Monomer: propylene oxide

The reaction scheme composes of six reactions in total. First, monomer propylene oxide (PO) attaches to the initiator o-toluenediamine (TDA) to form the mono-substituted species (M). Then, M reacts with PO to form di-substituted species D_{11} and D_{12}. There is a minor difference between D_{11} and D_{12}, as shown in Fig. 3.1. In D_{11}, two POs attach to the same amine group, but in D_{12} they attach to different amine groups. D_{11} and D_{12} then continue to react with PO to produce tri-substituted (T) species. Last, T and PO form quad-substituted (Q) species.

$$\text{TDA} + \text{PO} \xrightarrow{k_1} \text{M}$$

$$\text{M} + \text{PO} \xrightarrow{k_2} \text{D}_{12}$$

$$\text{M} + \text{PO} \xrightarrow{k_3} \text{D}_{11}$$

$$\text{D}_{12} + \text{PO} \xrightarrow{k_4} \text{T}$$

$$\text{D}_{11} + \text{PO} \xrightarrow{k_5} \text{T}$$

$$\text{T} + \text{PO} \xrightarrow{k_6} \text{Q}$$

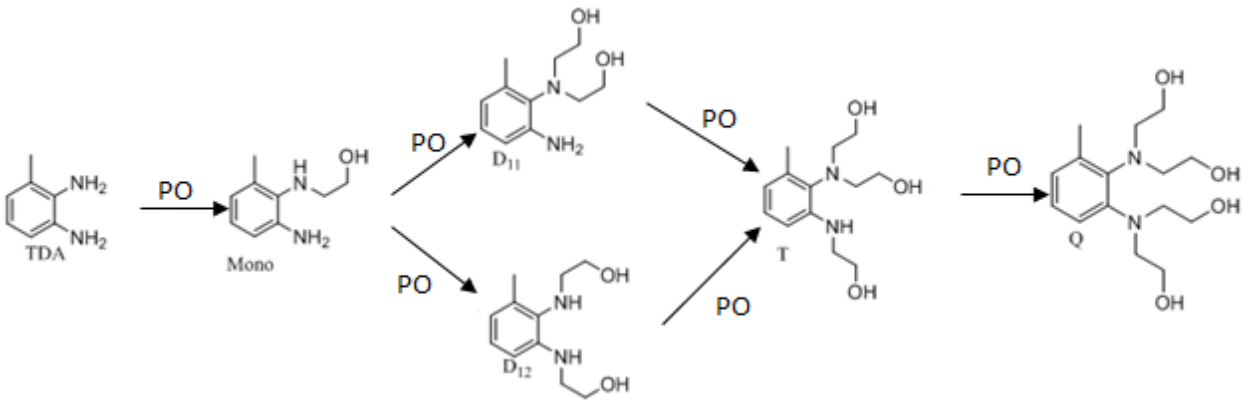

Figure 3.1. Reaction Mechanism

Although there are six reactions, only two rate constants k_1 and k_3 are independent. The rest of the rate constants are connected with either k_1 or k_3, as described below:

$$\begin{aligned} \mathrm{k}_2 &= \frac{1}{2}\mathrm{k}_1 \\ \mathrm{k}_4 &= 2\,\mathrm{k}_3 \\ \mathrm{k}_5 &= \frac{1}{2}\mathrm{k}_1 \\ \mathrm{k}_6 &= \mathrm{k}_3 \end{aligned} \tag{3.1}$$

According to the Arrhenius equation below, activation energies Ea_1 and Ea_3 are required, in order to obtain the rate constants at various temperatures.

$$k_i = k_i^{ref} e^{\frac{Ea_i}{RT_{ref}}(1-\frac{T_{ref}}{T})}, \quad i = 1, 3 \tag{3.2}$$

Furthermore, it is known that tertiary amines act as catalysts in these reactions. It is suggested to modify the reaction rates by introducing two enhancement factors $keff_1$ and $keff_3$.

$$TARE_i = 1 + keff_i(C_{D11} + C_T + 2C_Q), \quad i = 1, 3 \tag{3.3}$$

In the end, the rate equations can be modified with six kinetic parameters in this process: k_1, k_3,

Ea_1, Ea_3, $keff_1$ and $keff_3$.

$$
\begin{aligned}
r_1 &= k_1 C_{TDA} C_{PO} * TARE_1 \\
r_2 &= \frac{1}{2} k_1 C_M C_{PO} * TARE_1 \\
r_3 &= k_3 C_M C_{PO} * TARE_3 \\
r_4 &= 2k_3 C_{D12} C_{PO} * TARE_3 \\
r_5 &= \frac{1}{2} k_1 C_{D11} C_{PO} * TARE_1 \\
r_6 &= k_3 C_T C_{PO} * TARE_3
\end{aligned}
\tag{3.4}
$$

3.3 Data Set

For this rigid polyol production, two kinds of data sources are available for the kinetic parameter estimation. One data set is from a BASF patent [2], and the other one comes from the Dow Chemical Company as confidential data.

3.3.1 BASF Data

In the BASF patent, two experiments involving the continuous stirred tank reactor (CSTR) and three examples involving the plug flow reactor (PFR) with multiple monomer injections. The behavior of a CSTR is often approximated or modeled by that of an ideal CSTR, which assumes perfect mixing. In a perfectly mixed reactor, reagent is instantaneously and uniformly mixed throughout the reactor upon entry. Consequently, the output composition is identical to composition of the material inside the reactor, which is a function of residence time and reaction rate. Fig. 3.2 shows the set up of a typical CSTR. For the CSTR data set, the available information includes the reactor temperature, residence time, PO/TDA feed ratio and weight percentage of free TDA and PO at the outlet stream. Moreover, the CSTR material balance is $F_i^0 - F_i = -r_i V$,

where i represents the components in this process, F_i^0 and F_i are the inlet and outlet molar flow rate of component i, respectively. r_i is the generation rate of reactant i, and V represents the reactor volume. The CSTR mass balance can be summarized as following:

$$\begin{aligned}
F_{TDA}^0 - F_{TDA} &= r_1 * V \\
F_M^0 - F_M &= (-r_1 + r_2 + r_3) * V \\
F_{D11}^0 - F_{D11} &= (-r_3 + r_5) * V \\
F_{D12}^0 - F_{D12} &= (-r_2 + r_4) * V \\
F_T^0 - F_T &= (-r_4 - r_5 + r_6) * V \\
F_Q^0 - F_Q &= -r_6 * V \\
F_{PO}^0 - F_{PO} &= \sum_{n=1}^{6} r_i * V
\end{aligned} \tag{3.5}$$

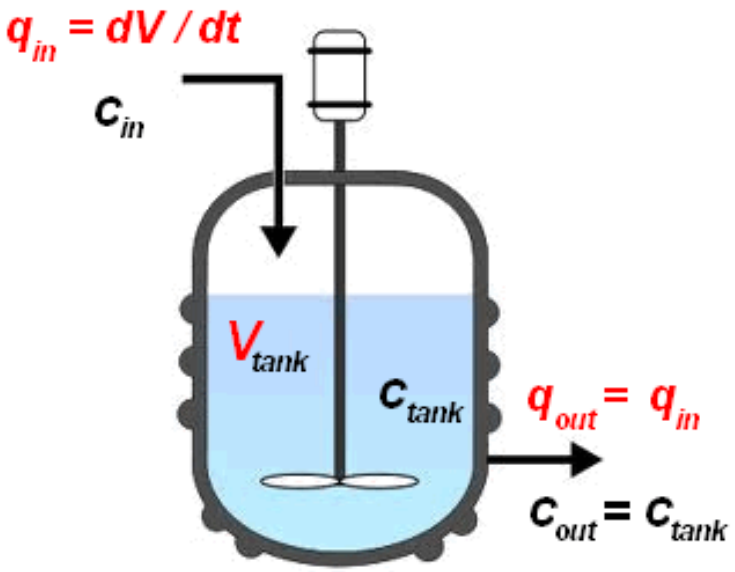

Figure 3.2. Set Up of a CSTR

Fluid going through a PFR can be modeled as flowing through the reactor as a series of infinitely thin coherent plugs, each with a uniform composition, traveling in the axial direction of the reactor, and each plug has a different composition from the ones before and after it. The key assumption is

that as a plug flows through a PFR, the fluid is perfectly mixed in the radial direction but not in the axial direction (forwards or backwards). Each plug of different volume is considered as a separate entity, effectively an infinitesimally small continuous stirred tank reactor, limiting to zero volume. As it flows down the tubular PFR, the residence time of the plug is a function of its position in the reactor. For the PFR data set, what are available are the reactor temperature, residence time, PO/TDA feed ratio, weight percentage of free PO at the outlet stream, and the number of feeding points. However, there is no information about the exact amount or location of each injection point. Hence, it is assumed that the feed is evenly distributed among the feeding points and the injection points are evenly distributed along the PFR reactor, as shown in Fig. 3.3. Furthermore, the design equation for PFR is $\frac{dF_i}{dV} = r_i$, where F_i stands for the molar flow rate of component i, V represents the reactor volume, r_i is the reaction rate of reactant i. The PFR mass balance can be summarized as follows:

$$\begin{aligned}
\frac{dF_{TDA}}{dV} &= -r_1 \\
\frac{dF_M}{dV} &= r_1 - r_2 - r_3 \\
\frac{dF_{D11}}{dV} &= r_3 - r_5 \\
\frac{dF_{D12}}{dV} &= r_2 - r_4 \\
\frac{dF_T}{dV} &= r_4 + r_5 - r_6 \\
\frac{dF_Q}{dV} &= r_6 \\
\frac{dF_{PO}}{dV} &= -\sum_{n=1}^{6} r_i
\end{aligned} \tag{3.6}$$

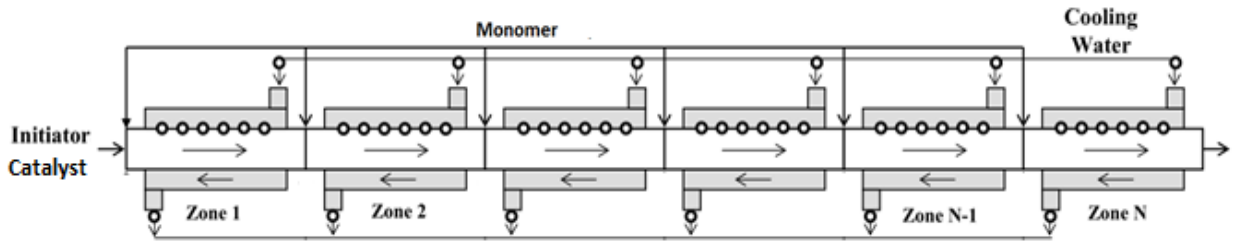

Figure 3.3. Set Up of a PFR with Multiple Monomer Injection Points

3.3.2 Dow Data

The confidential Dow data contains four sets of semi-batch data. Semi-batch reactors (see Fig. 3.4) operate much like batch reactors in that they take place in a single stirred tank with similar equipment. However, they are modified to allow reactant addition in time. A normal batch reactor is filled with the reactants in a single stirred tank at time zero and the reaction proceeds. On the contrary, a semi-batch reactor allows partial filling of reactants with the flexibility of adding more reactant as time progresses. Stirring in both types is very efficient, which allows batch and semi-batch reactors to assume a uniform composition and temperature throughout the reactor.

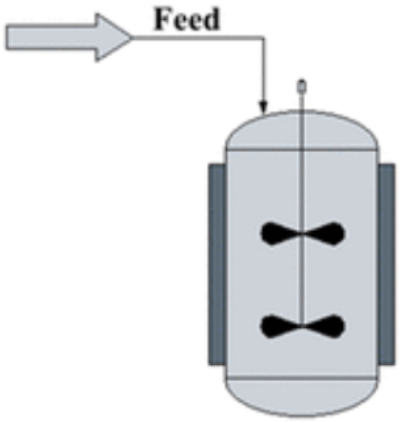

Figure 3.4. Set Up of a Semi-batch Reactor

Each semi-batch data set includes the reactor temperature and pressure at every minute, molar flow rate of monomer PO, the amount of TDA fed to the reactor and the reactor volume. Since pressure

data are available instead of concentration data, Wilson equation is used to convert pressure to concentration.

$$ln\gamma_i = 1 - ln(\sum_j A_{ij}x_j) - \sum_j \frac{A_{ji}x_j}{\sum_k A_{jk}x_k} \tag{3.7}$$

$$lnA_{ij} = a_{ij} + \frac{b_{ij}}{T} + c_{ij}lnT + d_{ij}T + \frac{e_{ij}}{T} \tag{3.8}$$

$$P = \sum_i x_i P_i^{sat} \gamma_i \tag{3.9}$$

where, x_i represents the molar fraction of component i in the liquid phase. γ_i stands for activity coefficient, and A_{ij} is a parameter, which can be calculated using the second equation above. Last, reactor pressure can be obtained by the last equation, where p_i^{sat} is the saturation pressure of component i. Finally, the material balance for semi-batch reactor is $\frac{dN_i}{dt} = F_i + r_i V$, where N_i is the number of moles of component i, t stands for time, F_i represents the feeding rate of component i, V is the reactor volume. The semi-batch mass balance can be summarized as following:

$$\begin{aligned}
\frac{dN_{TDA}}{dt} &= F_{TDA} - r_1 * V \\
\frac{dN_M}{dt} &= (r_1 - r_2 - r_3) * V \\
\frac{dN_{D11}}{dt} &= (r_3 - r_5) * V \\
\frac{dN_{D12}}{dt} &= (r_2 - r_4) * V \\
\frac{dN_T}{dt} &= (r_4 + r_5 - r_6) * V \\
\frac{dN_Q}{dt} &= r_6 * V \\
\frac{dN_{PO}}{dt} &= F_{PO} - \sum_{n=1}^{6} r_i * V
\end{aligned} \tag{3.10}$$

3.4 Solution Strategy

3.4.1 Semi-Batch and Plug Flow Reactor Models

The semi-batch and plug flow reactor models can be written in a general form as a dynamic optimization problem:

$$\begin{aligned} min \quad & \sum_{n} (\theta_n - \theta_n^{data})^2 \\ s.t. \quad & \dot{z} = f(z(x), y(x), u), \quad z(0) = z_0 \\ & g(z(x), y(x), u) = 0 \\ & z^L \leq z(x) \leq z^U \\ & y^L \leq y(x) \leq y^U \\ & u^L \leq u \leq u^U \end{aligned} \tag{3.11}$$

θ here represents weight fraction when dealing with the BASF data and stands for pressure when handling the Dow data. In addition, x represents time in the semi-batch model and stands for reactor volume in the PFR model. The objective function is the difference between actual data and model prediction. Moreover, z and y are differential and algebraic state variables, respectively, and u denotes the decision variables that are the six kinetic parameters in this case. Furthermore, differential equations are denoted by $f(\cdot)$, which come from the material balance. $g(\cdot)$ denotes the equality process constraints, which results from the pressure or weight fraction calculations, such as Wilson equation. The last three equations represent the upper and lower bounds for differential, algebraic and decision variables, respectively.

The simultaneous collocation method can be adopted to deal with the dynamic optimization problem in Eqn. 3.11. This method follows a full discretization methodology, in which orthogonal collocation on a fixed/moving finite element mesh is introduced to represent the continuous time/volume horizon. Meanwhile, the state variables are also discretized in the time/volume di-

mension. More specifically, for the differential states variables, a Runge-Kutta basis representation is introduced:

$$z(x) = z_{i-1} + h_i \sum_{j=1}^{K} \Omega_j(\tau)\dot{z}_{i,j} \tag{3.12}$$

where i corresponds to the index of finite elements, j is the index of collocation points up to K. h_i is the length of element i. $\tau \in [0, 1]$ represents the normalized time/volume in an element with $x = x_{i-1} + h_i\tau$. Moreover, z_{i-1} is the value of the differential variable at the beginning of the element, $\dot{z}_{i,j}$ is the value of the derivatives at the collocation point j in element i, and Ω_j is a polynomial of degree K, defined as the following:

$$\Omega_j = \int_0^{\tau} l_j(\tau')d\tau' \tag{3.13}$$

$$l_j(\tau) = \prod_{k=1,\neq j}^{K} \frac{(\tau - \tau_k)}{(\tau_j - \tau_k)} \tag{3.14}$$

In addition, to ensure the continuity condition across the element boundary, the following equation is introduced:

$$z_i = z_{1-1} + h_i \sum_{j=1}^{K} \Omega_j(1)\dot{z}_{i,j} \tag{3.15}$$

The algebraic states y are treated as K^{th} order Lagrange polynomials, but without the continuity condition across finite elements. By using the collocation method, a dynamic optimization problem

is translated into an NLP problem without any differential equations.

$$
\begin{aligned}
min \quad & \sum_{n} (\theta_n - \theta_n^{data})^2 \\
s.t. \quad & \dot{z}_{i,j} = f(z_{i,j}, y_{i,j}, u), \quad z_{1,0} = z_0 \\
& z_{i,j} = z_{i-1} + h_i \sum_{j=1}^{K} \Omega(\tau_j) \dot{z}_{i,j} \\
& z_i = z_{i-1} + h_i \sum_{j=1}^{K} \Omega(1) \dot{z}_{i,j} \\
& g(z_{i,j}, y_{i,j}, u) = 0 \\
& z^L \leq z_{i,j} \leq z^U \\
& y^L \leq y_{i,j} \leq y^U \\
& u^L \leq u \leq u^U
\end{aligned}
\tag{3.16}
$$

3.4.2 Continuous Stirred Tank Reactor Model

The general form for the CSTR model is simpler, since it does not contain any differential equations. Hence, all the constraints are in algebraic form, and the CSTR problem is a nonlinear programming problem (NLP) instead of a differential-algebraic equation (DAE) optimization problem. The CSTR model can be directly developed in platforms, such as GAMS, AMPL, Pyomo, and solved by NLP solvers. In addition, the objective function is still the difference between actual data and model prediction for the CSTR model.

$$
\begin{aligned}
min \quad & (\theta_{PO} - \theta_{PO}^{data})^2 \\
s.t. \quad & g(y, u) = 0 \\
& y^L \leq y \leq y^U \\
& u^L \leq u \leq u^U
\end{aligned}
\tag{3.17}
$$

where θ represents weight fraction, y stands for the algebraic state variables, u is the decision variables, which are the six kinetic parameters. $g(\cdot)$ denotes the equality constraints that come from the material balance.

3.5 Results and Discussion

The kinetic parameter estimation results are displayed in Table 3.1. The optimal results obtained by using the BASF data are presented in the left two columns. Both results in the last two columns are estimated based on the Dow data. The lower bounds for Ea_1 and Ea_3 are 120 $\frac{kJ}{mol}$ and 95 $\frac{kJ}{mol}$, respectively for BASF 1 and Dow 1. On the other hand, there is no restriction on activation energies for the BASF 2 and Dow 2 cases. The reason why lower bounds of activation energies are added for BASF 1 and Dow 1 cases is that the open literature states the values of Ea_1 amd Ea_3 are around 120 $\frac{kJ}{mol}$ and 95 $\frac{kJ}{mol}$, respectively. The units for k_i, Ea_i and $keff_i$ in Table 3.1 are $\frac{cm^3}{mol*min}$, $\frac{J}{mol}$ and $\frac{cm^3}{mol}$, respectively, $i \in \{1, 3\}$, and the reference temperature is 122 °C.

Table 3.1 Optimal Results for Kinetic Parameter Estimation

	BASF 1	BASF 2	Dow 1	Dow 2
Obj	936.310	0.0989	80.921	57.541
k_1	$6.96 \pm 1.89 * 10^{-5}$	5.76 ± 3.35	$3.87 \pm 4.56 * 10^{-3}$	6.47 ± 0.68
k_3	$0.20 \pm 4.69 * 10^{-6}$	1.05 ± 1.31	8.92 ± 0.63	3.23 ± 0.67
Ea_1	$1.20 * 10^5$	$6.06 * 10^3 \pm 2.98 * 10^4$	$1.20 * 10^5$	$3.72 * 10^4 \pm 1.69 * 10^4$
Ea_3	$9.50 * 10^4$	$6.56 * 10^{-2} \pm 9.27 * 10^2$	$9.50 * 10^4$	$9.69 * 10^3 \pm 1.05 * 10^3$
$keff_1$	$3.47 * 10^3 \pm 9.12 * 10^{-2}$	$1.75 * 10^4 \pm 8.55 * 10^3$	$6.71 * 10^3 \pm 465$	$6.84 * 10^3 \pm 7.73 * 10^2$
$keff_3$	$2.23 * 10^4 \pm 5.97 * 10^{-1}$	$2.48 * 10^4 \pm 5.04 * 10^4$	$1.34 * 10^{-4} \pm 0.13$	$1.09 * 10^{-4} \pm 0.11$

According to Table 3.1, the value of the objective function is much lower when there is no restriction on the activation energies. In addition, the optimal results solve to lower bounds when bounds for Ea_i are added. However, the standard deviations of kinetic parameters are much higher without

the activation energy bounds.

After solving the model and obtaining the optimal results, a covariance check is carried out to figure out which kinetic parameter cannot be determined independently. The eigenvalues of the reduced hessian matrix are shown in Table 3.2. According to this, all kinetic parameters can be determined for the BASF 1 case. However, recall that, the activation energies solve to lower bounds. Moreover, four eigenvalues of the reduced hessian matrix are very small for the BASF 2 case, which means these four kinetic parameters have large variances. Hence these parameters cannot be determined independently. On the other hand, when solving the model using the Dow data, and adding the activation energy bounds, only one kinetic parameter $keff_1$ has large variance. In addition, Ea_1, Ea_3 and $keff_1$ cannot be determined independently when the lower bounds for activation energies are not present. In conclusion, more kinetic parameters can be determined independently when the lower bounds of activation energies are incorporated in the model. However, activation energies solve to their lower bounds, which implies they are not independent and we would obtain a lower objective when there is no activation energy restriction.

Table 3.2 Eigenvalues of the Reduced Hessian Matrix

BASF 1	BASF 2	Dow 1	Dow 2
2.8 - $keff_3$	$3.9 * 10^{-10}$ - $keff_3$	$6.3 * 10^{-5}$ - $keff_1$	$2.4e^{-9}$ - Ea_3
$1.2 * 10^{2}$ - $keff_1$	$1.1 * 10^{-9}$ - Ea_1	55.5 - $keff_3$	$4.5 * 10^{-9}$ - Ea_1
$5.1 * 10^{9}$ - k_1	$3.1 * 10^{-8}$ - $keff_1$	$3.9 * 10^{9}$ - k_3	$5.4 * 10^{-6}$ - $keff_1$
$5.5 * 10^{11}$ - k_3	$1.2 * 10^{-6}$ - Ea_3	$7.4 * 10^{11}$ - k_1	$8.4 * 10^{1}$ - $keff_3$
	$3.0 * 10^{1}$ - k_1		$1.1 * 10^{8}$ - k_3
	$2.3 * 10^{3}$ - k_3		$2.3 * 10^{10}$ - k_1

We further simplify the kinetic model by setting $keff_1$ and $keff_3$ to zero and removing the lower bounds for Ea_1 and Ea_3. The optimal nominal values and corresponding standard deviations obtained by applying the BASF and Dow data are recorded in the second and third columns of

Table 3.3, respectively. Moreover, the corresponding eigenvalues of the reduced Hessian matrix are listed in Table 3.4. From these two tables we can tell that Ea_1 and Ea_3 still cannot be determined independently even when $keff_1$ and $keff_3$ are fixed to zero.

Table 3.3 Optimal Results After Setting $keff_1$ and $keff_3$ to Zero

	BASF	Dow
Obj	8.1	118.1
$k_1(\frac{cm^3}{mol*min})$	69.8 $\pm$1.0	8.1 $\pm$0.02
$k_3(\frac{cm^3}{mol*min})$	29.5 $\pm$6.0	40.9 $\pm$2.4
$Ea_1(\frac{J}{mol})$	2128.3 $\pm$1153	8.3*10^{-6} $\pm$ 0.1
$Ea_3(\frac{J}{mol})$	2675.9 $\pm$15251	5.5*10^{-4} $\pm$ 7.7

Table 3.4 Eigenvalues of the Reduced Hessian Matrix After Setting $keff_1$ and $keff_3$ to Zero

BASF	Dow
$7.9 * 10^{-9}$ - Ea_3	$1.4 * 10^{-2}$ - Ea_3
$4.5 * 10^{-5}$ - Ea_1	$1.7 * 10^{-1}$ - Ea_1
$1.4 * 10^{4}$ - k_3	$7.3 * 10^{1}$ - k_3
$1.8 * 10^{7}$ - k_1	$4.2 * 10^{13}$ - k_1

We also try to simplify the kinetic model by setting Ea_1 and Ea_3 to zero. The optimal nominal values and corresponding standard deviations obtained by applying the BASF and Dow data are recorded in the second and third columns of Table 3.5, respectively. Moreover, the corresponding eigenvalues of the reduced Hessian matrix are listed in Table 3.6. From these two tables we can tell that $keff_1$ and $keff_3$ still cannot be determined independently even when Ea_1 and Ea_3 are fixed to zero.

Table 3.5 Optimal Results After Setting Ea_1 and Ea_3 to Zero

	BASF	Dow
Obj	8.1	118.1
$k_1(\frac{cm^3}{mol*min})$	5.6 $\pm$0.3	8.3 $\pm$0.03
$k_3(\frac{cm^3}{mol*min})$	2.2 $\pm$0.7	5.9 $\pm$3.1
$keff_1(\frac{J}{mol})$	18740 $\pm$6132	4965 $\pm$2310
$keff_3(\frac{J}{mol})$	11200 $\pm$2903	564 $\pm$525

Table 3.6 Eigenvalues of the Reduced Hessian Matrix After Setting Ea_1 and Ea_3 to Zero

BASF	Dow
$2.2 * 10^{-8}$ - $keff_1$	$1.3 * 10^{-5}$ - $keff_1$
$1.5 * 10^{-6}$ - $keff_3$	$5.6 * 10^{-5}$ - $keff_3$
$1.4 * 10^{2}$ - k_1	$1.8 * 10^{8}$ - k_1
$1.4 * 10^{5}$ - k_3	$2.5 * 10^{11}$ - k_3

3.6 Conclusions

In this chapter, we first go over the motivation behind the kinetic parameter estimation. Then, we explore the reaction scheme for this particular rigid polyol and the material balances for different types of reactors. Two data sources are available for this rigid poyol production. One is from a BASF patent, the other one is provided by the Dow Chemical Company. Next, we model the parameter estimation problems as dynamic optimization problems, and apply the simultaneous collocation method to discretize the continuous time or volume horizon to convert the DAE problems into NLPs. Finally, we examine and compare the estimation results obtained from the BASF patent and the Dow data.

The optimal results obtained from the two data sources are not consistent with each other. This may be caused by the incompatibility between these two data sources. First, the BASF data are based on continuous reactors, such as CSTR and PFR. On the contrary, the Dow data is obtained from semi-batch reactors. Second, the objective of reference is different. In the BASF patent, what we know is the outlet weight percentage of unreacted monomer and initiator. Therefore, the objective is to minimize the difference between the predicted and the actual outlet weight percentage. For the Dow data, what we have available is pressure data, which is a function of time. Hence, we aim to minimize the difference between the predicted and the target pressure. Both objective of references have their own advantages and disadvantages. For instance, weight percentage data is more accurate than pressure data, since we do not need to make any assumptions to convert concentration to pressure. However, the outlet weight percentage data is inadequate, since it lacks weight percentage data along the reactor volume.

Despite which data source is applied, the kinetic parameter estimation results do not turn out as expected. When the bounds for activation energies are not present, more than half of the kinetic parameters cannot be determined independently. This is mainly caused by the insufficiency of the data. After adding the activation energy bounds, fewer parameters have large standard deviations, but activation energies solve to lower bounds. The reason behind this is that the temperature ranges of these data sets are narrow, between 110 and 150 °C. Hence, it is hard to estimate the activation energies over this small range.

Since the kinetics cannot be fully understand, our next step is to consider processes that take KOH as catalyst, since the kinetics of KOH is fully discovered, and we can adopt it directly in the continuous network design problem.

Chapter 4 Continuous Reactor Network Design for Rigid Polyol Production

In this chapter, we focus on developing continuous reactor network models that are capable of producing rigid polyols under strict product and safety specifications. At the same time, we determine the optimal decision profiles that lead to minimum capital cost. Decision variables include the feeding rates of initiator, monomer, and catalyst, reactor temperature, residence time, number and location of monomer injection points. Moreover, we narrow down the types of continuous reactors that can be part of the network to two: plug flow reactor (PFR) with multiple feed injection points and continuous stirred tank reactor (CSTR). The PFR model can be written as a differential algebraic equation (DAE) optimization problem. The simultaneous collocation method is applied to transform the DAE into a mixed integer nonlinear programming (MINLP) problem. An iterative algorithm is proposed to solve the MINLP, where binary variables are manually fixed. The results obtained from this strategy show that a PFR with ten monomer injection points is the reactor configuration that has the lowest capital cost.

4.1 Literature Review

Nie et al. [76] studied the recipe optimization of polyether polyol processes, where a well defined reaction model was proposed for polyol production and it is adopted in this work as well, since the same reaction mechanism applies to rigid polyols with shorter chain length. The reaction scheme

contains four kinds of reactions: initiation, propagation, transfer and exchange. Among the four reactions, the rates of exchange reactions are higher than other reaction rates. The difference in reaction rates leads to a two-time scale model and results in a stiff system that is hard to solve. Hence, the quasi-steady state assumption (QSSA) is applied through a nullspace projection proposed in [76] to simplify the differential-algebraic equation (DAE) reactor model. The basic idea is to model the fast reactions using QSSA to separate the slow and fast components and reformulate the stiff system to a non-stiff, index-1 DAE reactor model. However, in [76] only operating recipes were examined for the semi-batch reactor. Furthermore, Di Serio et al. [77] studied the kinetics of propoxylation process in the presence of catalyst KOH, and these kinetics are adopted in Nie's work, as well as the case study in this work.

In 2016, Zhang et al. [5] developed the optimization of continuous reactor networks for a polymerization process. Simple flowsheet configurations with two CSTRs in series and in parallel are frequently used in practice. However, due to the limitations of these conventional reactor network structures, many polymer grades, especially high-quality ones, may not be achievable even under a wide range of operating conditions. Hence, a more flexible process flowsheet configuration was constructed in Zhang's study. The superstructure was constructed to incorporate all possible structural alternatives of interest. The basic idea was to place splitters at the exit of each CSTR, and then allow all CSTRs to be fully connected with each other. In Zhang's work, the configurations with one to four CSTRs were carried out to meet the target molecular weight distribution. The proposed superstructure was very flexible and allows recycles to occur, but it does not contain PFRs.

In 1994, Kokossis and Floudas. [4] proposed a reactor network that includes both CSTRs and PFRs. The key advantage of this approach is that the objective value, optimal reactor network and operating conditions can be determined simultaneously. One of the limitations of this superstructure approach is that the model formulations typically are nonconvex, and the subspaces of the response surface are often "flat", leading to many near-optimal solutions. In addition, the optimal solution is only as rich as the initial superstructure; therefore, the global optimal reactor network cannot be found if it is not contained within the superstructure. However, there is a trade

off between the richness of the superstructure and the size and complexity of the model. In addition, some optimal reactor configurations are rather complex (contain multiple recycle streams) and hard to validate in reality.

Another way to formulate the reactor network is through the attainable region (AR) in concentration space, which finds the set of all possible outputs for all possible reactor configurations [6]. Every point in or on the AR is an output of a reactor combination. Once we have the region, we are assured that it contains the optimal solution. However, for this polymerization problem, attainable regions with more than two dimensions would be required, since there are more than two independent reactants in the process. And such AR is hard to construct. In 2000, Feinberg analyzed the optimal reactor design from a geometric viewpoint [7], [8]. The first work focused on critical differential sidestream reactors (DSR), while the second one analyzed critical CSTRs. Critical reactors are the ones whose products lie entirely on the attainable region's boundary. Both critical DSR and CSTR play important roles in shaping the attainable region's boundary. In these studies, Feinberg determined the necessary conditions for a DSR/CSTR to be critical. These properties apply regardless of the problem dimension, although computational cost increases dramatically with the problem dimension. In addition, Feinberg did not discuss if these conditions held true when path constraints were considered. Nevertheless, these AR studies inspired our study to focus on the reactor networks that contain DSRs (i.e., a PFR with multiple monomer injection points) and/or CSTRs.

Lakshmanan and Biegler [9] proposed a superstructure framework as a sequence of modules, each consisting of a CSTR and DSR in parallel. These reactor modules are solved as a sequence of optimization problems with additional degrees of freedom. Because of this, the sequence leads to a monotonically decreasing objective function. An optimal network is assumed to have been found, when there are no further improvements within tolerance. This approach combines AR properties with superstructure techniques. From a geometric property that shows that network recycles and recycle reactors are unlikely to lie on the AR, Lakshmanan and Biegler [9] argued that the modular network is sufficiently rich to yield the optimum network. In addition, higher dimensional prob-

lems are addressed directly through the MINLP formulation.

Our approach combines the ideas in Feinberg's works [7],[8] (CSTR and DSR play important roles in shaping the AR boundary) with the findings in Lakshmanan and Biegler's paper [9] (solving reactor modules in an increasing manner). First, we examine the reactor network with one CSTR or a PFR with multiple sidestreams. Then, we enrich the reactor design by adding one more CSTR/DSRs in series, and we continue this procedure, until no improvement (within a tolerance of $1e^{-3}$) in the objective function is observed. Finally, five reactor networks are derived and compared, as shown in Fig. 4.1: one CSTR, two CSTRs in series, a single DSR, a CSTR followed by a DSR, and a DSR followed by a CSTR.

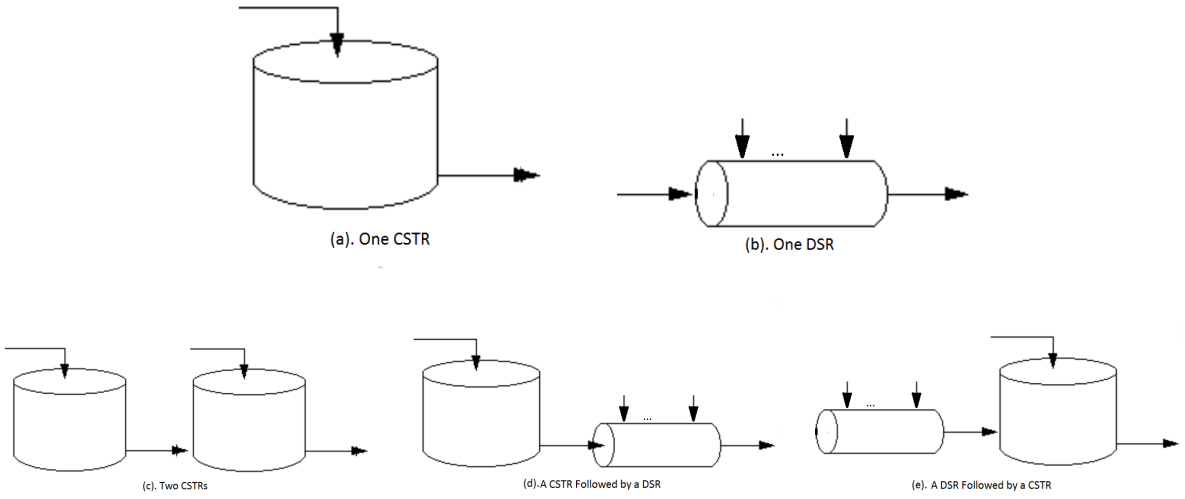

Figure 4.1. Examined Reactor Networks

This chapter is organized as follows; Section 2 introduces the complex reaction scheme for rigid polyol production and corresponding kinetic parameters. In Section 3, the development of both CSTR and DSR models is presented. The solution strategy utilized for solving the reactor network optimization models is given in Section 4. Section 5 presents and further compares the numerical results for each reactor network. Section 6 summaries the study and concludes the chapter.

4.2 Kinetics for Rigid Polyol Production

The kinetics for rigid polyol are based on Sorbitol initiator, which has six hydroxyl groups per molecule of Sorbitol with a molecular weight of 182 g/mol. Sorbitol is propoxylated (addition of propylene oxide (PO) monomer) to a molecular weight less than 1000 g/mol. Therefore, the typical chain length for rigid polyol is less than 10. For the lower molecular weight rigid polyols, the propoxylation is done via anionic polymerization with KOH catalyst. Typically, the alkoxide is produced by adding KOH catalyst to an aqueous sorbitol solution and then removing the water. Therefore, all the catalyst is fed at the beginning of the reactor. The melt needs to be maintained at a temperature above 100 °C to remain pumpable. Finally, it is desirable that the mole fraction for the unalkoxylated OH groups to be less than 0.05.

4.2.1 Reaction Scheme

The reaction kinetics generally follow the reaction kinetics reported in Nie's work [76], except that hydrolysis reactions are excluded, because water in aqueous sorbitol solution is removed before adding to the reactor. In addition, the detailed reaction scheme is displayed in Table 4.1. The following notation is used in the remainder of this chapter. PO denotes the propylene oxide monomer. P_n represents one of six branches in the sorbitol initiator $CH(PO)_n$. Both n and m indicate the number of repeating units. Meanwhile, U_n denotes the unsaturated chains with double-bond end groups $CH_2 = CHCH_2(PO)_n$, formed by the chain transfer step and subsequent growth step. Moreover, depending on the different functional end groups, we define the following:

G_n growing product chains of length n $(P_nO^-K^+)$

D_n dormant product chains of length n (P_nOH)

Q_n growing unsaturated chains of length n $(U_nO^-K^+)$

R_n dormant unsaturated chains of length n (U_nOH)

Table 4.1 Reaction Scheme for Rigid Polyol

Initiation
$G_0 + PO \xrightarrow{k_i} G_1$
Propagation
$G_n + PO \xrightarrow{k_p} G_{n+1}\ (n \geq 1)$
$Q_n + PO \xrightarrow{k_p} Q_{n+1}\ (n \geq 1)$
Transfer
$G_n + PO \xrightarrow{k_t} D_n + Q_0\ n \geq 0)$
$Q_n + PO \xrightarrow{k_t} R_n + Q_0\ (n \geq 0)$
Exchange
$G_n + D_m \xrightarrow{k_e} D_n + G_m\ (n, m \geq 0)$
$Q_n + R_m \xrightarrow{k_e} R_n + Q_m\ (n, m \geq 0)$
$G_n + R_m \overset{k_e}{\rightleftharpoons} D_n + Q_m\ (n, m \geq 0)$

The population balance of polymer chains in the CSTR model is described in Eqn. 4.1, where the subscripts i, p, t and e represent the initiation, propagation, transfer and exchange reactions, respectively. Also, F represents the molar flow rate. C stands for concentration. V is the volume.

$$F^0_{G_0} - F_{G_0} = -V * k_i * C_{G_0} * C_{PO} - V * k_t * C_{G_0} * C_{PO} - V * k_e * C_{G_0} * \sum_{m=0}^{N}(C_{D_m} + C_{R_m}) + V * k_e * C_{D_0} * \sum_{m=0}^{N}(C_{G_m} + C_{Q_m})$$

$$F^0_{G_1} - F_{G_1} = V * k_i * C_{G_0} * C_{PO} - V * (k_p + k_t) * C_{G_1} * C_{PO} - V * k_e * C_{G_1} * \sum_{m=0}^{N}(C_{D_m} + C_{R_m}) + V * k_e * C_{D_1} * \sum_{m=0}^{N}(C_{G_m} + C_{Q_m})$$

$$F^0_{G_n} - F_{G_n} = V * k_p * (C_{G_{n-1}} - C_{G_n}) * C_{PO} - V * k_t * C_{G_n} * C_{PO} - V * k_e * C_{G_n} * \sum_{m=0}^{N}(C_{D_m} + C_{R_m}) + V * k_e * C_{D_n} * \sum_{m=0}^{N}(C_{G_m} + C_{Q_m})$$

$$G_n = G_2, ..., G_{N-1}$$

$$F^0_{G_N} - F_{G_N} = V * k_p * C_{G_{N-1}} * C_{PO} - V * k_t * C_{G_N} * C_{PO} - V * k_e * C_{G_n} * \sum_{m=0}^{N}(C_{D_m} + C_{R_m}) + V * k_e * C_{D_n} * \sum_{m=0}^{N}(C_{G_m} + C_{Q_m})$$

$$F^0_{D_n} - F_{D_n} = V * k_t * C_{G_n} * C_{PO} + V * k_e * C_{G_n} * \sum_{m=0}^{N}(C_{D_m} + C_{R_m}) - V * k_e * C_{D_n} * \sum_{m=0}^{N}(C_{G_m} + C_{Q_m})$$

$$D_n = D_0, ..., D_N$$

$$F^0_{Q_0} - F_{Q_0} = -V * (k_i + k_t) * C_{Q_0} * C_{PO} + V * k_t * \sum_{m=0}^{N}(C_{G_m} + C_{Q_m}) * C_{PO} - V * k_e * C_{Q_0} * \sum_{m=0}^{N}(C_{D_m} + C_{R_m}) + V * k_e * C_{R_0} * \sum_{m=0}^{N}(C_{G_m} + C_{Q_m})$$

$$F^0_{Q_1} - F_{Q_1} = V * (k_i * C_{Q_0} - k_p * C_{Q_1}) * C_{PO} - V * k_t * C_{Q_1} * C_{PO} - V * k_e * C_{Q_1} * \sum_{m=0}^{N}(C_{D_m} + C_{R_m}) + V * k_e * C_{R_1} * \sum_{m=0}^{N}(C_{G_m} + C_{Q_m})$$

$$
\begin{aligned}
F^0_{Q_n} - F_{Q_n} &= V * k_p * (C_{Q_{n-1}} - C_{Q_n}) * C_{PO} - V * k_t * C_{Q_n} * C_{PO} \\
&\quad - V * k_e * C_{Q_n} * \sum_{m=0}^{N} (C_{D_m} + C_{R_m}) + V * k_e * C_{R_n} * \sum_{m=0}^{N} (C_{G_m} + C_{Q_m}) \\
Q_n &= Q_2, ..., Q_{N-1} \\
F^0_{Q_N} - F_{Q_N} &= V * k_p * C_{Q_{N-1}} * C_{PO} - V * k_t * C_{Q_N} * C_{PO} \\
&\quad - V * k_e * C_{Q_n} * \sum_{m=0}^{N} (C_{D_m} + C_{R_m}) + V * k_e * C_{R_n} * \sum_{m=0}^{N} (C_{G_m} + C_{Q_m}) \\
F^0_{R_n} - F_{R_n} &= V * k_t * C_{Q_n} * C_{PO} \\
&\quad + V * k_e * C_{Q_n} * \sum_{m=0}^{N} (C_{D_m} + C_{R_m}) - V * k_e * C_{R_n} * \sum_{m=0}^{N} (C_{G_m} + C_{Q_m}) \\
R_n &= R_0, ..., R_N
\end{aligned}
\tag{4.1}
$$

Among the four major reactions, the rates of the exchange reactions are significantly higher than other reaction rates. This explains why it is necessary to add less catalyst than the number of OH groups in the reactor. The difference in the rate constants results in a two-time scale model and leads to a stiff system, which cannot be easily solved. Hence, the exchange reactions are modeled using the quasi-steady state assumption and two pseudo-species X and Y are introduced [76] to solve this problem, where $X_n = G_n + D_n$ and $Y_n = Q_n + R_n$. The resulting population balances

for the CSTR and DSR models are demonstrated in Eqn. 4.2 and 4.3, respectively.

$$
\begin{aligned}
F^0_{X_0} - F_{X_0} &= -k_i * C_{G_0} * C_{PO} \\
F^0_{X_1} - F_{X_1} &= (k_i * C_{G_0} - k_p * C_{G_1}) * C_{PO} \\
F^0_{X_n} - F_{X_n} &= (k_p * C_{G_{n-1}} - k_p * C_{G_n}) * C_{PO} \quad n = 2, ..., N-1 \\
F^0_{X_N} - F_{X_N} &= k_p * C_{G_{N-1}} * C_{PO} \\
F^0_{Y_0} - F_{Y_0} &= -k_i * C_{Q_0} * C_{PO} + k_t * \sum_{n=0}^{N} (C_{G_n} + C_{Q_n}) * C_{PO} \\
F^0_{Y_1} - F_{Y_1} &= (k_i * C_{Q_0} - k_p * C_{Q_1}) * C_{PO} \\
F^0_{Y_n} - F_{Y_n} &= (k_p * C_{Q_{n-1}} - k_p * C_{Q_n}) * C_{PO} \quad n = 2, ..., N-1 \\
F^0_{Y_N} - F_{Y_N} &= k_p * C_{Q_{N-1}} * C_{PO}
\end{aligned}
\tag{4.2}
$$

$$
\begin{aligned}
\frac{dF_{X_0}}{dV} &= -k_i * C_{G_0} * C_{PO} \\
\frac{dF_{X_1}}{dV} &= (k_i * C_{G_0} - k_p * C_{G_1}) * C_{PO} \\
\frac{dF_{X_n}}{dV} &= (k_p * C_{G_{n-1}} - k_p * C_{G_n}) * C_{PO} \quad n = 2, ..., N-1 \\
\frac{dF_{X_N}}{dV} &= k_p * C_{G_{N-1}} * C_{PO} \\
\frac{dF_{Y_0}}{dV} &= -k_i * C_{Q_0} * C_{PO} + k_t * \sum_{n=0}^{N} (C_{G_n} + C_{Q_n}) * C_{PO} \\
\frac{dF_{Y_1}}{dV} &= (k_i * C_{Q_0} - k_p * C_{Q_1}) * C_{PO} \\
\frac{dF_{Y_n}}{dV} &= (k_p * C_{Q_{n-1}} - k_p * C_{Q_n}) * C_{PO} \quad n = 2, ..., N-1 \\
\frac{dF_{Y_N}}{dV} &= k_p * C_{Q_{N-1}} * C_{PO}
\end{aligned}
\tag{4.3}
$$

4.2.2 Model Parameters

Kinetic parameters stated by Nie et al. [76] are applied to this case study, and listed in the Table 4.2 below. This is a major assumption since these kinetics are brought up for long polymer chains

which are not necessarily the same as those for the short chains in this work. Moreover, initiation and propagation steps have different kinetics, which implies that polymer chains with monomers attached behave differently than the initiator.

Table 4.2 Kinetic Parameters

Reaction Type	Initiation	Propagation	Transfer
Arrhenius Constant $(\frac{m^3}{mol*s})$	396400	8504	950410
Activation Energy $(\frac{kJ}{kmol})$	77822	69172	105018
Heat of Reaction $(\frac{kJ}{kmol})$	92048	92048	0

Tables 4.3, 4.4, 4.5 list the parameters used to calculate the capital cost for CSTR, PFR, and oxide recovery system [78]. These costs are relative.

Table 4.3 Capital Cost Parameters for CSTR

CSTR component	Basis	Installed Base cost ($K)	Exponent
Tank Reactor	3 hr RT	1000	0.7
Agitators	Per reactor	300	1
Pump		50	1
Oxide Injection	Per injection	50	1
Catalyst Injection	Per injection	20	1
Heat Exchanger	1465 $\frac{kJ}{s}$	100	0.7

Table 4.4 Capital Cost Parameters for PFR

PFR component	Basis	Installed Base cost ($K)	Exponent
Piping Segment	15 minutes	100	0.7
Pump	every hour	50	1
Oxide Injection	Per injection	50	1
Catalyst Injection	Per injection	20	1
Heat Exchanger	293 $\frac{kJ}{s}$	50	0.7

Table 4.5 Capital Cost Parameters for Oxide Recovery System

Recovery System component	Basis	Installed Base cost ($K)	Exponent
Vacuum	1% oxide	200	0.7
Flash Tank	1% oxide	200	0.7
Condenser	1% oxide	100	0.7

4.3 Optimization Model for Rigid Polyol Reactor

The model consists of three main parts: material balance, energy balance, product specifications and safety constraints, which are explored in the following subsections. In addition, n denotes either the index of each CSTR or the index of each DSR zone. c and m stands for the components involved in the process, and monomer respectively. rxn represents the reaction index. Finally, $FR_{m,n}$ is the feed rate of monomer to n^{th} CSTR/DSR zone.

4.3.1 Material Balance

First, rate constants can be calculated using the Arrhenius equation (4.4), where k, A, Ea, R and T represent the rate constant, Arrhenius constant, activation energy, gas constant and reactor temperature, respectively.

$$k_{rxn,n} = A_{rxn} e^{-\frac{Ea_{rxn}}{RT_n}}, rxn \in \{i, p, t\}, n \in N \tag{4.4}$$

Second, reaction rates for different reactions can be expressed using Eqn. 4.5, where r is the reaction rate, and C represents concentration. All the reactions are of second order. The subscripts 1 and 2 in Eqn. 4.5, represent the first and second components involved in the reaction, respectively.

$$r_{rxn,n} = k_{rxn,n} * [C_{1,n}] * [C_{2,n}], rxn \in \{i, p, t\}, n \in N \tag{4.5}$$

Eqns. 4.6a, and 4.6b enforce the continuity between CSTRs or DSR zones. F^0 and F denote the inlet and outlet molar flow rate, respectively. Since fresh monomers are allowed to be added at the beginning of each CSTR/DSR zone, the inlet molar flow rate equals the summation of outlet molar flow rate from previous CSTR/DSR zone and the feeding rate of fresh monomer. For other components, the inlet molar flow rate equals the outlet molar flow rate of the previous CSTR/DSR zone.

$$F^0_{m,n} = F_{m,n-1} + FR_{m,n}, n \in \{1..N\} \tag{4.6a}$$

$$F^0_{c,n} = F_{c,n-1}, \quad c \neq m, n \in \{1..N\} \tag{4.6b}$$

Reactor volume, volumetric flow rate and concentration for each zone n can be calculated using Eqn. 4.7a, 4.7b and 4.7c, respectively. V represents the reactor volume, $\dot{V}$ is the volumetric flow

rate and MW denotes the molecular weight of component c.

$$V_n = \dot{V}_n * \tau_n, n \in N \tag{4.7a}$$

$$\dot{V}_n = \sum_c \frac{F^0_{c,n} * MW_c}{\rho_{c,n}}, n \in N \tag{4.7b}$$

$$C_{c,n} * \dot{V}_n = F_{c,n}, c \in C, n \in N \tag{4.7c}$$

Finally, CSTR and DSR follow different design equations. For CSTR, the design equation is in algebraic form (Eqn. 4.8):

$$F^0_{c,n} - F_{c,n} = -r_{c,n} * V_n, c \in C, n \in N \tag{4.8}$$

while the design equation for DSR is a differential equation (Eqn. 4.9).

$$\frac{dF_{c,n}}{dV_n} = -r_{c,n}, c \in C, n \in N \tag{4.9}$$

4.3.2 Energy Balance

Fresh monomer feed has a cooling effect, since its temperature is at least 100 °C lower than the reactor temperature. Monomer cooling is represented by H^m_{cool} in Eqn. 4.10. In addition, C^m_p is the heat capacity of monomer and T^m_f denotes the feed temperature of monomer.

$$H^{m,n}_{cool} = \int_{T^m_f}^{T_n} C^m_p \, dT, n \in N \tag{4.10}$$

Second, total mass flow rate $\dot{M}$ can be obtained from Eqn. 4.11, which is required in the energy balance calculation.

$$\dot{M}_n = \sum_c F^0_{c,n} * MW_c, n \in N \tag{4.11}$$

Moreover, we need to ensure the energy is conserved across CSTRs/DSR zones (Eqn. 4.12a, 4.12b). $\dot{M}^m$ is the mass flow rate of monomer. Superscript b represents the solution mixture inside

of the reactor.

$$(\dot{M}_n - \dot{M}_n^m) * \int_{T_n^0}^{T_f^b} C_p^b dT = \sum_m H_c^{m,n} * FR^{m,n} * MW^m, \quad n = 1 \tag{4.12a}$$

$$\dot{M}_n * \int_{T_n^0}^{T_{n-1}} C_p^b dT = \sum_m H_c^{m,n} * FR^{m,n} * MW^m, \quad n \in \{1..N\} \tag{4.12b}$$

The final element in energy balance is the amount of heat released during the reaction, H_r. For CSTR, it can be obtained using Eqn. 4.13, where H_{rxn} represents the heat of reaction, which is different for different monomers.

$$H_r^n = \sum_m (F_{m,n}^0 - F_{m,n}) * H_{rxn}^m, n \in N \tag{4.13}$$

For DSR, the heat released can be calculated based on the rate of reactions as shown in Eqn. 4.14:

$$H_r^n = -\sum_m r_{m,n} * H_{rxn}^m, n \in N \tag{4.14}$$

Finally, the energy balances for CSTR and DSR are different, with the former one in algebraic form (Eqn. 4.15a), and the latter one in differential form (Eqn. 4.15b). Moreover, H_p represents the extra cooling that needs to be provided.

$$\dot{M}_n * C_p^b * T_n^0 + H_r^n - H_p^n = \dot{m}_n * C_p^b * T_n, n \in N \tag{4.15a}$$

$$\dot{M}_n * C_p^b * \frac{dT_n}{dV_n} = H_r^n - H_p^n, n \in N \tag{4.15b}$$

4.3.3 Product Quality & Safety Constraints

This model includes six product specifications and two safety constraints. First, there is a minimum target production rate (Eqn. 4.16), where N represents the final reactor or the last zone in the network.

$$\sum_c F_{c,N} \geq PR^* \tag{4.16}$$

Second, a lower bound for the average molecular weight is given by Eqn. 4.17:

$$\overline{MW} = \frac{\sum_c F_{c,N} * MW_c}{\sum_c F_{c,N}} \geq \overline{MW}^* \tag{4.17}$$

Third, an upper bound for unalkoxylated active sites of initiator is given by Eqn. 4.18:

$$\sigma = \frac{moles\,of\,unalkoxylated\,active\,sites}{moles\,of\,initiator} \leq \sigma^* \tag{4.18}$$

Fourth, there are specifications for outlet weight percentage of monomer m and catalyst (Eqn. 4.19a, 4.19b).

$$wt\%_{m,N} \leq wt\%_m^* \tag{4.19a}$$

$$wt\%_{cat,N} \leq wt\%_{cat}^* \tag{4.19b}$$

Finally, the amounts of monomer, initiator and catalyst are limited (Eqn. 4.20a). In addition, monomer feeding rate should equal to zero if reactor n has no monomer injection point (the corresponding binary variable $\beta_n = 0$).

$$FR_c \leq FR_c^*, \quad c = \{ini, cat\} \tag{4.20a}$$

$$FR_{m,n} \leq \beta_n * FR_m^*, \quad \beta_n \in \{0, 1\}, n \in N \tag{4.20b}$$

The first safety constraint is implemented to avoid runaway reactions when the cooling system fails. κ in Eqn. 4.21 is a constant between one and ten. Basically, this constraint limits the weight percentage of unreacted monomers in the reactor. In a PFR, runaway will dramatically increase the reactor temperature and eventually lead to overpressure the storage tank that the PFR empties into.

$$\kappa * wt\%_{m,n} \leq T_{safety} - T_n, n \in N \tag{4.21}$$

The second safety constraint provides the reactor temperature range as shown in Eqn. 4.22.

$$T_{LB} \leq T_n \leq T_{UB}, n \in N \tag{4.22}$$

4.4 Solution Strategy

4.4.1 CSTR Model

The MINLP problem of continuous stirred tank reactor (Eqns. 4.2, 4.4 - 4.8, 4.10 - 4.13, 4.15a & 4.16-4.22) can be summarized in Eqn. 4.23:

$$\begin{aligned} min \quad & CC = \sum_{n=1}^{N} (f_1(H_p(n)) + f_2(\tau(n)) + f_3(\beta_n)) + f_4(wt\%_{m,N}) + f_5 \\ s.t. \quad & g(y_n, u_n) = 0 \\ & h(y_n, u_n, \beta_n) \leq 0 \\ & y_n^L \leq y_n \leq y_n^U \\ & u_n^L \leq u_n \leq u_n^U \\ & \beta_n \in \{0, 1\} \end{aligned} \tag{4.23}$$

where n represents the index of CSTRs and N denotes the final CSTR. The objective function is capital cost (CC), which includes the reactor cost and the cost for oxide recovery system (f_4), which is used to separate the unreacted monomer from the polyol product. In addition, the reactor cost includes the cost of reactor tank (f_2), agitator, pump, catalyst injection (these three costs are constants and denoted by f_5), monomer injection (f_3) and heat exchanger (f_1). Notice that, monomer injection is represented by binary variable β_n. If the feeding rate of monomer m to CSTR n is greater than zero then $\beta_n = 1$, otherwise $\beta_n = 0$. In order to formulate the problem as an NLP instead of a MINLP, the binary term is manually fixed to either 1 or 0. Moreover, y stands for algebraic state variables, and u denotes the decision variables that are the reactor temperature,

residence time, injection points of monomer, feeding rates of monomer, catalyst and initiator. $g(\cdot)$ denotes the equality process constraints, which result from the mass balance (Eqn. 4.2) as well as the energy balance. $h(\cdot)$ represents the inequality constraints which result from the process constraints, such as the adiabatic temperature rise, heat removal and product specification constraints. The last two equations represent the upper and lower bounds for algebraic and decision variables, respectively.

4.4.2 DSR Model

The DSR model (Eqns. 4.3, 4.4 - 7, 4.9 - 12, 4.14 & 4.15b - 4.22) can be written in a general form as a dynamic optimization problem (Eqn. 4.24). The objective function of the DSR model is capital cost. In addition, f_1 calculates the cost for heat exchanger. f_2 estimates the reactor cost. The monomer injection cost is denoted by f_3, followed by the cost for monomer recovery system (f_4). Finally, f_5 represents the cost for agitator, pump and catalyst injection. Moreover, z and y are differential and algebraic state variables, respectively. u denotes the decision variable that includes the reactor temperature, residence time and injection points of monomer, feeding rates of monomer, catalyst and initiator. Furthermore, differential equations are denoted by f, which result from the mass balance (Eqn. 4.3) as well as the energy balance and g denotes the algebraic equality constraints. h stands for inequality constraints that come from the product and safety specifications. The next three equations represent the upper and lower bounds for differential, algebraic and decision variables, respectively. Monomer injection points are represented by binary variable β_V.

$$
\begin{aligned}
min \quad & CC = f_1(H_p) + f_2(\tau) + \sum_{n=1}^{N} f_3(\beta_V) + f_4(wt\%_{m,V_f}) + f_5 \\
s.t. \quad & \dot{z}(V) = f(z(V), y(V), u(V)) = 0 \\
& g(z(V), y(V), u(V)) = 0 \\
& h(z(V), y(V), u(V), \beta_V) \leq 0 \\
& z(V)^L \leq z(V) \leq z(V)^U \\
& y(V)^L \leq y(V) \leq y(V)^U \\
& u(V)^L \leq u(V) \leq u(V)^U \\
& \beta_V \in \{0, 1\}
\end{aligned}
\tag{4.24}
$$

The dynamic optimization model can be solved by the simultaneous collocation method. This method discretizes the continuous volume horizon into a finite element mesh, and then the differential-algebraic equation optimization problems are converted into nonlinear programming problems. A detailed description for simultaneous collocation method can be found in Chapter 2. In this study, a mesh of 40 finite elements along with a two-point Radau collocation is applied to the DSR model. We observe that this combination gives accurate solutions, while maintaining a computationally solvable model, shown in Fig. 4.2. Each DSR is discretized into 40 elements with equal volume and each element is treated as one DSR zone. Initiator and catalyst are added at the beginning of DSR. Monomer can be added at the beginning of each DSR zone. Therefore, there are forty possible monomer injection points per DSR and over a trillion (2^{40}) injection profiles. More importantly, the model is highly nonlinear. Through several trials, we observe that solution of the nonconvex MINLP in Eqn. 4.24, is beyond the capabilities of current MINLP solvers, such as BARON, DICOPT, SBB and BONMIN. Therefore, instead of using MINLP solvers, an efficient algorithm is proposed to determine the injection profile that would lead to a minimum capital cost.

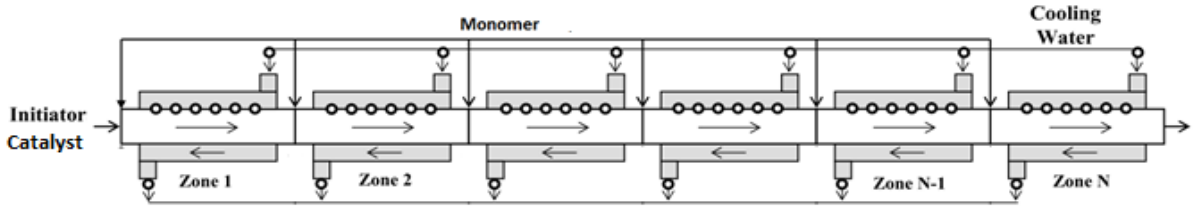

Figure 4.2. Discretized DSR

Below are the steps to determine the optimal injection profile for a DSR:

- Step 1. Relax the binary variables to nonnegative variables between 0 and 1. Then, solve the relaxed DSR model and obtain its optimal decision profiles. Based on the monomer feeding rates, sort the injection points from the highest to the lowest. Set $i = 1$

- Step 2. Select only the first i injection points (β_n) from the sorted list and set them to one. Fix other injection points to zero. Define the set $J_i = \{n|\beta_n = 1\}$. Solve the DSR model with injection profile J_i. If the model is infeasible, set $i = i + 1$. Repeat step 2, until the DSR model becomes feasible (able to produce desired rigid polyol without violating the safety constraint in Eqn. 4.21). Then, the minimum number of injection points required for the rigid polyol production is obtained, with injection profile given by J_i, which includes the first i elements in the sorted injection point list.

- Step 3. Re-visit the optimized solution of the model with injection profile J_i. Based on the KKT multiplier of the constraint displayed in Eqn. 4.20b for $n \notin J_i$, add the injection point with the largest multiplier to injection profile J_{i+1} (fix the binary variable to one instead of zero). Repeat this step, until no further improvement in the objective function (within a tolerance of 10^{-3}).

- Step 4 (Optional). Permute between different profiles with i injection points by shifting injection points one by one to the near by positions or dividing the injection points more evenly. If the new profile yields a lower objective, update profile J_i. Repeat this step until exhausted.

Our alternative approach offers no guarantee of a global optimal solution, since it is not possible to examine all permutations when i is large. Nevertheless, we find this multiplier-based approach determines high quality local solutions with modest computational costs. As shown in the Section 4.5.1, reactor configurations with similar monomer injection profiles all converge to a similar relative capital cost. This also shows that the objective function is flat due to the non-linearity. Furthermore, CSTR model yields to the same results using either NLP solver IPOPTH or MINLP solver SBB. And FR_{ini} is consistent between CSTR and DSR models. All of the consistency between models shows that the multiplier-based approach determines high quality local solutions.

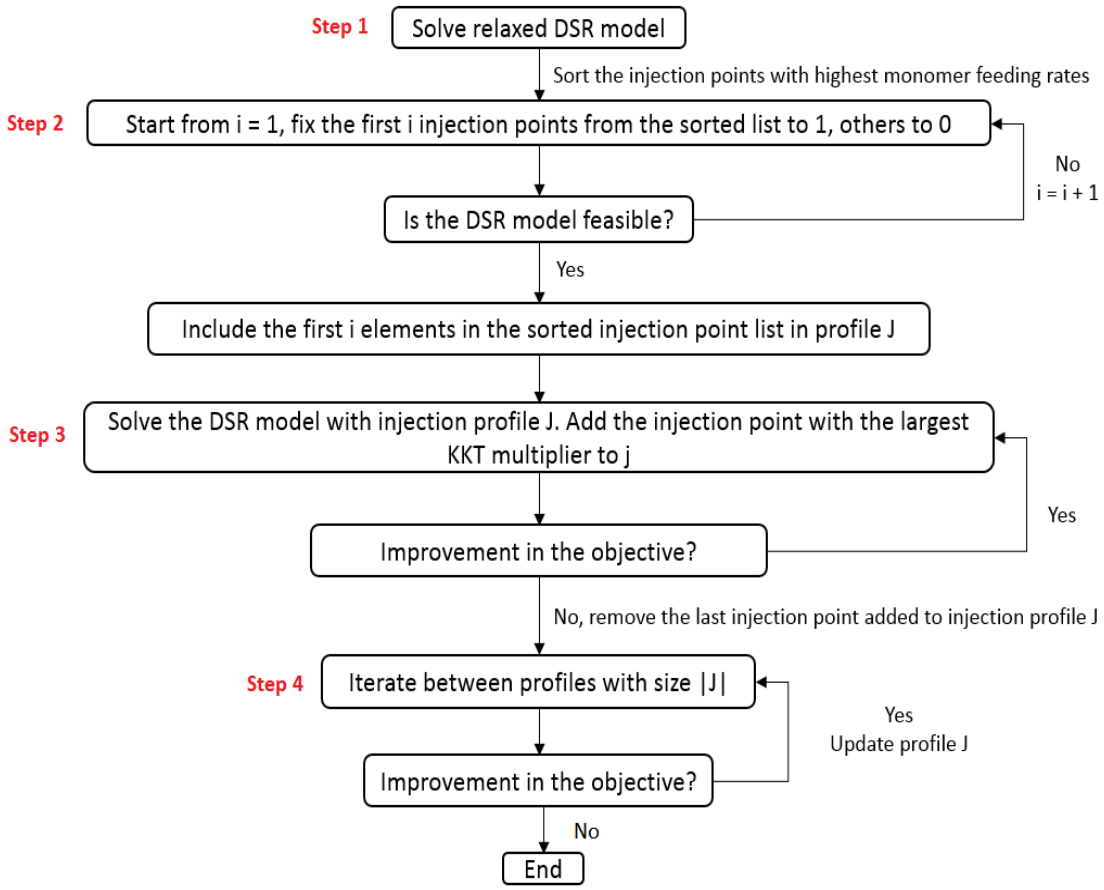

Figure 4.3. Flow Chart of Finding Optimal Injection Profile

Both CSTR and DSR models are implemented in GAMS and solved by NLP solver IPOPTH.

4.5 Results and Discussions

In this section, five different reactor networks for polyol production are examined: one CSTR, two CSTRs in series, one DSR, a CSTR followed by a DSR, and a DSR followed by a CSTR. The corresponding optimal capital cost, and operation conditions are presented in the following subsections. Due to confidentiality, results are scaled based on the optimal solution of the single DSR model. Moreover, the maximum chain length of the rigid polyol is set to 10 in this study.

4.5.1 One DSR

The DSR model is presented in Eqn. 4.24 and the steps in Fig. 4.3 are applied to obtain the optimal injection profile.

First, the binary variables are relaxed into variables between 0 and 1. The relaxed DSR model is then solved. The relative capital cost of the relaxed DSR model (optimal DSR cost $= 1$) is 0.572. However, this capital cost represents a lower bound of the solution, since the optimal values for variables β_n lead to fractional injection points with unrealistic costs. The relative capital cost is 1.322 after setting the fractional β_n to unity for the injection points. The optimal feed profile of the relaxed DSR model is plotted in Fig. 4.4. According to this, fresh PO feeds are added to first 22 zones. The weight percentage curve oscillates in the first half of the reactor, since monomers are constantly added to the reactor. Moreover, there is a spike in the weight percentage of PO, and a drop of PO feeding rate when the normalized volume equals to 0.2. This is caused by the adiabatic temperature rise constraint, which limits the weight percentage of unreacted PO in the reactor. Since, the weight percentage of PO is high at that point, it is reasonable for the system to decrease the PO feeding rate at the same point. Based on the monomer feeding rates, the injection points are sorted from the largest to the smallest as follows: 1, 2, 3, 5, 7, 4, 6, 9, 8, 10, 11, 12, 13, 14, 15, 16, 17, 18, 19, 20, 21, 22.

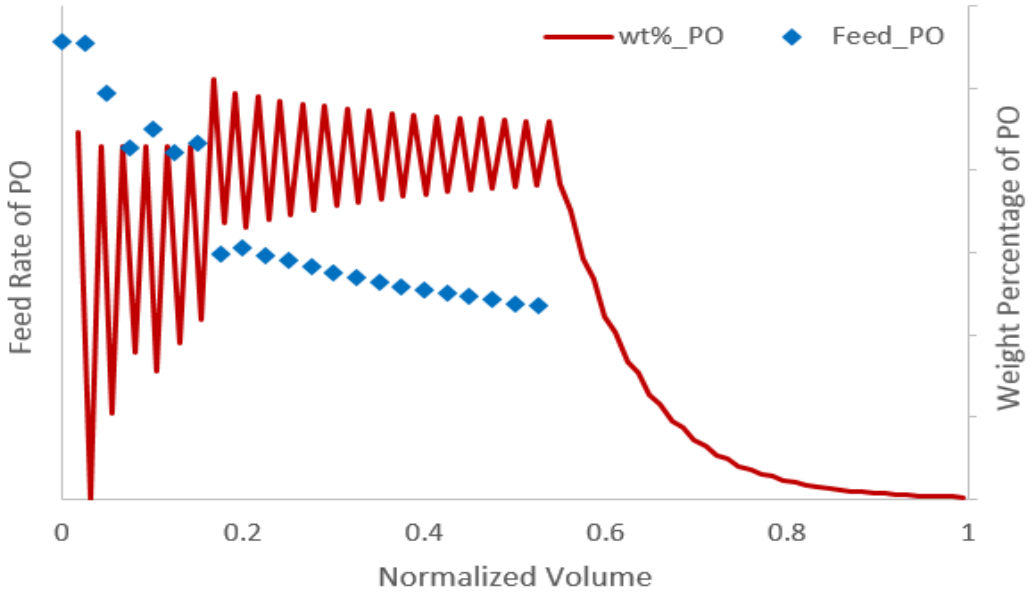

Figure 4.4. Feed Profile for the Relaxed DSR Model

Then, we move to step 2 and find that at least five injection points are required for model feasibility. Next, we solve the DSR model with injection profile $J_5 = \{1, 2, 3, 5, 7\}$ (the first five injection points in the sorted list above). Based on the KKT multiplier for the injection points that are not presented in J_5, injection point at zone 4 is added to the profile. Step 3 is repeated, until additional injection points no longer improves the objective function. Fig. 4.5 shows the change in capital cost as a function of the number of monomer injection points. According to this plot, capital cost starts to drop as more injection points are incorporated. However, after 10 injection points, adding more feeding points does not lead to a significant improvement in capital cost, since the savings in reactor cost do not cover the cost of additional injection point.

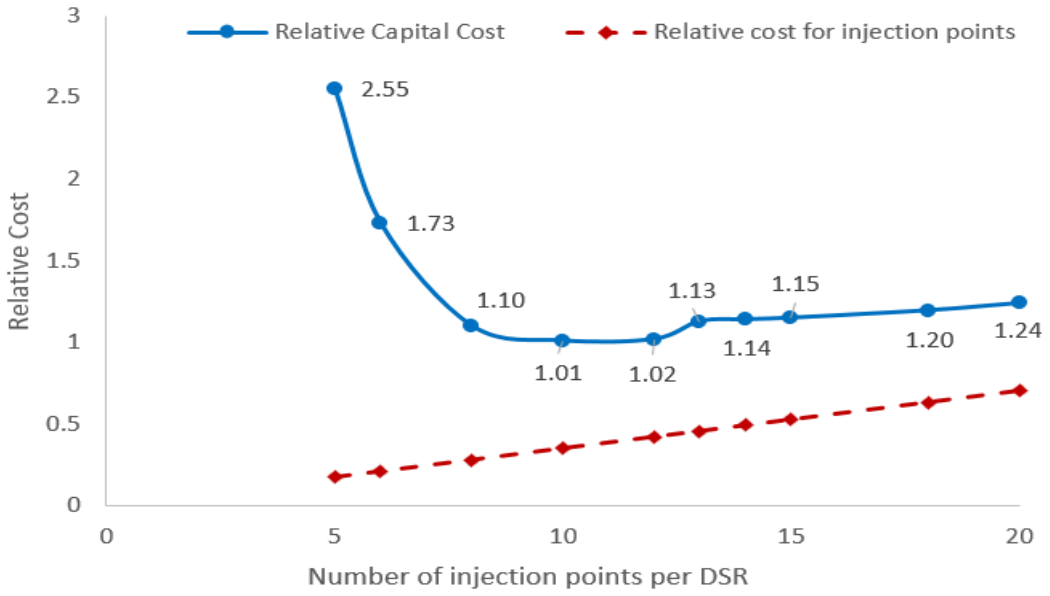

Figure 4.5. Relative Capital Cost Versus Number of Monomer Injection Points (Scaled to Optimal Objective in Table 4.6 No.5 Iteration)

After step 3, the profile J_{10} includes injection points at zones 1, 2, 3, 4, 5, 7, 9, 12, 15, and 25. The last injection point (at zone 25) is far away from its previous injection point (at zone 15). Moving the last injection point towards the front, would extend the DSR digestion period, and might reduce the capital cost. In order to obtain the relationship between capital cost and the optimal position of the final injection point, the last injection point is moved towards the beginning of the reactor one zone at a time, while keeping the other injection points fixed. According to Fig. 4.6, as the final injection point moves from zone 25 to zone 22, the relative capital cost decreases, although moving it to zone 20 increases the capital cost. Therefore, the injection profile is updated to $J_{10} = \{1, 2, 3, 4, 5, 7, 9, 12, 15, 22\}$.

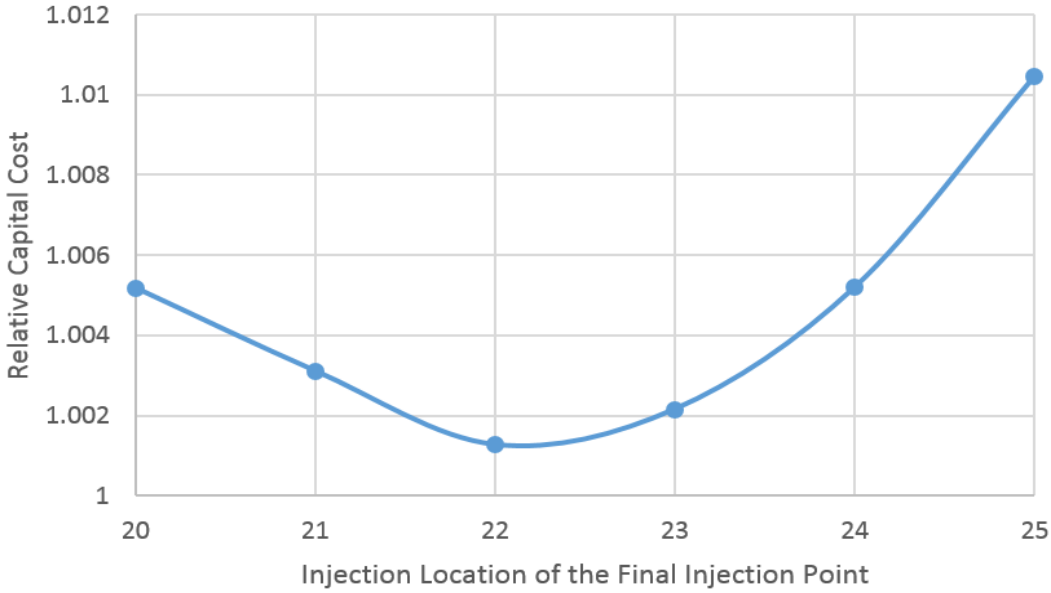

Figure 4.6. Relative Capital Cost Versus the Position of the Final Injection Point (Scaled to Optimal DSR Objective in Table 4.6 No.5 Iteration)

We also consider spreading the injection point more evenly to reduce the capital cost. Eight of the closest injection profiles to profile J_{10} are explored, and Table 4.6 shows the optimal relative capital cost for each profile. The fifth iteration has the lowest capital cost and its optimal solution is set as the baseline. Hence, the relative capital cost of a DSR with injection profile $J_{10} = \{1, 2, 3, 5, 7, 9, 11, 13, 17, 23\}$ is 1. Moreover, when the final injection point is at zone 22, spreading the injection points along the first half of the reactor does not reduce the capital cost, although it decreases the capital cost when the final injection point is at zone 23. All of these injection profiles have similar values for the objective function, which demonstrates that the response surface is fairly flat. Furthermore, the capital cost with injection profile found after step 3 (iteration 0 in Table 4.6) is 1.001, which is slightly higher than the optimal capital cost (iteration 5 in Table 4.6). The approach proposed in Fig. 4.3 offers no guarantee of a global optimal solution, since not all permutations are explored. Nevertheless, based on the assumption that injection points have a monotonic effect on the objective function and the fact that all reactor configurations with ten injection points have similar capital cost, we conclude that the solution obtained by applying the steps described in Fig. 4.3 should be close to the global optimal point. The monotonic assumption

may apply to other reactor type, as long as the monomer injection point accounts for a major part in the objective function.

Table 4.6 Optimal Relative Capital Cost for Injection Profiles with 10 Monomer Feeds (Scaled Based on the 5^{th} Iteration)

No. Iteration	Monomer Injection Locations	Relative Capital Cost
0	1,2,3,4,5,7,9,12,15,22	1.001
1	1,2,3,5,7,9,12,15,18,22	1.005
2	1,2,3,5,7,9,13,15,17,22	1.007
3	1,3,5,7,9,11,13,15,17,22	1.025
4	1,2,3,4,5,7,9,12,15,23	1.002
5	1,2,3,5,7,9,13,15,17,23	1.000
6	1,2,3,5,7,9,11,13,15,23	1.012
7	1,2,3,7,9,11,13,15,17,23	1.016
8	1,2,3,5,7,9,13,17,19,23	1.010

The optimal feed and temperature profiles of single DSR with $J_{10} = \{1, 2, 3, 5, 7, 9, 11, 13, 17, 23\}$ are plotted in Fig. 4.7. In this figure, we see that monomer feeding rates increase along the 10 injection points. This trend can be explained by the limits on monomer feeds imposed by the adiabatic temperature constraint ($T_{ad} \leq T_{ad}^{*}$), as seen at the injection points in Fig. 4.7b. As polymer product is formed along the reactor, the composition change influences the determination of T_{ad}, which leads to higher feed rates along the length of the reactor, e.g., at normalized volumes of 0.4 and 0.5 in Fig. 4.7b.

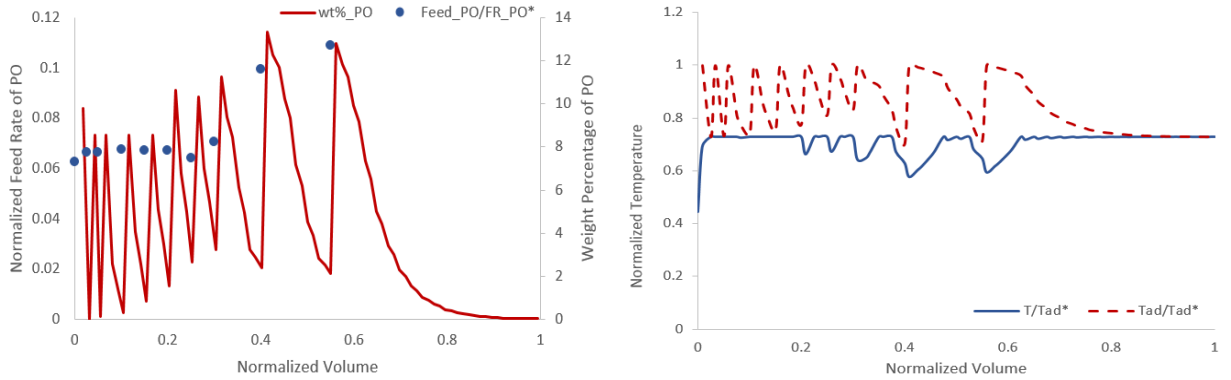

(a) Feed Profile

(b) Temperature Profile

Figure 4.7. Decision Profiles of the DSR Model

Table 4.7 shows the constraints that are active in this reactor network, and the corresponding impacts on the objective function (scaled to optimal objective in Table 4.6 iteration 5). The impact is obtained based on the value of the KKT multiplier at the optimal solution, which equals the rate of change in the maximal value of the objective function as the constraint is relaxed. A larger KKT multiplier indicates greater impact on the objective if the constraint is changed by one unit.

Table 4.7 Active Constraints in the Single DSR Model

Active Constraint	Impact on the Objective Function
Outlet weight percentage of KOH	2.642
Un-alkoxylated OH group	2.204
Production rate	0.210
Adiabatic temperature	0.001

The feeding rates of initiator and catalyst are $0.78FR^*_{Sorbitol}$ and $0.07FR^*_{KOH}$, respectively. Recall that, $FR^*_{Sorbitol}$ and FR^*_{KOH} represent the upper bounds for the feeding rates of sorbitol and KOH, respectively. For confidentiality, optimal results are scaled based on this optimal solution: a DSR with injection profile $J_{10} = \{1, 2, 3, 5, 7, 9, 13, 15, 17, 23\}$. Therefore, the relative PDI of the final

polymer obtained by a reactor network containing one DSR is 1. Its relative total heat removal is also scaled to 1. Normalized chain length distribution is plotted in Fig. 4.8 (scaled to $FR^*_{Sorbitol}$). Furthermore, the weight percentage of PO at the outlet stream is $0.017wt\%^*_{PO}$.

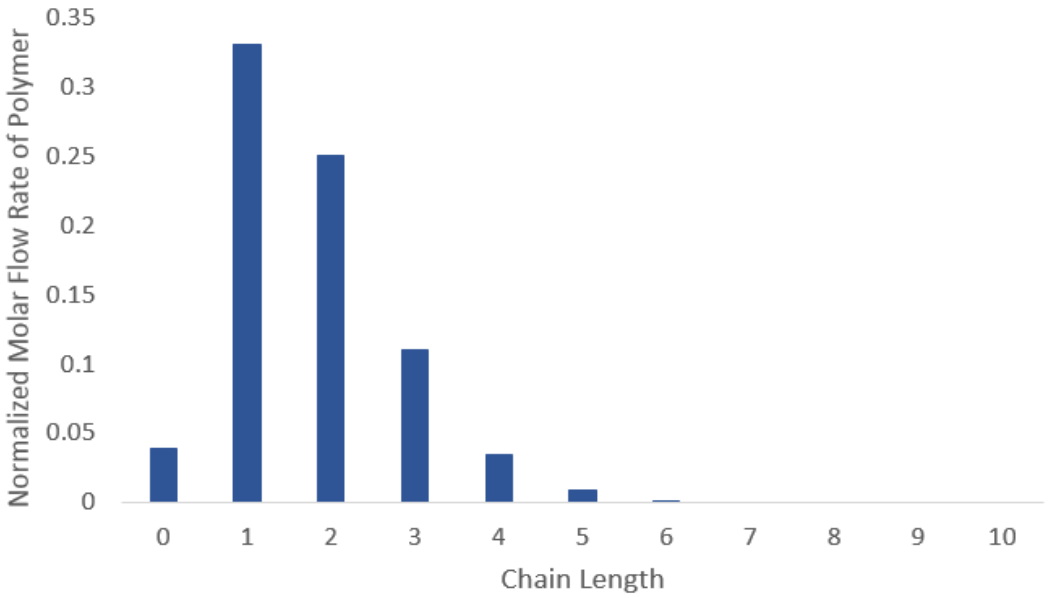

Figure 4.8. Chain Length Distribution for the DSR Model

4.5.2 One CSTR

If only one CSTR is utilized, polymer that satisfies the product specifications cannot be produced without violating the safety constraints. All the constraints cannot be satisfied at the same time and the model in Eqn. 4.23 with $N = 1$ has no feasible solution.

4.5.3 Two CSTRs in Sequence

The relative capital cost of two CSTRs in series is 2.64. In addition, the optimal decision profiles are sketched in Fig. 4.9. Majority of the monomers are fed to the first reactor where the weight fraction of monomer is high. Therefore, the adiabatic temperature is at its upper bound. Moreover, the residence time of the second reactor is greater than that of the first reactor. Hence, digestion is

the main function of the second CSTR to reduce the weight percentage of unreacted monomer in the outlet stream below its specified value.

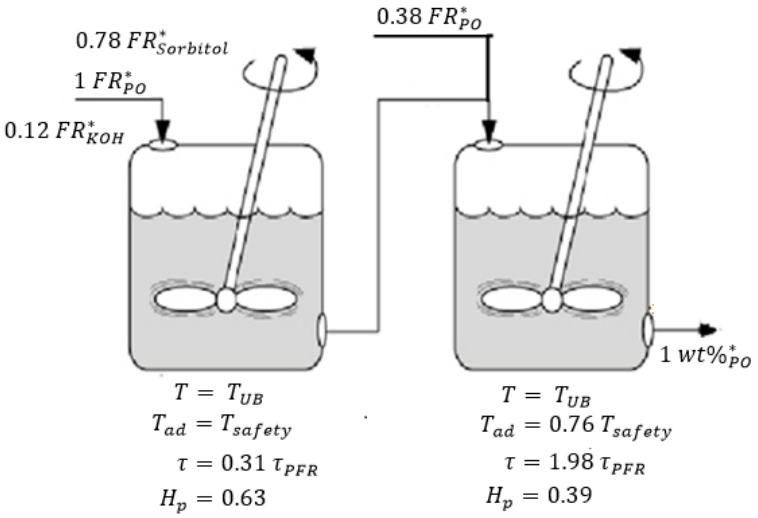

Figure 4.9. Optimal Results of the 2 CSTRs Model

Table 4.8 shows the constraints that are active in this reactor network, and their corresponding impacts on the objective function (scaled based on the optimal objective in Section 4.4.2).

Table 4.8 Active Constraints in the 2 CSTRs in Series Reactor Network

Active Constraint	Impact on the Objective Function
Un-alkoxylated OH group	15.963
Outlet weight percentage of KOH	6.832
Production rate	3.168
Outlet weight percentage of PO	0.563
Feeding rate of PO to the first CSTR	0.071
Adiabatic temperature of the first CSTR	0.002

Furthermore, the normalized chain length distribution is plotted in Fig. 4.10 (scaled to $FR^*_{Sorbitol}$). The relative PDI to the single DSR model and the relative average molecular weight of final product are 1.16 and 1.64, respectively.

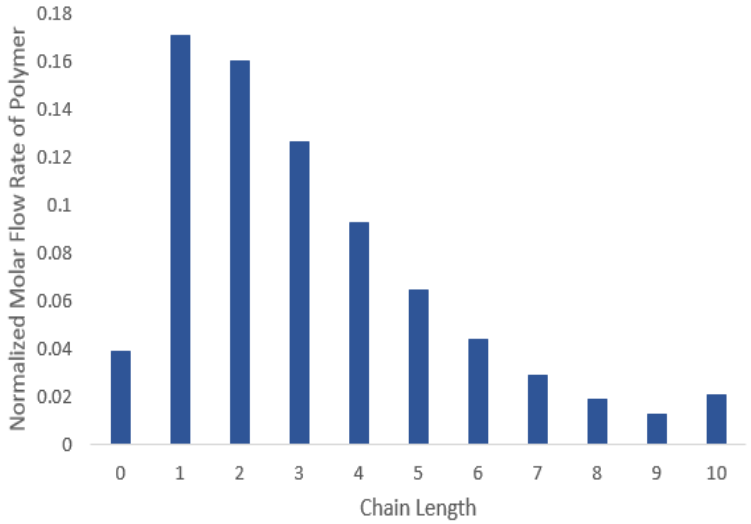

Figure 4.10. Chain Length Distribution for the 2 CSTRs Model

4.5.4 CSTR Followed by a DSR

As with the previous case, DSR is discretized using a fine mesh of 40 finite elements along with a two-point Radau collocation. Moreover, for this reactor network, two monomer injection points per DSR are enough to produce the desired rigid polyol. The injection profile is found by first solving the relaxed model. Then, starting with $i = 1$, fix the first i injection points with the highest monomer feeding rates to 1 and others to zero. This step is repeated until the problem becomes feasible. Since the CSTR followed by a DSR model becomes feasible when $i = 2$ (two injection points per DSR), there is no need to loosen the last constraint in model 4.24. Therefore, step 3 and 4 in Fig. 4.3 are skipped. In this reactor configuration, the majority of the reactions occur within the CSTR. And the DSR is used to further digest the unreacted monomer in the reactor. Therefore, it does not require feeding a lot of monomers to the DSR and two injection points are sufficient to

produce the desired polymers.

The capital cost of this reactor configuration is 1.2. The optimal decision profile of the CSTR is presented in Fig. 4.11. Based on this, both reactor and adiabatic temperatures are at upper bounds, to accelerate the reactions to their maximum rate. In addition, the optimal feed profile and temperature profile of the DSR after the CSTR are plotted in Fig. 4.12. Fresh PO feeds are added to zones 5 and 13. At these two points, the weight percentage of unreacted monomer increases. Although the feeding rate at zone 13 is higher, its weight percentage of unreacted PO is less compared to zone 5. Because the PO feeding rates at zones 5 and 13 do not differ a lot (one is 0.11*FR^*_{PO} and the other is 0.12*FR^*_{PO}). Also, the weight percentage of PO just before the injection is higher at zone 5. Furthermore, based on the temperature profile, the adiabatic temperature constraint is only active in zones 5 and 13. At the same position, reactor temperature is lowered to avoid runaway reaction. Besides the adiabatic temperature constraint, the outlet weight percentage of KOH, production rate, and the un-alkoxylated OH group constraints are also active. Their impacts on the objective function are shown in Table 4.9 (scaled to optimal objective in Section 4.4.2). Finally, the relative PDI of the final polymer is 1.13.

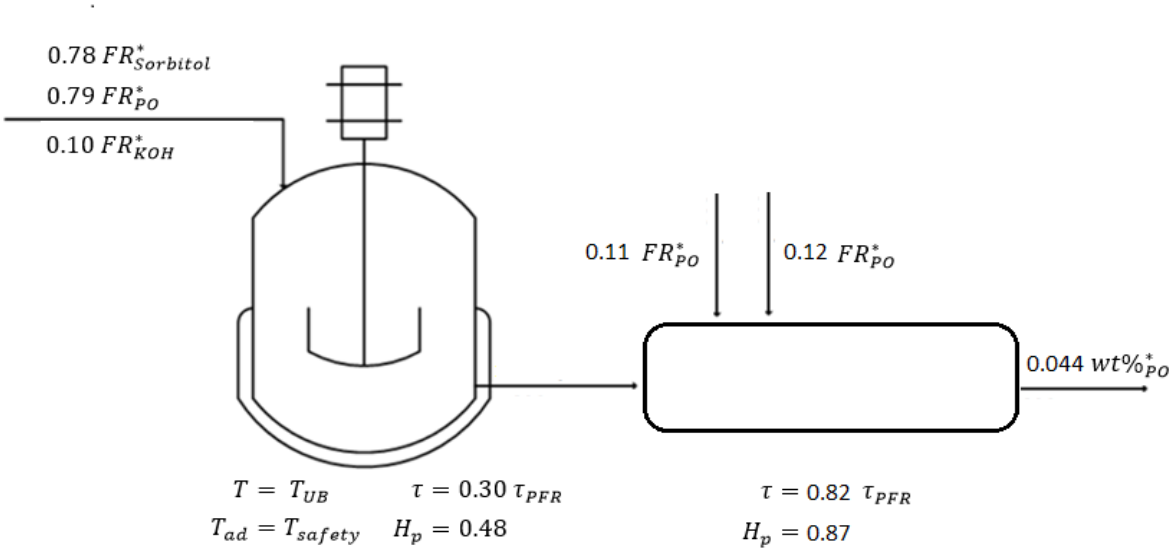

Figure 4.11. Optimal Results of the CSTR Followed by a DSR Model

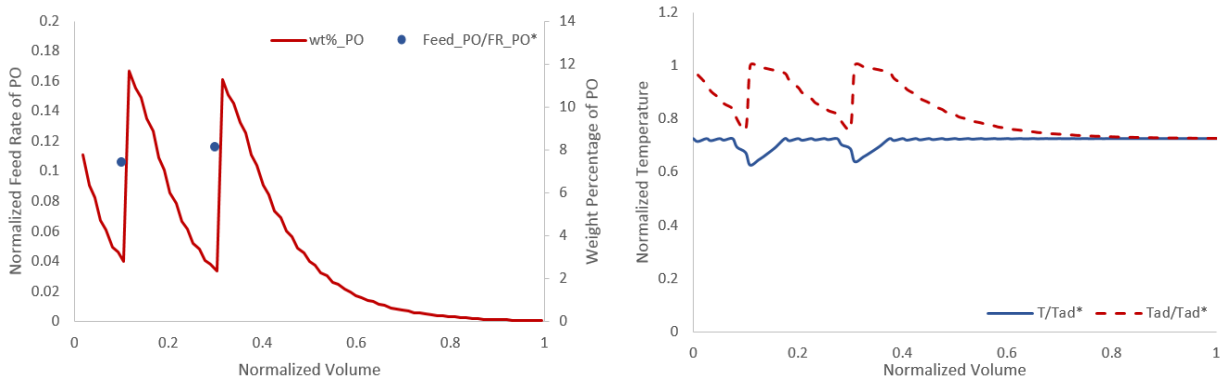

(a) Feed Profile

(b) Temperature Profile

Figure 4.12. Decision Profiles of the CSTR Followed by a DSR Model

Table 4.9 Active Constraints in the CSTR Followed by a DSR Reactor Network

Active Constraint	Impact on the Objective Function
Outlet weight percentage of KOH	2.992
Un-alkoxylated OH group	2.516
Production rate	0.058
Adiabatic temperature	0.002

Fig. 4.13 shows the normalized chain length distribution (scaled to $FR^*_{sorbitol}$). According to this, the majority of branches have one PO or two POs attached to them. Few branches have more than five POs.

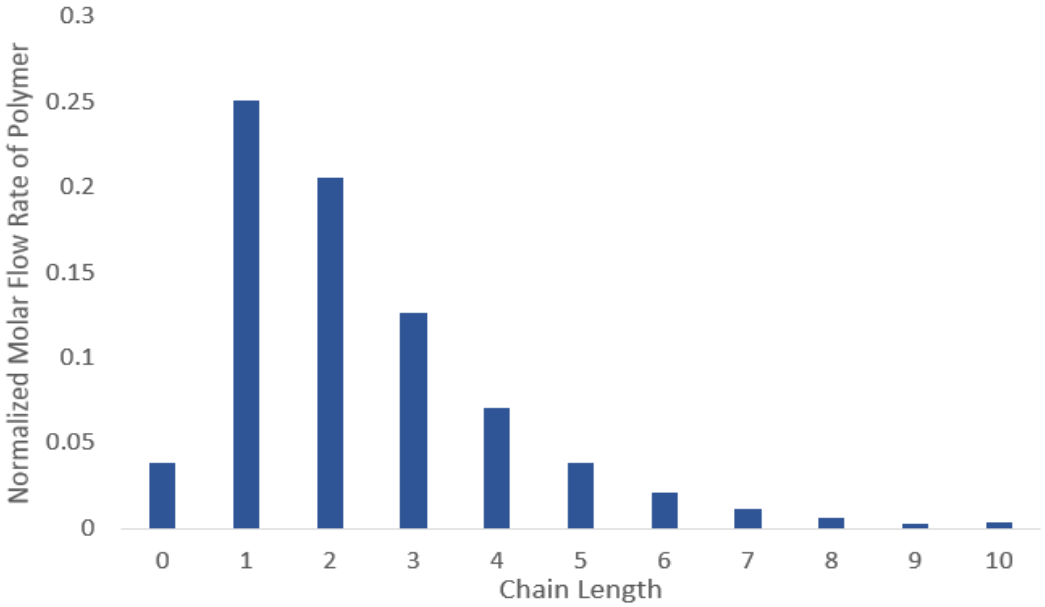

Figure 4.13. Chain Length Distribution for the CSTR Followed by a DSR Model

4.5.5 DSR Followed by a CSTR

In Section 4.4.2, DSR is discretized using a fine mesh of 40 finite elements along with a two-point Radau collocation. The same discretization scheme is adopted in the section. And steps in Fig. 4.3 are carried out to determine the optimal injection profile for the system. Moreover, this reactor network requires at least four monomer feeding points. Fig. 4.14 shows the relationship between the number of injection points and the CSTR residence time, which is normalized by dividing the residence time of single DSR. The relative capital cost is based on the optimal capital cost of the single DSR model. As the number of monomer injection points increases, the residence time of CSTR decreases to its lower bound, which is 0.1 min. This suggests that adding a CSTR at the end of DSR would not improve the capital cost. Hence, it is better to use a DSR alone. In summary, this reactor network is not suitable for this rigid polyol production. If few injection points (less than 6) are applied, the problem is either infeasible or has a high capital cost compared to other reactor designs. On the contrary, when more injection points are utilized, the CSTR becomes useless.

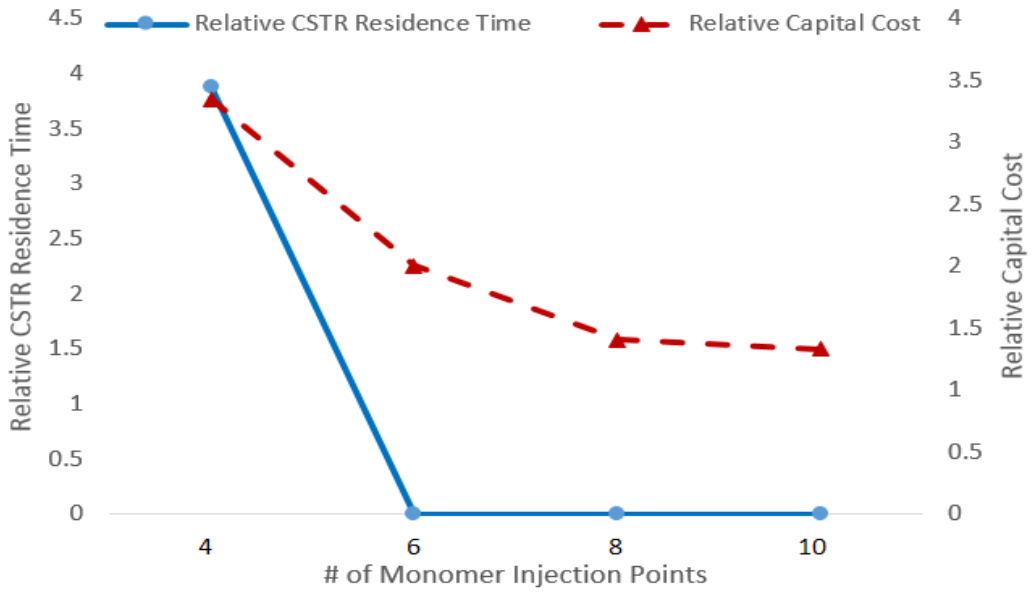

Figure 4.14. Number of Injection Point Versus CSTR Residence Time

The optimal solution of one DSR followed by a CSTR with four monomer injection points is shown in this section. The relative capital cost of this configuration is 3.380. The optimal feed profile and temperature profile of the DSR are plotted in Fig. 4.15. According to this, fresh PO are added to zones 1,3,5 and 7. Furthermore, based on the temperature profile, the adiabatic temperature constraint is active when monomers are added to the DSR. And this is why the temperature profile oscillates before the normalized volume reaches 0.2. Moreover, the temperature profile and the weight percentage of unreacted PO drop at volume = 0.4, which implies digestion begins at that point and most of reactions are carried out before this point. However, the reactor volume cannot be reduced, since it will violate the adiabatic temperature constraint.

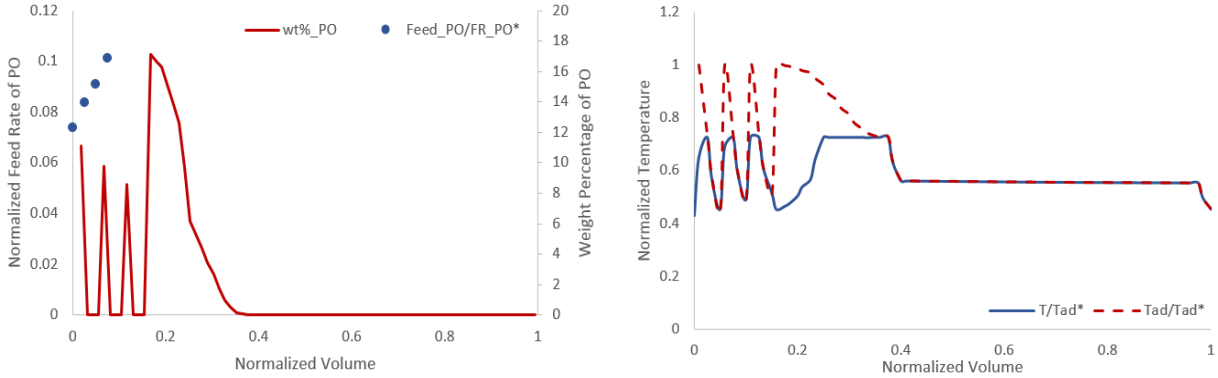

(a) Feed Profile

(b) Temperature Profile

Figure 4.15. Decision Profiles of the DSR Followed by a CSTR Model

The spikes in reactor and adiabatic temperature profiles occur when monomers are added to the reactor. And temperature profile becomes steady after all the monomer injections. Because weight percentage of unreacted monomer increases after monomer has been added to the reactor. Then, the reactor temperature is decreased to ensure the adiabatic temperature would not exceed its upper bound. After a while, monomer reacts to grow the polymer chain length. Hence, the weight percentage of unreacted monomer decreases and the reactor temperature increases to speed up the reactions. In addition, the optimal decision profile of the CSTR is sketched in Fig. 4.16. Based on this, the adiabatic temperature constraint is inactive. On the other hand, the feeding rate of monomer to the CSTR, outlet weight percentages of KOH and PO, production rate, and unalkoxylated OH group constraints are active. Their impacts on the objective are listed in Table 4.10 (scaled to optimal objective in Section 4.4.2).

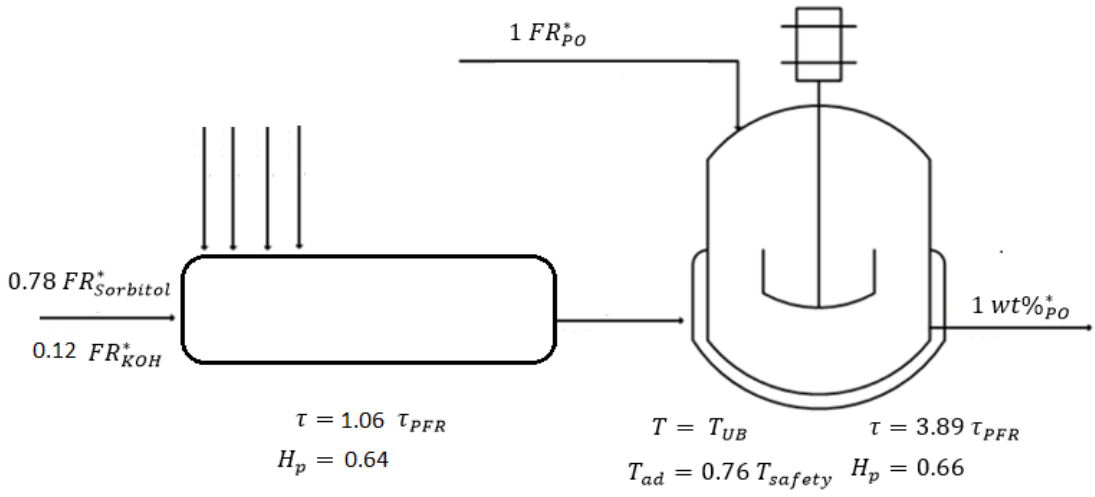

Figure 4.16. Optimal Results of the DSR Followed by a CSTR Model

Table 4.10 Active Constraints in the DSR Followed by a CSTR Reactor Network

Active Constraint	Impact on the Objective Function
Un-alkoxylated OH group	15.723
Outlet weight percentage of KOH	11.348
Outlet weight percentage of PO	1.052
Production rate	0.972
Feeding rate of monomer to the CSTR	0.018
Adiabatic temperature	0.006

Finally, the relative PDI of the final polymer is 1.20, and the normalized chain length distribution is displayed in Fig. 4.17 (scaled to $FR^*_{sorbitol}$). When comparing the chain length distributions among different reactor configurations (Fig. 4.8 4.10, 4.13, and 4.17), it is clear that using a CSTR at the end would result in more polymers with higher chain length. This is caused by the mixing

nature of CSTR, and the unreacted monomer constraint.

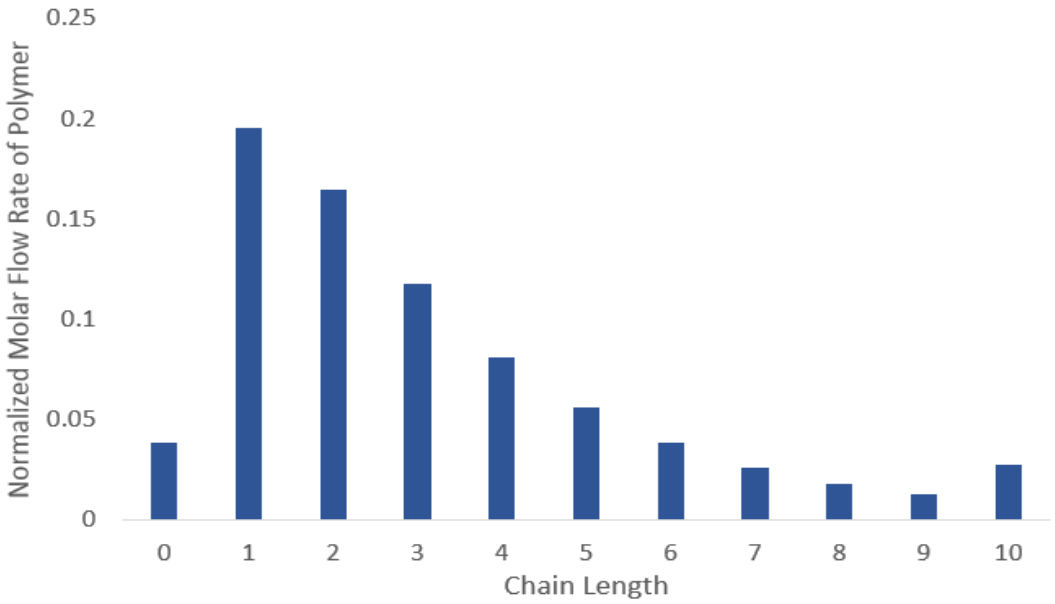

Figure 4.17. Molecular Weight Distribution for the DSR Followed by a CSTR Model

4.5.6 Results Summary

Table 4.11 summarizes the optimal results normalized to the optimal solution of single DSR for different reactor configurations, where UB represents the optimal result is at the upper bound. The reason why DSR outperforms other reactor networks is that it has the highest monomer conversion (lowest weight percentage of monomers in the outlet stream). The DSR has a digestion phase where the weight percentage of unreacted monomer in the mixture decreases after the last monomer injection, as shown in Fig. 4.7. On the other hand, a CSTR does not have a digestion phase, since its reactor concentration equals its outlet concentration. If the monomer concentration in the outlet stream is low, then its concentration in the reactor is also low. Therefore, the reaction rates decrease, since they are proportional to the monomer concentration in the reactor. In order to react more monomer in a CSTR, the monomer concentration needs to be increased. For this reason

adding a DSR after CSTR is more effective than adding a CSTR after a DSR; DSRs can help digest the unreacted monomers, but CSTRs cannot. Also, since capital cost includes the reactor and heat exchanger costs, as well as the costs for injection points and monomer separation unit, having less monomer in the outlet stream means reducing the cost of monomer separation unit.

Table 4.11 Optimal Results for Different Reactor Networks

	DSR	2 CSTRs	CSTR + DSR	DSR + CSTR
Relative Capital Cost	1.00	2.64	1.20	3.38
Relative Residence Time	1.00	2.29	0.82	4.95
Relative Total Feed of PO	1.00	1.87	1.36	1.82
Relative Feed of Sorbitol	1.00	1.00	1.00	1.00
Relative Feed of KOH	1.00	1.71	1.43	1.71
Relative PDI	1.00	1.16	1.13	1.20
Relative Total Heat Removal	1.00	1.03	0.87	1.30
Relative wt% of PO in the Outlet Stream	1.00	58.82 (UB)	2.59	58.82 (UB)

Finally, all reactor optimization models are MINLPs, but as these models are large (as shown in Table 4.12) and highly nonlinear, MINLP solvers are not capable of solving these problems. In particular, DSR models could not be handled because of the excessive number of binary variables. Instead, the binary variables are manually fixed to either 0 or 1 based on a detailed NLP-based algorithm where the optimization models are solved with IPOPTH in GAMS.

Table 4.12 Model Size for Different Reactor Networks

	# of Variables	# of Equality Constraints	# of Inequality Constraint
2 CSTRs	505	497	11
DSR	16657	16534	205
CSTR + DSR	16909	16783	209
DSR + CSTR	16909	16783	209

4.6 Conclusions

The focus of this study is to determine a continuous reactor network along with its operating conditions that minimize the capital cost for rigid polyol production. Based on Feinberg's studies [7], [8] we narrowed the reactor types to CSTRs and DSRs. The main strategy is to start with the most basic reactor network (contains one CSTR or DSR), and then enlarge the reactor network by adding more CSTRs/DSRs until there is no improvement in the objective function. Hence, we first examined the reactor networks, with only one CSTR or DSR. For the single CSTR case, we find that it cannot produce the target rigid polymer without violating the safety constraints. For the reactor configuration with one DSR, at least five monomer injections points are required to produce polymer that satisfies the product specifications. A DSR with ten monomer injection points has the lowest capital cost. Then, one more reactor (CSTR/DSR) is added after the CSTR/DSR to determine if an extra reactor would provide a better option. Adding another CSTR/DSR after the CSTR enables the rigid polyol production to satisfy the safety and product constraints. However, it fails to improve the objective function, since its capital cost is higher than the one of single DSR. We also examined the reactor configuration with a single DSR followed by a CSTR, to analyze if an extra CSTR would reduce the objective function. The results show that adding a CSTR can not decrease the capital cost and improve performance simultaneously. Because the reactor

networks with two reactors do not outperform the one with one reactor, we conclude that one DSR with 10 injection points is the appropriate reactor network design for this particular rigid polyol production.

The optimal reactor network is sensitive to the cost parameters, as well as the target product. Moreover, it is clearly inefficient if the continuous reactor network can only produce one product. In order to remain competitive, companies are required to operate their systems at nearby optimal conditions for multiple products. Therefore, we consider the reactor network design for multiple rigid polyols in the next chapter.

Chapter 5 Continuous Reactor Network Design for Multiple Rigid Polyol Productions

This study focuses on developing continuous reactor network models to produce multiple rigid polyol products under strict product and safety specifications. We first determine reactor networks and operating decisions for minimum capital cost, and then find reactor networks with optimal profit through multi-criteria optimization, using a Pareto chart to analyze the relationship between capital cost and net sales. Based on our previous study [85], we narrow down the types of continuous reactors to two: plug flow reactor (PFR) with multiple feed injection points and a network of continuous stirred tank reactors (CSTR). The CSTR model can be written as a mixed integer nonlinear programming (MINLP) problem. The DSR model is a differential algebraic equation (DAE) optimization problem. The simultaneous collocation method is applied to transform the resulting DAE model into a MINLP, which is solved as a NLP by fixing the binary terms. Both capital cost and multi-criteria problems are formulated as multi-scenario optimization problems to determine the best single network design for producing multiple polymer products.

5.1 Literature Review

Recent related studies for continuous multi-product polymerization plants include [79, 39, 40]. Shi et al. [39] developed an optimization strategy for polymer grade transitions for a multi-product continuous loop reactor. In this work, a rigorous mathematical model was developed for the entire reactor-based process. Optimal transition recipes were generated through dynamic optimization to guide the transition between polymer A and polymer B. These recipes efficiently shorten the transition time and significantly reduce the off-transition products. A similar approach was proposed by Wang et al. [40], where a multi-stage dynamic optimization was implemented on a gas-phase fluidized bed polymerization process. In addition to off-line optimization, they extended this approach to shrinking horizon nonlinear model predictive control, along with an expanding horizon weighted least-squares estimator for process states and unknown parameters.

Moreover, there have been a number of general optimization studies for multi-product continuous processes. These include the integration of optimal design and control for reactor systems [80], simultaneous control and scheduling for a multi-product CSTR [81, 82] as well as scheduling and operation optimization for generic multi-plant models. A comprehensive review of this work was summarized by L. D. R. Beal group [83].

In addition, optimization methods have been extended to integrate the design, control and scheduling for polyol processes [84], since it provides more reliable optimal solutions. However, for large-scale problems, the simultaneous method requires a high computational cost, since the numbers of variables and equations involved are quite large. Some problems also include binary variables. Moreover, the problem formulation can become more complex when uncertainty in kinetic parameters comes into play.

Multi-product polymer processes lead to further design advantages, as well as convenience and versatility. On the other hand, obtaining an optimal design solution can be challenging, since these problems/models are large and non-convex, and involve binary variables. For optimal design and operation of multi-product processes, a simultaneous optimization strategy is the most straight-

forward, where optimal decision profiles are generated simultaneously for all the products. Once designed, the optimal process meets the performance and capacity requirements for all products, which are produced in single product campaigns separated by grade transitions. This optimization study focuses on the recipe design of this process. In this work, the simultaneous approach is adopted to generate optimal multi-product reactor networks. Since, the reaction kinetics for each polymer product may be quite different, it is a challenge to satisfy feasibility requirements for each product scenario. Therefore, an approach combines the ideas that CSTR and DSR play important roles in shaping the AR boundary [7],[8] and solving reactor modules in an increasing manner [9] are adopted in this work. As shown in Chapter 4, DSRs offered long digestion times, which implied putting the DSR at the end of the reactor network. In addition, single DSR is often sufficient to produce rigid polyol. On the other hand, existing semi-batch reactors can be converted to CSTRs, which are easier to control than DSR. To meet these requirements, three reactor networks are derived and considered here. As shown in Fig. 5.1, these are single DSR, CSTRs in series, and a CSTR followed by a DSR.

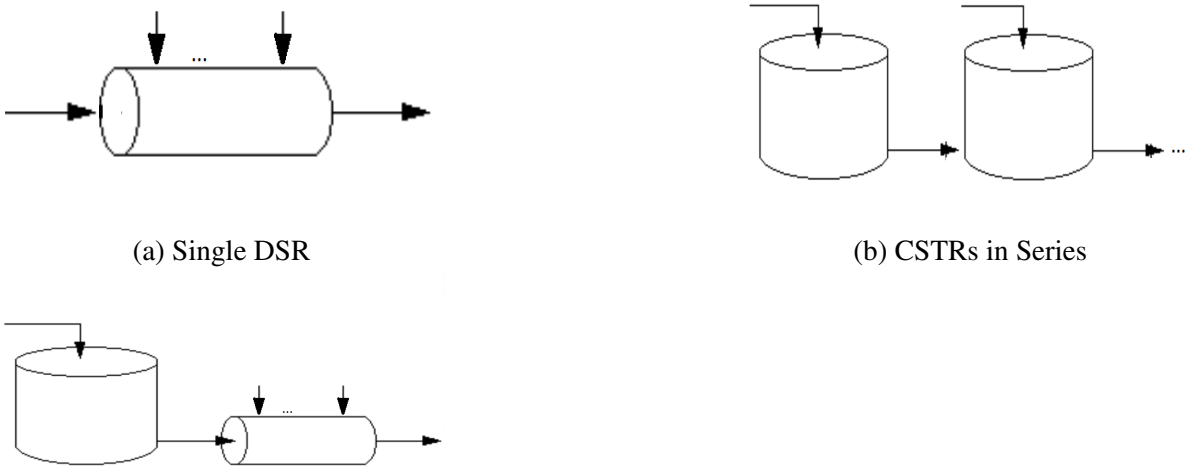

(a) Single DSR

(b) CSTRs in Series

(c) Single CSTR Followed by a DSR

Figure 5.1. Examined Reactor Networks

This chapter is organized as follows. Section 5.2 introduces the complex reaction scheme for rigid

polyol productions, corresponding kinetic parameters and the reactor network models. In Section 5.3, the solution strategy utilized for solving the reactor network optimization models is presented, as well as constraint specifications. Section 5.4 presents and compares the numerical results for each reactor network. Section 5.5 summarizes the study and concludes the chapter.

5.2 Reactor Models for Rigid Polyol Production

5.2.1 Reaction Scheme

We follow the reaction kinetics reported in Nie's work [76], except that hydrolysis reactions are excluded, because water in the aqueous initiator solution is removed before adding to the reactor. Each polymer product is formed by different initiators and monomers, as described in Table 5.1. The catalyst is KOH for all the products. In addition, the detailed reaction scheme is displayed in Table 5.2. The following notation is used in the remainder of the study. MO denotes monomer oxide. P_l represents one of the branches from the initiator without the active site $CH(MO)_l$. Both l and s indicate the number of repeating units. G_0 is a branch of the initiator. Meanwhile, U_l denotes the unsaturated chains with double-bond end groups $CH_2 = CHCH_2(MO)_l$, formed by the chain transfer step and subsequent growth step. Moreover, depending on the different functional end groups, we define the following components, where $L \leq 10$. Based on the average molecular weight of rigid polymers, the expected average chain length is less than 5. Therefore, we assume the maximum chain length is less than 10.

G_l growing product chains of length l $(P_lO^-K^+)$, $l = 1, ...L$

D_l dormant product chains of length l (P_lOH), $l = 1, ...L$

Q_l growing unsaturated chains of length l $(U_lO^-K^+)$, $l = 1, ...L$

R_l dormant unsaturated chains of length l (U_lOH), $l = 1, ...L$

Table 5.1 Reactants of Each Rigid Polymer

Polymer	Initiator	Monomer
Polymer A	Sorbitol	Propylene oxide (PO)
Polymer B	Glycerin	Ethylene oxide (EO)
Polymer C	Glycerin	Propylene oxide (PO)

Table 5.2 Reaction Scheme for Rigid Polyol

Initiation
$G_0 + MO \xrightarrow{k_i} G_1$
Propagation
$G_l + MO \xrightarrow{k_p} G_{l+1}\ (l \geq 1)$
$Q_l + MO \xrightarrow{k_p} Q_{l+1}\ (l \geq 1)$
Transfer
$G_l + MO \xrightarrow{k_t} D_l + Q_0\ l \geq 0)$
$Q_l + MO \xrightarrow{k_t} R_l + Q_0\ (l \geq 0)$
Exchange
$G_l + D_s \xrightarrow{k_e} D_l + G_s\ (l, s \geq 0)$
$Q_l + R_s \xrightarrow{k_e} R_l + Q_s\ (l, s \geq 0)$
$G_l + R_s \xrightleftharpoons{k_e} D_l + Q_s\ (l, s \geq 0)$

Since the maximum chain length L is small, we can include all of the population balances for each species up to L into the model. To illustrate the population balance of polymer chains, we first present a CSTR model in Eqn. 5.1, where the subscripts $ini, prop, trf$ and exc represent the initiation, propagation, transfer and exchange reactions, respectively. Here, V is the volume, F_c^0 and F_c represent the total inlet and outlet molar flow rate of component c. C_c stands for concentration of component c in set COMP, which includes initiator, monomer, catalyst and growing/dormant product/unsaturation chains.

$$\frac{F^0_{G_0} - F_{G_0}}{V} = -\,k_{ini}\,C_{G_0}\,C_{MO} -\; k_{trf}\,C_{G_0}\,C_{MO} - \;k_{exc}\,C_{G_0}\,\sum_{s=0}^{S}(C_{D_s}+C_{R_s}) +\; k_{exc}\,C_{D_0}\,\sum_{s=0}^{S}(C_{G_s}+C_{Q_s})$$

$$\frac{F^0_{G_1} - F_{G_1}}{V} = \;k_{ini}\,C_{G_0}\,C_{MO} -\; (k_{prop}+k_{trf})\,C_{G_1}\,C_{MO} - \;k_{exc}\,C_{G_1}\,\sum_{s=0}^{S}(C_{D_s}+C_{R_s}) +\; k_{exc}\,C_{D_1}\,\sum_{s=0}^{S}(C_{G_s}+C_{Q_s})$$

$$\frac{F^0_{G_l} - F_{G_l}}{V} = \;k_{prop}\,(C_{G_{l-1}} - C_{G_l})\,C_{MO} -\; k_{trf}\,C_{G_l}\,C_{MO} - \;k_{exc}\,C_{G_l}\,\sum_{s=0}^{S}(C_{D_s}+C_{R_s}) +\; k_{exc}\,C_{D_l}\,\sum_{s=0}^{S}(C_{G_s}+C_{Q_s})$$

$$for\;\; G_l = G_2, ..., G_{L-1}$$

$$\frac{F^0_{G_L} - F_{G_L}}{V} = \;k_{prop}\,C_{G_{L-1}}\,C_{MO} -\; k_{trf}\,C_{G_L}\,C_{MO} - \;k_{exc}\,C_{G_l}\,\sum_{s=0}^{S}(C_{D_s}+C_{R_s}) +\; k_{exc}\,C_{D_l}\,\sum_{s=0}^{S}(C_{G_s}+C_{Q_s})$$

$$\frac{F^0_{D_l} - F_{D_l}}{V} = \;k_{trf}\,C_{G_l}\,C_{MO} + \;k_{exc}\,C_{G_l}\,\sum_{s=0}^{S}(C_{D_s}+C_{R_s}) -\; k_{exc}\,C_{D_l}\,\sum_{s=0}^{S}(C_{G_s}+C_{Q_s})$$

$$for\;\; D_l = D_0, ..., D_L$$

$$\frac{F^0_{Q_0} - F_{Q_0}}{V} = -\,(k_{ini}+k_{trf})\,C_{Q_0}\,C_{MO} +\; k_{trf}\,\sum_{s=0}^{S}(C_{G_s}+C_{Q_s})\,C_{MO} - \;k_{exc}\,C_{Q_0}\,\sum_{s=0}^{S}(C_{D_s}+C_{R_s}) +\; k_{exc}\,C_{R_0}\,\sum_{s=0}^{S}(C_{G_s}+C_{Q_s})$$

$$\frac{F^0_{Q_1} - F_{Q_1}}{V} = \;(k_{ini}\,C_{Q_0} - k_{prop}\,C_{Q_1})\,C_{MO} -\; k_{trf}\,C_{Q_1}\,C_{MO} - \;k_{exc}\,C_{Q_1}\,\sum_{s=0}^{S}(C_{D_s}+C_{R_s}) +\; k_{exc}\,C_{R_1}\,\sum_{s=0}^{S}(C_{G_s}+C_{Q_s})$$

$$
\begin{aligned}
\frac{F^0_{Q_l} - F_{Q_l}}{V} &= k_{prop}\,(C_{Q_{l-1}} - C_{Q_l})\,C_{MO} - k_{trf}\,C_{Q_l}\,C_{MO} \\
&\quad - k_{exc}\,C_{Q_l}\sum_{s=0}^{S}(C_{D_s} + C_{R_s}) + k_{exc}\,C_{R_l}\sum_{s=0}^{S}(C_{G_s} + C_{Q_s}) \\
&\quad for\;\; Q_l = Q_2, ..., Q_{L-1} \\
\frac{F^0_{Q_L} - F_{Q_L}}{V} &= k_{prop}\,C_{Q_{L-1}}\,C_{MO} - k_{trf}\,C_{Q_L}\,C_{MO} \\
&\quad - k_{exc}\,C_{Q_l}\sum_{s=0}^{S}(C_{D_s} + C_{R_s}) + k_{exc}\,C_{R_l}\sum_{s=0}^{S}(C_{G_s} + C_{Q_s}) \\
\frac{F^0_{R_l} - F_{R_l}}{V} &= k_{trf}\,C_{Q_l}\,C_{MO} \\
&\quad + k_{exc}\,C_{Q_l}\sum_{s=0}^{S}(C_{D_s} + C_{R_s}) - k_{exc}\,C_{R_l}\sum_{s=0}^{S}(C_{G_s} + C_{Q_s}) \\
&\quad for\;\; R_l = R_0, ..., R_L
\end{aligned}
\tag{5.1}
$$

Since the rates of the exchange reactions are significantly higher than other reaction rates. The exchange reactions are modeled using the quasi-steady state assumption and two pseudo-species X and Y are introduced [76] to solve this problem, where $X_l = G_l + D_l$ and $Y_l = Q_l + R_l$. The resulting population balances for the CSTR and PFR models are presented in Eqns. 5.2 and 5.3, respectively.

$$
\begin{aligned}
F^0_{X_0} - F_{X_0} &= -k_{ini}\,C_{G_0}\,C_{MO} \\
F^0_{X_1} - F_{X_1} &= (k_{ini}\,C_{G_0} - k_{prop}\,C_{G_1})\,C_{MO} \\
F^0_{X_l} - F_{X_l} &= (k_{prop}\,C_{G_{l-1}} - k_{prop}\,C_{G_l})\,C_{MO}, \quad l = 2, ..., L-1 \\
F^0_{X_L} - F_{X_L} &= k_{prop}\,C_{G_{L-1}}\,C_{MO} \\
F^0_{Y_0} - F_{Y_0} &= -k_{ini}\,C_{Q_0}\,C_{MO} + k_{trf}\sum_{l=0}^{L}(C_{G_l} + C_{Q_l})\,C_{MO} \\
F^0_{Y_1} - F_{Y_1} &= (k_{ini}\,C_{Q_0} - k_{prop]}\,C_{Q_1})\,C_{MO} \\
F^0_{Y_l} - F_{Y_l} &= (k_{prop}\,C_{Q_{l-1}} - k_{prop}\,C_{Q_l})\,C_{MO}, \quad l = 2, ..., L-1 \\
F^0_{Y_L} - F_{Y_L} &= k_{prop}\,C_{Q_{L-1}}\,C_{MO}
\end{aligned}
\tag{5.2}
$$

$$
\begin{aligned}
\frac{dF_{X_0}}{dV} &= -k_{ini}\, C_{G_0}\, C_{MO} \\
\frac{dF_{X_1}}{dV} &= (k_{ini}\, C_{G_0} - k_{prop}\, C_{G_1})\, C_{MO} \\
\frac{dF_{X_l}}{dV} &= (k_{prop}\, C_{G_{l-1}} - k_{prop}\, C_{G_l})\, C_{MO}, \quad l = 2, ..., L-1 \\
\frac{dF_{X_L}}{dV} &= k_{prop}\, C_{G_{L-1}}\, C_{MO} \\
\frac{dF_{Y_0}}{dV} &= -k_{ini}\, C_{Q_0}\, C_{MO} + k_{trf} \sum_{l=0}^{L} (C_{G_l} + C_{Q_l})\, C_{MO} \\
\frac{dF_{Y_1}}{dV} &= (k_{ini}\, C_{Q_0} - k_{prop}\, C_{Q_1})\, C_{MO} \\
\frac{dF_{Y_l}}{dV} &= (k_{prop}\, C_{Q_{l-1}} - k_{prop}\, C_{Q_l})\, C_{MO}, \quad l = 2, ..., L-1 \\
\frac{dF_{Y_L}}{dV} &= k_{prop}\, C_{Q_{L-1}}\, C_{MO}
\end{aligned}
\tag{5.3}
$$

Model Parameters

As a proof of concept, the kinetic parameters stated in Nie et al. [76] are applied to this study, and are listed in Tables 5.3 and 5.4 below. They apply to long polymer chains and are suitable for this study, even though they are not necessarily the same as those for the short chains. Moreover, initiation and propagation steps have different kinetics, which implies that polymer chains with monomers attached behave differently than the initiator. Generally, monomer EO reacts faster than monomer PO, due to larger rate constants.

Table 5.3 Kinetic Parameters of PO

Reaction Type	Initiation	Propagation	Transfer
Arrhenius Constant $(m^3/mol/s)$	396,400	13,504.2	1,509,000
Activation Energy (kJ/kmol)	77,822	69,172	105,018
Heat of Reaction (kJ/kmol)	92,048	92,048	0

Table 5.4 Kinetic Parameters of EO

Reaction Type	Initiation	Propagation	Transfer
Arrhenius Constant $(m^3/mol/s)$	322,030,000	24,104	1,509,000
Activation Energy (kJ/kmol)	90,854	66,107	105,018
Heat of Reaction (kJ/kmol)	112,968	112,968	0

5.2.2 Reactor Network Model

The reactor network model consists of three main parts as our previous work [85]: material balance, energy balance, product specifications and safety constraints, which are explored in the following subsections. In addition, n denotes either the index of each CSTR or the index of each DSR zone. Indices c and m refer to the components and monomer, respectively, that are involved in the process, p indicates the process model that produces polymer products A, B and C, rxn is the reaction index, $FR_{m,n}$ is the feed rate of monomer to n^{th} CSTR/DSR zone.

Material Balance

First, rate constants can be calculated using the Arrhenius Eqn. 5.4, where k, A, Ea, R and T represent the rate constant, Arrhenius constant, activation energy, gas constant and reactor temperature, respectively.

$$k_{rxn,n,p} = A_{rxn} e^{-\frac{Ea_{rxn}}{RT_{n,p}}}, \quad rxn \in \{ini, prop, trf\}, \quad n \in \{1..N\}, \quad p \in \{A, B, C\} \tag{5.4}$$

Second, reaction rate for different reactions can be expressed using Eqn. 5.5, where r is the reaction rate, and C_c represents the concentration of components. All the reactions are second order. The subscripts c_1 and c_2 in Eqn. 5.5 represent the first and second components involved in reaction

rxn, respectively.

$$r_{rxn,n,p} = k_{rxn,n,p}\, C_{c_1,n,p}\, C_{c_2,n,p}, \quad rxn \in \{ini, prop, trf\}, \quad n \in \{1..N\}, \quad p \in \{A, B, C\} \tag{5.5}$$

Third, Eqns. 5.6a and 5.6b enforce the continuity between CSTRs/DSR zones. F^0 and F denote the inlet and outlet molar flow rates, respectively. Since fresh monomer can be added at the beginning of each CSTR/DSR zone, the inlet molar flow rate equals the summation of outlet molar flow rate from the previous CSTR/DSR zone and the feeding rate of fresh monomer. For other components, the inlet molar flow rate equals the outlet molar flow rate of the previous CSTR/DSR zone.

$$F^0_{m,n,p} = F_{m,n-1,p} + FR_{m,n,p}, \quad n \in \{1..N\}, \quad p \in \{A, B, C\} \tag{5.6a}$$

$$F^0_{c,n,p} = F_{c,n-1,p}, \quad c \neq m, \quad n \in \{1..N\}, \quad p \in \{A, B, C\} \tag{5.6b}$$

Reactor volumetric flow rate and concentration can be calculated using the Eqns. 5.7a and 5.7b for each zone n, respectively. $\dot{V}$ is the volumetric flow rate and MW denotes the molecular weight of reactant.

$$\dot{V}_{n,p} = \sum_c \frac{F^0_{c,n,p}\, MW_c}{\rho_{c,n,p}}, \quad n \in \{1..N\}, \quad p \in \{A, B, C\} \tag{5.7a}$$

$$C_{c,n,p}\, \dot{V}_{n,p} = F_{c,n,p}, \quad c \in COMP, \quad n \in \{1..N\}, \quad p \in \{A, B, C\} \tag{5.7b}$$

Finally, CSTRs and DSRs follow different design equations. For the CSTR, the design equation is an algebraic equation (Eqn. 5.8).

$$F_{c,n,p} - F^0_{c,n,p} = -r_{c,n,p}\, V_n, \quad c \in COMP, \quad n \in \{1..N\}, \quad p \in \{A, B, C\} \tag{5.8}$$

while the design equation for DSR is in differential form (Eqn. 5.9).

$$\frac{dF_{c,n,p}}{dV_n} = -r_{c,n,p}, \quad c \in COMP, \quad n \in \{1..N\}, \quad p \in \{A, B, C\} \tag{5.9}$$

Energy Balance

To develop the energy balance, we introduce monomer cooling. Fresh monomer feed has a cooling effect, since its temperature is at least 100 °C lower than the reactor temperature. Monomer cooling is represented by H^m_{cool} in Eqn. 5.10. In addition, C^m_p is the heat capacity of monomer and T^m_f denotes the feed temperature of monomer.

$$H^{m,n,p}_{cool} = \int_{T^m_f}^{T_{n,p}} C^m_p \, dT, \quad n \in \{1..N\}, \quad p \in \{A, B, C\} \tag{5.10}$$

Second, total mass flow rate $\dot{M}$ can be obtained from Eqn. 5.11. It is required in the energy balance calculation.

$$\dot{M}_{n,p} = \sum_{c \in COMP} F^0_{c,n,p} \, MW_c, \quad n \in \{1..N\}, \quad p \in \{A, B, C\} \tag{5.11}$$

Moreover, we need to ensure that energy is conserved across CSTRs/DSR zones (Eqn. 5.12a, 5.12b). Here $\dot{M}^m$ is the mass flow rate of monomer and superscript b represents the solution mixture inside of the reactor.

$$(\dot{M}_{n,p} - \dot{M}^m_{n,p}) \int_{T^0_{n,p}}^{T^b_f} C^b_p dT = H^{m,n,p}_c \, FR^{m,n,p} \, MW^m, \quad n = 1, \quad m \in MON, \quad p \in \{A, B, C\} \tag{5.12a}$$

$$\dot{M}_{n,p} \int_{T^0_{n,p}}^{T_{n-1,p}} C^b_p dT = H^{m,n,p}_c \, FR^{m,n,p} \, MW^m, \quad n \in \{1..N\}, \quad p \in \{A, B, C\} \tag{5.12b}$$

The final element in energy balance is the amount of heat released during the reaction, H_r. For CSTR, this can be obtained using Eqn. 5.13, where H_{rxn} represents the heat of reaction, which is

different for each monomer.

$$H_r^{n,p} = (F_{m,n,p}^0 - F_{m,n,p})\, H_{rxn}^{m,p}, \quad n \in \{1..N\}, \quad p \in \{A, B, C\} \tag{5.13}$$

For DSR, heat released $\bar{H}_r$ can be calculated based on the rates of reactions, as shown in Eqn. 5.14:

$$\bar{H}_r^{n,p} = -r_{m,n,p}\, H_{rxn}^{m,p}, \quad n \in \{1..N\}, \quad p \in \{A, B, C\} \tag{5.14}$$

Finally, the energy balances for CSTR and DSR are different, with the former one in algebraic form (Eqn. 5.15a), and the latter one in differential form (Eqn. 5.15b). Moreover, HX represents the extra cooling that needs to be provided.

$$\dot{M}_{n,p}\, C_p^b\, T_{n,p}^0 + H_r^{n,p} - HX^{n,p} = \dot{M}_{n,p}\, C_p^b\, T_{n,p}, \quad n \in \{1..N\}, \quad p \in \{A, B, C\} \tag{5.15a}$$

$$\dot{M}_{n,p}\, C_p^b\, \frac{dT_{n,p}}{dV_n} = \bar{H}_r^{n,p} - HX^{n,p}, \quad n \in \{1..N\}, \quad p \in \{A, B, C\} \tag{5.15b}$$

Product Quality & Safety Constraints

This model includes six product specifications and two safety constraints. First, there is a minimum target production rate (Eqn. 5.16) for each of the polymer, where subscript N refers to the final reactor in the network.

$$\sum_{c \in COMP} F_{p,c,N} \geq PR_p^*, \quad p \in \{A, B, C\} \tag{5.16}$$

Second, a lower and upper bound for the OH number can be obtained through Eqn. 5.17:

$$OH\ Number_p = \frac{56.1 * 1000}{EW_p}, \quad p \in \{A, B, C\} \tag{5.17a}$$

$$EW_p = \frac{\overline{MW}_p}{Functionality_p} \tag{5.17b}$$

$$Functionality_p = \frac{total\ moles\ OH\ of\ polymer\ p}{total\ moles\ polyol\ of\ polymer\ p}, \quad p \in \{A, B, C\} \tag{5.17c}$$

$$\overline{MW}_p = \frac{\sum_c F_{c,N,p}\, MW_c}{\sum_c F_{c,N,p}}, \quad p \in \{A, B, C\} \tag{5.17d}$$

$$OH\ Number_{LB,p} \leq OH\ Number_p \leq OH\ Number_{UB,p}, \quad p \in \{A, B, C\} \tag{5.17e}$$

Third, an upper bound for polydispersity index (PDI) is given by Eqn. 5.18, where Mw and Mn stand for weight and number average molecular weight, respectively.

$$PDI_p = \frac{Mw_p}{Mn_p} = \frac{\sum_{c \in COMP} F_{p,c} * MW_{p,c}^2 * \sum_{c \in COMP} F_{p,c}}{(\sum_{c \in COMP} F_{p,c} * MW_{p,c})^2} \leq PDI_p^*, \quad p \in \{A, B, C\} \tag{5.18}$$

Fourth, there is a specification for the outlet weight percentage of catalyst.

$$FR_{cat,p} \geq \sum_l (G_{l,n,p} + Q_{l,n,p}) \quad l = 1...L, n, = 1...N, p \in \{A, B, C\} \tag{5.19a}$$

$$wp_{cat,p,N} = \frac{FR_{cat,p} * MW_{cat,p}}{\dot{M}_{N,p}} \leq wp_{cat,p}^*, \quad p \in \{A, B, C\} \tag{5.19b}$$

Finally, the monomer, initiator and catalyst amounts are limited (Eqn. 5.20a). In addition, monomer feeding rate should equal zero if reactor n has no monomer injection point (the corresponding binary variable $\beta_n = 0$).

$$FR_{c,p} \leq FR_{c,p}^*, \quad c \in \{ini, cat\}, \quad p \in \{A, B, C\} \tag{5.20a}$$

$$FR_{m,n,p} \leq \beta_n\, FR_{m,p}^*, \quad \beta_n \in \{0, 1\}, \quad n \in \{1..N\}, \quad p \in \{A, B, C\} \tag{5.20b}$$

The first safety constraint (Eqn. 5.21) is implemented to limit the adiabatic temperature rise to

($T_{safety} - T_{n,p}$) if the cooling system fails; in Eqn. 5.21 κ is a constant between one and ten. Note that this rise is directly related to weight percentage of unreacted monomers in the reactor. In a PFR or DSR, runaway will dramatically increase the reactor temperature and eventually overpressure the storage tank that the reactor empties into.

$$\kappa\, wp_{m,n,p} \leq T_{safety} - T_{n,p}, \quad n \in \{1..N\}, \quad p \in \{A, B, C\} \tag{5.21}$$

The second safety constraint provides the reactor temperature range, as shown in Eqn. (5.22).

$$T_{LB,p} \leq T_{n,p} \leq T_{UB,p}, \quad n \in \{1..N\}, \quad p \in \{A, B, C\} \tag{5.22}$$

5.3 Optimization Formulations and Solution Strategy

Our optimization approach derives reactor networks with minimum capital costs and maximum net sales. This multi-objective optimization problem is solved in two stages. In this section we first consider minimizing capital cost, followed by an $\epsilon-$constrained approach [86] that traces a Pareto curve with maximum net sales.

5.3.1 Stage 1 - Minimizing capital cost

The aim of stage 1 is to construct continuous reactor networks that are able to produce multiple rigid polyols with strict product and safety specifications. At the same time, optimal decision profiles that would lead to a minimum capital cost are determined. Decision variables include the feeding rates of initiator, monomers and catalyst, reactor temperature, reactor volume, injecting location of monomers, capacity of heat exchange and the separation unit. Feeding rates and reactor temperature can take different values in order to produce different polymer products. All other decision variables are common variables, which means they take the same values for different polymer products.

CSTR Optimization Model

The MINLP problem of the continuous stirred tank reactor (Eqns. 5.2, 5.4 - 5.8, 5.10 - 5.13, 5.15a, 5.16-5.22) are incorporated into Eqn. 5.23:

$$\begin{aligned} min \quad & CC = \sum_{n=1}^{N}(f_1(HX(n)) + f_2(V) + f_3(\beta_n)) + f_4(wp_{m,N}) + f_5 \\ s.t. \quad & g_p(y_p(n), u_p(n)) = 0, \quad p \in \{A, B, C\} \\ & h_p(y_p(n), u_p(n), \beta_n) \leq 0, \quad p \in \{A, B, C\} \\ & y_p(n)^L \leq y_p(n) \leq y_p(n)^U, \quad p \in \{A, B, C\} \\ & u_p(n)^L \leq u_p(n) \leq u_p(n)^U, \quad p \in \{A, B, C\} \\ & \beta_n \in \{0, 1\} \end{aligned} \tag{5.23}$$

where n is the index of CSTRs, N denotes the final CSTR and $p \in \{A, B, C\}$ stands for the product process model. The objective is to minimize the capital costs (CC), which includes the cost for the heat exchangers (f_1), reaction vessel (f_2), monomer injectors (f_3), oxide recovery system (f_4), which is used to separate the unreacted monomer from the polyol product, and agitator, pump, catalyst injection (taken as constants and denoted by f_5).

Notice that monomer injection is represented by binary variable β_n. If the feed of monomer m to CSTR n is greater than zero then $\beta_n = 1$, otherwise $\beta_n = 0$. This model can either be solved as a MINLP using SBB, or solved as an NLP using IPOPTH with binary variables fixed. Both methods lead to same optimal decision profiles. Moreover, y_p stands for algebraic state variables, and u_p denotes the decision variables for each polymer product; these are the reactor temperature, feeding rates of monomer, catalyst and initiator. $g_p(\cdot)$ denotes the equality process constraints, which result from the mass balcnce (Eqn. 5.2) as well as the energy balances, and $h_p(\cdot)$ represents the inequality constraints which result from the process constraints, such as adiabatic temperature, and product specification constraints. The last two constraints in Eqn. 5.23 represent the upper and lower bounds for algebraic and decision variables, respectively.

DSR Optimization Model

The DSR model (Eqns. 5.3, 5.4 - 5.7, 5.9 -5.12, 5.14, 5.15b -5.22) can be written in a general form as a dynamic optimization problem (Eqn. 5.24). The objective function of the DSR model is to minimize the capital cost. Here, f_1 calculates the cost for heat exchanger, f_2 estimates the reactor cost and the monomer injection cost is denoted by f_3, followed by the cost for monomer recovery system (f_4). Finally, f_5 represents the cost for agitator, pump and catalyst injection. Moreover, the subscript p refers to the product process model, z_p and y_p are differential and algebraic state variables, respectively, and u_p denotes the decision variables, which consist of the reactor temperature, feeding rates of monomer, catalyst and initiator. Other than these individual decision variables, there are four common ones: capacity of the heat exchangers HX, reactor volume V, monomer injection points β_n, and monomer recovery system's capacity wp_{m,V_f}. Also, the derivatives in differential equations are denoted by $\dot{z}_p$, which result from the material balance (Eqn. 5.3) as well as the energy balance, and g_p denotes the algebraic equality constraints. The next three equations represent the upper and lower bounds for differential, algebraic and decision variables, respectively. Monomer injection is represented by binary variable β_V. We aim to limit the number of injection points by setting this to β_{max} which is typically 10, and we relax it if the design is not feasible.

$$
\begin{aligned}
min \quad & CC = f_1(HX) + f_2(V) + \sum_{n=1}^{N} f_3(\beta_V) + f_4(wp_{m,V_f}) + f_5 \\
s.t. \quad & \dot{z}_p(V) = f(z_p(V), y_p(V), u_p(V)) = 0, \quad p \in \{A, B, C\} \\
& g_p(z_p(V), y_p(V), u_p(V)) = 0, \quad p \in \{A, B, C\} \\
& h_p(z_p(V), y_p(V), u_p(V), \beta_V) \leq 0, \quad p \in \{A, B, C\} \\
& z_p(V)^L \leq z_p(V) \leq z_p(V)^U, \quad p \in \{A, B, C\} \\
& y_p(V)^L \leq y_p(V) \leq y_p(V)^U, \quad p \in \{A, B, C\} \\
& u_p(V)^L \leq u_p(V) \leq u_p(V)^U, \quad p \in \{A, B, C\} \\
& \beta_V \in \{0, 1\} \\
& \sum_V \beta_V \leq \beta_{max}
\end{aligned}
\tag{5.24}
$$

The dynamic optimization model can be solved by the simultaneous collocation method. This method discretizes the continuous volume horizon into a finite element mesh, and then the differential-algebraic equation optimization problems are converted into nonlinear programming problems. A detailed description for the simultaneous collocation method can be found in Chapter 2. In this study, a mesh of 40 finite elements along with two-point Radau collocation is applied to the DSR model. We observe that this combination gives accurate solutions, while maintaining a computationally solvable model. As shown in Fig. 5.2, each DSR is discretized into 40 elements with unequal volumes and each element is treated as one DSR zone. Catalyst and initiator are added at the beginning of the DSR, while monomer can be added at the beginning of each DSR zone. Since the volume of each zone is a decision variable, the optimal injection profile and location can be found automatically for fixed number of injection points. In order to find the optimal number of monomer injection points, the following steps are applied:

- Step 1. Start with number of injection points $i = 1$. Fix the first i binary variable β_n to 1, and others to 0.

- Step 2. Solve the NLP problem. If it is infeasible, set $i = i + 1$.
- Step 3. Repeat Step 2, until the problem becomes feasible.
- Step 4. Keep increasing i by 1 and observe the change in capital cost with the number of injection points. Continue until there is no further improvement.

Compared with our previous algorithm, where DSR is divided into 40 zones with equal length, the new method is more flexible about the monomer injection location, and requires fewer iterations to obtain the optimal injection profile.

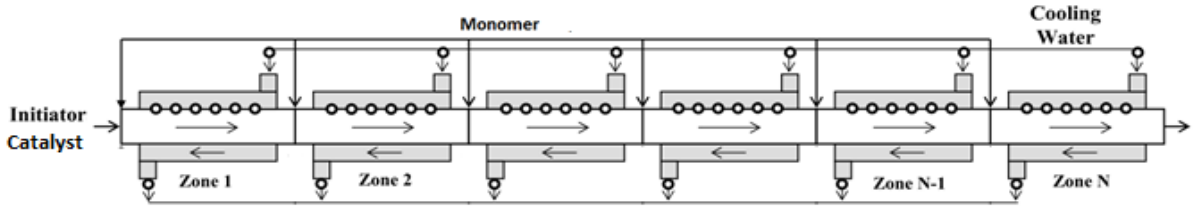

Figure 5.2. Discretized DSR

The simultaneous collocation method [51] follows a full discretization methodology, in which orthogonal collocation on a fixed/moving finite element mesh is introduced to represent the continuous volume horizon in the DSR model. Both CSTR and DSR models are implemented in GAMS and solved by NLP solver IPOPTH.

5.3.2 Stage 2 - Generate Pareto Chart Between Net Sales and Capital Cost

Stage 2 focuses on generating a Pareto chart between net sales and capital cost for each of the reactor configuration. This is achieved by increasing $\epsilon > 0$ in Eqn. 5.25 until net sales gradually levels off. Because the problem is nonconvex, we are only ensuring local solutions. However, we use multi-start and other features to make sure these are very good solutions, and assume them to be global solutions. Due to the nonconvexity, we use the ϵ constraint formulation for the multi-criteria optimization. This helps to promote unique solutions on the pareto curve. Stage 2 has the same decision variables as stage 1. But the objective switches from minimizing the capital cost to

maximizing the net sales. In addition, CC^* is the optimal capital cost obtained from Eqns. 5.23 and 5.24. γ_1, γ_2, and γ_3 are prices for polymer product, utility and raw material, respectively, as listed in Table 5.5. Although prices generally differ for different product, the selling price of each polymer is assumed to be the same in this study, as is the raw material cost. $g_p(\cdot)$ represents the equality constraints that come from the material and energy balances. $h_p(\cdot)$ represents the inequality constraints that result from the safety and product specifications.

$$\begin{aligned} max \quad & \sum_p net\, sales_p = \gamma_1\, sales_p - \gamma_2\, utility_p - \gamma_3\, raw\, material_p \\ s.t. \quad & g_p(z_p(V), y_p(V), u_p(V)) = 0, \quad p \in \{A, B, C\} \\ & h_p(z_p(V), y_p(V), u_p(V)) \leq 0, \quad p \in \{A, B, C\} \\ & CC \leq (1+\epsilon) * CC^* \end{aligned} \tag{5.25}$$

Table 5.5 Parameters for Estimating the Net Sales

	Price ($/kg)
Product	2.866
Utility	0.0123
Raw Material	2.176

5.3.3 Optimization Model Parameters

Tables 4.3 – 4.5 list the parameters used to calculate the capital cost for CSTR, PFR, and oxide recovery system [78]. Cost of component equals to the installed base cost multiplied by the ratio of component to base size raised to an exponent. These costs are normalized for confidentiality. Table 5.6 describes the product and safety specifications for each product model.

Table 5.6 Product & Safety Specifications

	Polymer A	Polymer B	Polymer C
$PR_p^*(\frac{kg}{min})$	28.87	28.87	28.87
OH Number Range ($\frac{mg\,KOH}{g\,of\,polymer}$)	460-495	260-280	370-396
PDI_p^*	1.3	1.5	1.4
$wp_{cat,p}^*$	0.15	0.1	3
$FR_{ini,p}^*(\frac{kmol}{min})$	0.45	0.45	0.45
$FR_{cat,p}^*(\frac{kmol}{min})$	2.7	1.35	1.35
$FR_{m,p}^*(\frac{kmol}{min})$	5	5	5
$T_{safety}(°C)$	220	220	220
$T_{LB,p}(°C)$	100	100	100
$T_{UB,p}(°C)$	160	160	160

5.4 Results and Discussion

5.4.1 Stage 1 - Minimizing Capital Cost

Single DSR

The aim is to minimize the capital cost, and the monomer injections represent a high percentage of those costs. Fig. 5.3 shows how the costs change with the number of monomer injection points. CC, SU, MI, R, and HE represent the costs for total capital, separation unit, monomer injection, reactor and heat exchange, respectively. All the costs are normalized to the optimal DSR capital cost. If a single DSR is used for production, at least 10 monomer injection points are required to meet the product specifications. Generally, optimal capital cost increases as the number of monomer injection points increases, due to the expense of new injection points. In addition, the weight per-

centage of unreacted monomer in the outlet stream remains at zero for all product cases A, B and C, which means DSR provides enough digestion time and can achieve high conversion. Moreover, the heat exchanger cost gradually reduces, and the reactor cost increases with the number of injection points. These are caused by the fact that with more injections, monomers are fed to the reactor more evenly and then, the temperature profile oscillates less dramatically, but the reactions slow down due to the reduction in monomer concentrations. Therefore, the heat exchanger duty decreases, but the reactor size increases in order to speed up the reactions.

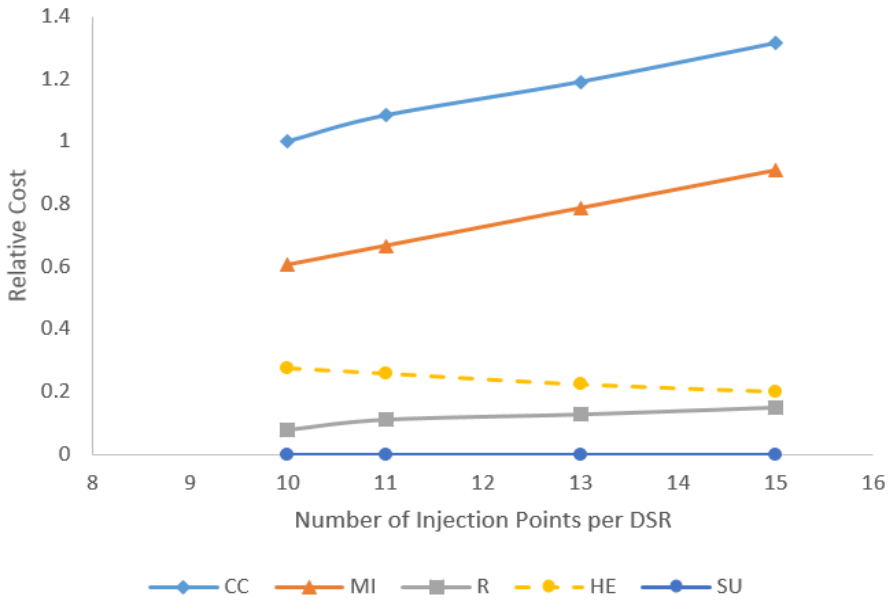

Figure 5.3. Number of Monomer Injection Points Versus Costs

This reactor design is dominated by polymer product B. Table 5.7 shows the constraints that are active in this reactor network, and their corresponding values of the constraint multipliers; higher values show a higher impact on the objective function. For all of these active constraints, Polymer B has the largest impact on the objective function among the three polymers, especially for the outlet weight percentage of KOH constraint. Therefore, we would expect that polymer B is the dominant product for the DSR network design.

In order to prove this point, we optimize the DSR model with 10 monomer injection points for each polymer product separately (Fig. 5.4). The relative optimal capital costs (scaled to the optimal capital cost of single DSR) for product A, B, and C are 0.84, 0.98 and 0.74, respectively. Polymer B has the highest capital cost and this cost is very close to the optimal cost of the multi-product process. Since, we fix the number of injection points to 10, all the products have the same monomer injection cost. Moreover, if we plan to use DSR to produce only polymers A and C, then only 5 monomer injection points are required, with a relative capital cost of 0.65. All of these demonstrate that Polymer B is the dominant product in the DSR network design.

Table 5.7 Active Constraints' Impact on the Objective Function (Constraint Multiplier) for the DSR Reactor Network

Active Constraint	Polymer A	Polymer B	Polymer C
OH Number	0.025	126.05	-
Outlet weight percentage of KOH	2.96	439.54	$1.14 * 10^{-4}$
Production rate	0.444	202.29	-
PDI	-	-	-
Adiabatic temperature	-	0.178	-
Reactor Temperature	0.52	41.05	-

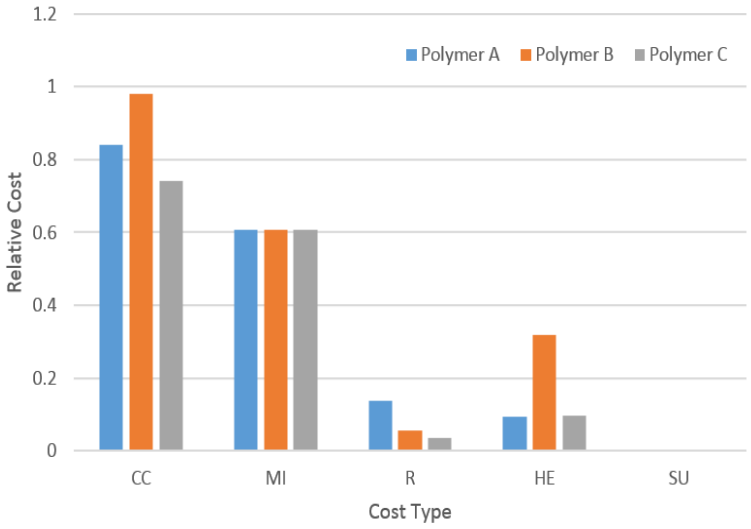

Figure 5.4. Capital Cost Breakdown for Each Polymer with DSR with 10 Monomer Injection Points

All the decision variables in Table 5.8 are relative values normalized to their upper bounds. According to it, for the dominant product B, the total feeding rates of initiator, monomer and catalyst stay the same, while the number of injection points increases from 10 to 15. On the other hand, we observe that the nondominating polymer C behaves differently; the feeding rates decrease as the number of injection points increases. No matter how many injection points are utilized, there is added capacity to produce more polymer C than is demanded, but reactor volume increases the yield of product C as the number of injection points increases and leads to adiabatic temperature violations (5.21). To avoid this, the feeding rates of polymer C must decrease as the number of injection points increases.

Table 5.8 Optimal Decision Profile of DSR vs. the Number of Monomer Injection Points

	10 INJ			11 INJ		
Product	A	B	C	A	B	C
FR_{ini}	0.093	0.11	0.44	0.087	0.11	0.46
FR_{cat}	$2.88 * 10^{-4}$	$3.85 * 10^{-4}$	0.037	$2.88 * 10^{-4}$	$3.85 * 10^{-4}$	0.039
Total FR_m	0.073	0.11	0.25	0.074	0.11	0.26
Volume	0.084			0.079		
HX	2.19			3.51		
$wp_{KOH,N}$	0			0		
	13 INJ			15 INJ		
Product	A	B	C	A	B	C
FR_{ini}	0.087	0.11	0.39	0.087	0.11	0.26
FR_{cat}	$2.88 * 10^{-4}$	$3.85 * 10^{-4}$	0.033	$2.88 * 10^{-4}$	$3.85 * 10^{-4}$	0.021
Total FR_m	0.074	0.11	0.22	0.075	0.11	0.14
Volume	0.041			0.053		
HX	6.47			5.55		
$wp_{KOH,N}$	0			0		

Figures 5.5, 5.6, and 5.7 show the relative temperature and feed profiles for polymers A, B and C, respectively. Temperatures and adiabatic temperatures are scaled relative to T_{safety}. All other variables in the plots are scaled to their upper bounds. In the feed profile, the feeding rate of monomer at that position is indicated by the dot, and the smooth line represents the weight percentage of unreacted monomer in the reactor. The temperature profiles and weight percentages of monomer for all the polymers stop oscillating after all the monomers are added to the reactor. In addition, polymer B's temperature profile oscillates dramatically compared with other products. This is expected, since polymer B uses EO instead of PO as its monomer. EO reacts much faster

than PO, and has a higher value of κ in Eqn. 5.21, which makes it more sensitive to the adiabatic temperature rise constraint. Therefore, when the weight percentage of monomer in the reactor is the same for all products, polymer B's reactor temperature needs to be the lowest among all the polymers. Moreover, the sharp decrease in polymer B's temperature profile requires the largest amount of heat exchanger capacity, since it requires a lot of cooling to bring temperature down from a high temperature to a low temperature within a small reactor volume. The faster kinetics also make polymer B the dominant product in this design. Since it is more sensitive to the adiabatic temperature rise constraints, monomers are required to be added more slowly, and this would lead to requiring more monomer injections.

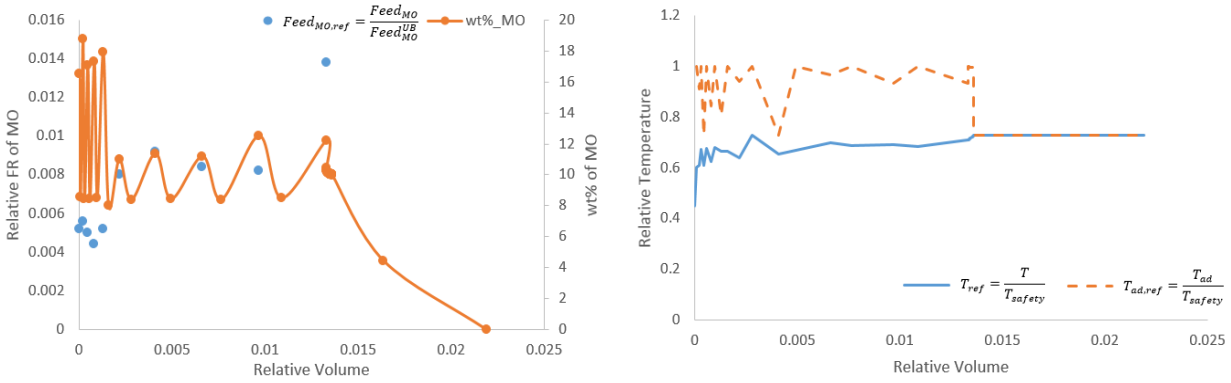

(a) Feed Profile (b) Temperature Profile

Figure 5.5. Decision Profiles of the DSR with 10 Injections for Product A

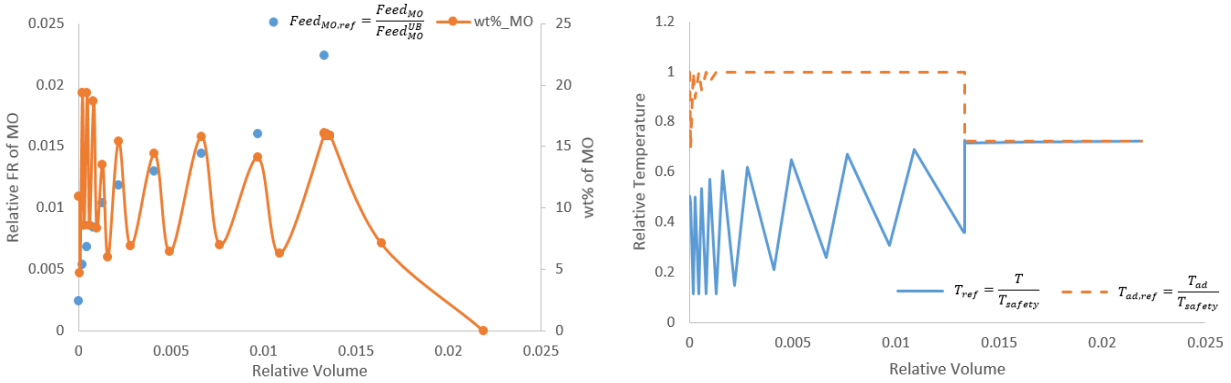

(a) Feed Profile (b) Temperature Profile

Figure 5.6. Decision Profiles of the DSR with 10 Injections for Product B

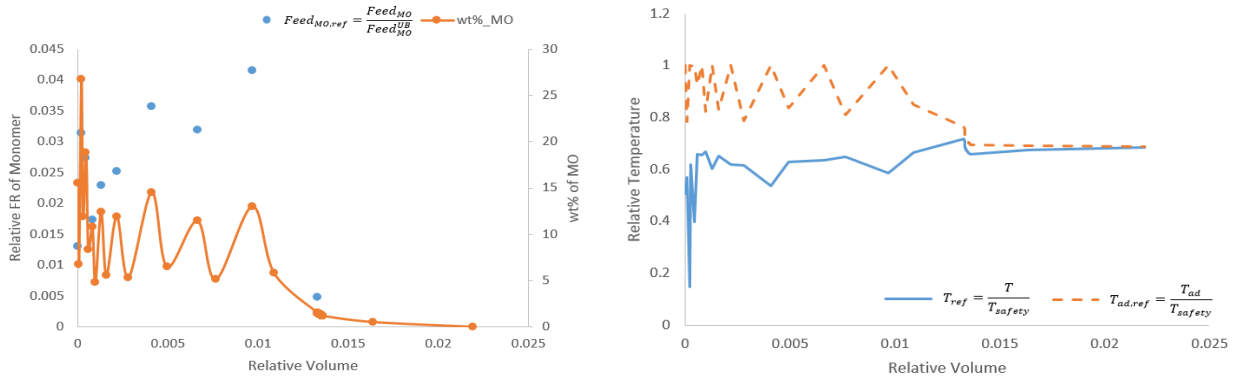

(a) Feed Profile

(b) Temperature Profile

Figure 5.7. Decision Profiles of the DSR with 10 Injections for Product C

Furthermore, the normalized chain length distribution is plotted in Fig. 5.8 (scaled to $FR^*_{ini,p}$). Product A and C do not include polymers with chain lengths longer than 8, and product B does not have polymers with chain length greater than 9. These prove that it is reasonable to assume the maximum chain length for these rigid products to be less than 10. The PDIs of the three products are 1.22, 1.15, and 1.20 respectively.

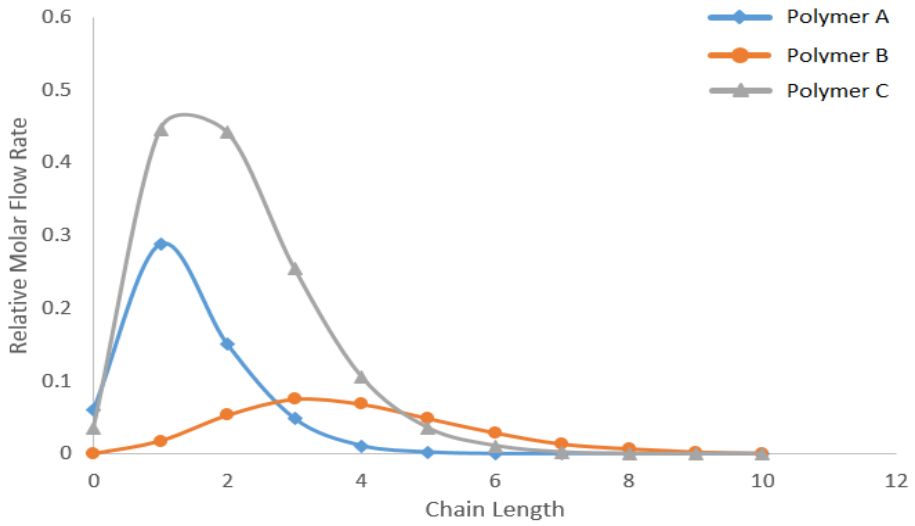

Figure 5.8. Chain Length Distribution for the DSR Model

CSTR in Series

Fig. 5.9 shows the relationship between the number of CSTRs in series and the relative capital cost (CC), along with other relative costs (normalized to the optimal capital cost of the single DSR case). SU, MI, R, and HE represent the cost for the separation unit, monomer injection, reactor and heat exchange, respectively. Other costs include the cost for catalyst injection, agitator, and pump. Capital cost increases as the number of CSTRs increases, due to the fact that extra CSTRs require extra pumps, and agitators. In contrast, the costs for the separation unit and the reactor decrease as the number of CSTRs increase, since more reactors provide longer residence time for digestion, and lower the weight percentage of unreacted monomer in the outlet stream. Moreover, when fewer than 4 CSTRs are utilized, PDI product specifications could not be satisfied, especially for polymers A and C, as they have a tighter bound than polymer B. Therefore, at least four CSTRs are required, and the relative capital cost of this configuration is 2.86.

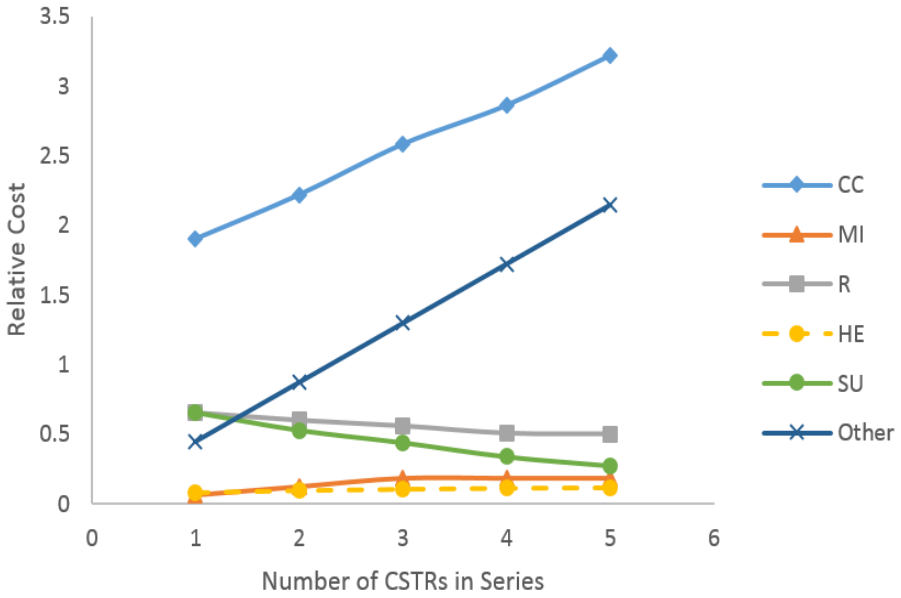

Figure 5.9. Number of CSTRs Versus Costs

This reactor structure is mainly determined by polymer A. Since polymer A has the shortest chain

length, its monomer feeding rates are the lowest among the three products. This would lead to a lower monomer concentration in the reactor, and slower reactions. Hence, larger reactors are needed to increase its reaction rates and its monomer conversion. Table 5.9 shows this to be the most constrained production case.

Table 5.9 Active Constraints' Impact on the Objective Function (Constraint Multiplier) for the 4CSTRs Reactor Network

Active Constraint	Polymer A	Polymer B	Polymer C
OH Number	-	0.067	-
Outlet weight percentage of KOH	1925.87	43.90	-
Production rate	10.00	2.23	-
PDI	11.81	-	-
Adiabatic temperature of the first CSTR	0.45	0.028	-
Reactor Temperature	10.21	0.23	-

The relative decision profiles (normalized to their upper bounds) are listed in Table 5.10. Although, no monomer is fed to the last CSTR, the last CSTR is necessary in order to provide more residence time for digestion, and to satisfy the PDI and other product specifications. Moreover, the last CSTR is ten times larger than the other CSTRs. Since the weight percentage of unreacted monomer in the last CSTR is small, it requires a larger reactor to achieve a higher conversion.

Table 5.10 Optimal Decision Profile of the 4 CSTRs in Series Model

Decision Variable	Polymer A	Polymer B	Polymer C
FR_{ini}	0.089	0.11	0.14
FR_{cat}	$2.88 * 10^{-4}$	$3.85 * 10^{-4}$	0.018
$FR_{m,1}$	0.032	0.024	0.012
$FR_{m,2}$	0.023	0.052	0.038
$FR_{m,3}$	0.020	0.036	0.031
$FR_{m,4}$	0.00	0.00	0.00
T_1	1.00	1.00	0.72
T_2	1.00	1.00	1.00
T_3	1.00	1.00	0.77
T_4	1.00	1.00	0.83
V_1	0.0027		
V_2	0.0051		
V_3	0.0072		
V_4	0.061		
HX^1	1.28		
HX^2	0.72		
HX^3	0.42		
HX^4	0.20		
SU	4360		

Table 5.9 shows the constraints that are active in this reactor network, and their corresponding multipliers. Larger multipliers imply higher impact on the objective function. For most of these active constraints, Polymer product A has the largest impact on the objective function among the three cases. Therefore, we observe that product A is the dominant one when it comes to the CSTR

network design.

In order to prove this point, we optimize the 4-serial CSTR model for each polymer product separately. The relative optimal capital costs (normalized to the optimal capital cost for single DSR) for product A, B, and C are 2.82, 2.32, and 2.04, respectively. Moreover, if the reactor configuration is used to produce B only, only one monomer injection point is required. To produce product C, only two injection points are required. Fig. 5.10 shows the detailed costs for each product case. All of these show that product A is dominant for the CSTR network design.

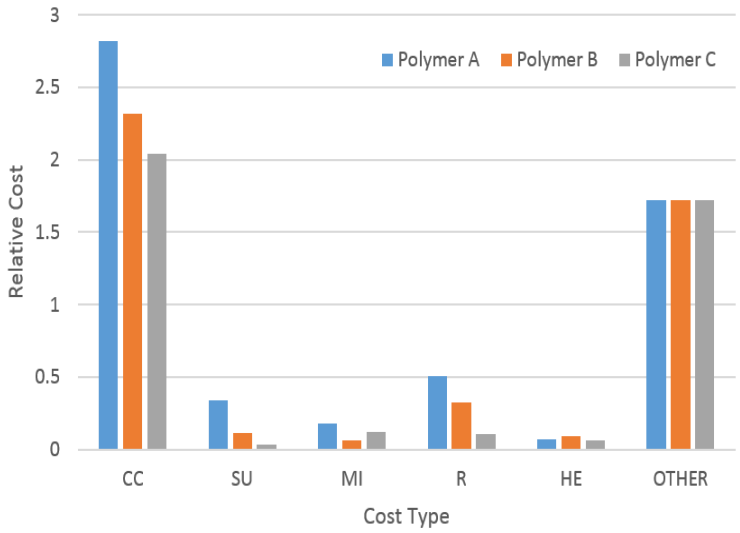

Figure 5.10. Capital Cost Breakdown for Each Polymer Product with 4 CSTRs in Series

Furthermore, the normalized chain length distribution is plotted in Fig. 5.11 (scaled to $FR^*_{ini,p}$). Product A and C do not contain polymers with chain lengths longer than 7, and product B has only a small amount of longer polymers. The PDIs for the three products are 1.3, 1.24, and 1.33 respectively.

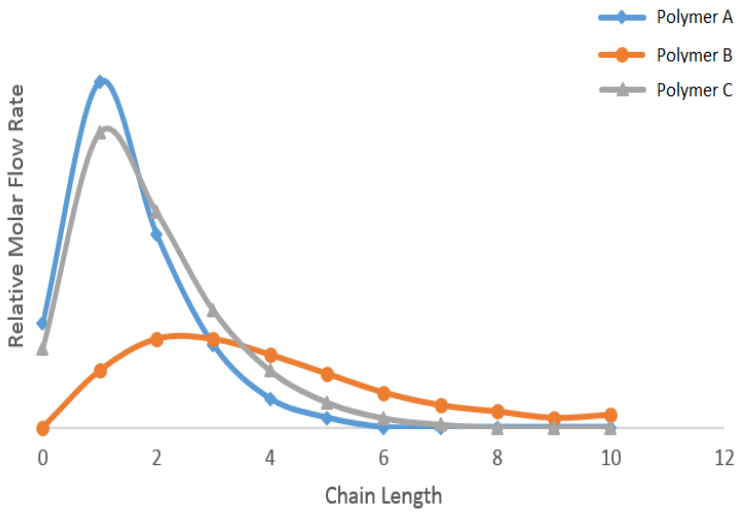

Figure 5.11. Chain Length Distribution for the 4 CSTRs Model

Single CSTR followed by a DSR

The last configuration is the design of a single CSTR followed by a DSR. This reactor design was chosen in previous work [85], where several additional network options were considered. In [85] this network was favored because it initially leads to better heat control, along with better digestion at the end. In contrast, the single DSR followed by a CSTR is inferior, as the CSTR does not offer enough digestion time and is not suitable to be placed at the end of a reactor network.

As in the previous sections, we study the relationship between costs and the number of monomer injection points within the DSR. All the costs in Fig. 5.12 are normalized to the optimal capital cost of a single DSR. This reactor design requires at least 6 injection points in total, one for the CSTR and 5 for the DSR. Also its relative optimal capital cost is 1.09. This reactor design is dominated by both product A and B, as these are the most constrained cases (see Table 5.13). Moreover, increasing the number of monomer injections increases the total capital cost. The separation unit cost is zero for all cases, since the weight percentage of unreacted monomer is negligible. This further demonstrates that DSRs provide longer digestion time to help increase the conversion.

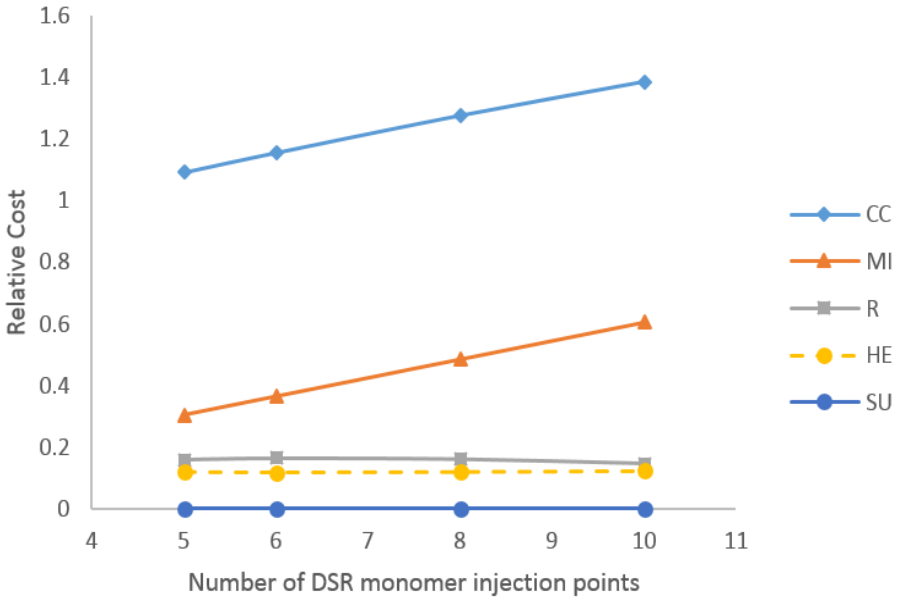

Figure 5.12. Number of Monomer Injection Points Within the DSR Versus Costs

The relative decision profiles (scaled to their upper bounds) for different number of monomer injection points are listed in Table 5.11. As with the single DSR model, the total feeding rates of monomer, initiator and catalyst for polymer C decrease with the number of injection points. Also, in order to achieve higher conversion for polymer product A and B, reactor volume is increased. However, for the nondominant product C, larger volume will lead to violation of the adiabatic temperature constraint, since the reaction rates would increase with the volume and more heat would be generated. Therefore, its raw material feeding rates reduce with increasing volume to avoid run-away reaction. The relative monomer feeding rates to the CSTR and to each DSR zone are listed in Table 5.12. Fig. 5.13 shows the relative temperature profiles (normalized to T_{safety}) for all product cases.

Table 5.11 Optimal Decision Profile of CSTR Followed by a DSR Vs. the Number of Monomer Injection Points within the DSR

	CSTR+DSR w/ 5 INJ			CSTR + DSR w/ 6 INJ		
Product	A	B	C	A	B	C
FR_{ini}	0.093	0.11	0.28	0.093	0.11	0.30
FR_{cat}	$2.88 * 10^{-4}$	$3.85 * 10^{-4}$	0.024	$2.88 * 10^{-4}$	$3.85 * 10^{-4}$	0.025
Total FR_m	0.073	0.11	0.16	0.073	0.11	0.17
Volume	0.025			0.027		
HX	2.83			2.78		
$wp_{KOH,N}$	0			0		
	CSTR + DSR w/ 8 INJ			CSTR + DSR w/ 10 INJ		
Product	A	B	C	A	B	C
FR_{ini}	0.093	0.11	0.28	0.093	0.11	0.26
FR_{cat}	$2.88 * 10^{-4}$	$3.85 * 10^{-4}$	0.024	$2.88 * 10^{-4}$	$3.85 * 10^{-4}$	0.021
Total FR_m	0.073	0.11	0.16	0.073	0.11	0.15
Volume	0.027			0.023		
HX	2.78			2.84		
$wp_{KOH,N}$	0			0		

Table 5.12 Relative FR_m for CSTR Followed by a DSR (5 INJ) Reactor Network

	Polymer A	Polymer B	Polymer C
$FR_{m,CSTR}$	0.049	0.085	0.14
FR_{m,DSR_1}	$8.0 * 10^{-3}$	$7.8 * 10^{-3}$	$3.8 * 10^{-5}$
FR_{m,DSR_2}	0.010	$4.2 * 10^{-3}$	$8.0 * 10^{-5}$
FR_{m,DSR_3}	$1.4 * 10^{-3}$	$4.4 * 10^{-3}$	$1.4 * 10^{-3}$
FR_{m,DSR_4}	$3.6 * 10^{-3}$	$4.2 * 10^{-3}$	0.018
FR_{m,DSR_5}	$8.0 * 10^{-4}$	$5.2 * 10^{-3}$	$2.8 * 10^{-3}$

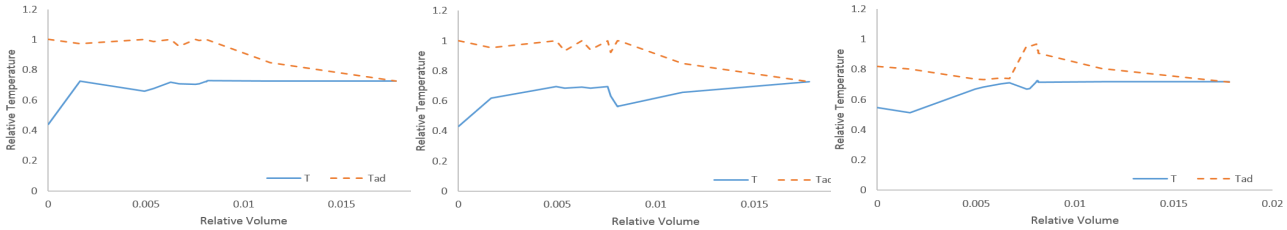

(a) Product A (b) Product B (c) Product C

Figure 5.13. Temperature Profiles of the CSTR Followed by a DSR Model

Table 5.13 shows the active constraints for this reactor network, and their corresponding constraint multipliers. Both product A and B play important roles when deciding the structure of this reactor network. This is what we expected, since product A and B dominate in the CSTR and DSR designs, respectively. Fig. 5.14 shows the detailed costs for each product case.

Table 5.13 Active Constraints' Impact on the Objective Function (Constraint Multiplier) for the CSTR Followed by a DSR Reactor Network

Active Constraint	Polymer A	Polymer B	Polymer C
OH Number	0.059	0.023	-
Outlet weight percentage of KOH	7.04	21.91	-
Production rate	1.46	4.17	-
PDI	66.03	-	0.20
Adiabatic temperature of the first CSTR	0.058	0.10	-
Reactor Temperature	0.77	0.31	-

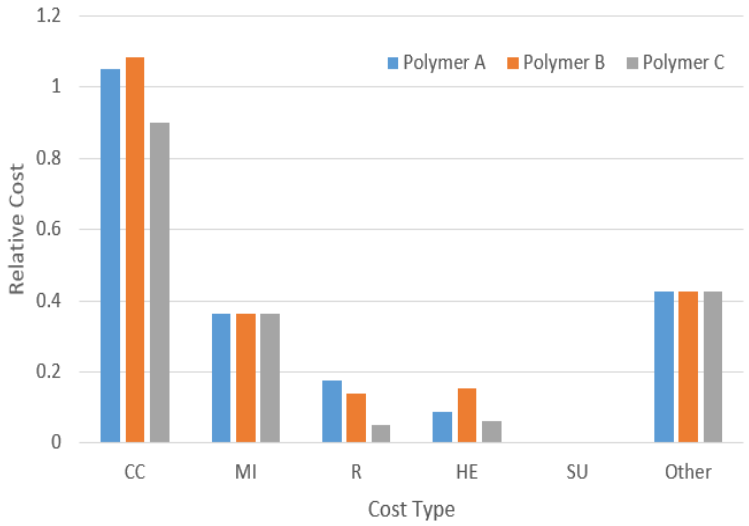

Figure 5.14. Capital Cost Breakdown for Each Polymer Product (Single CSTR Followed by a DSR)

Furthermore, the normalized chain length distribution is plotted in Fig. 5.15 (scaled to $FR^{*}_{ini,p}$). Product A does not contain polymers with chain length longer than 6. Products B and C have only a small amount of longer chain length polymers. The PDIs of the three products are 1.30, 1.26, and 1.40, respectively.

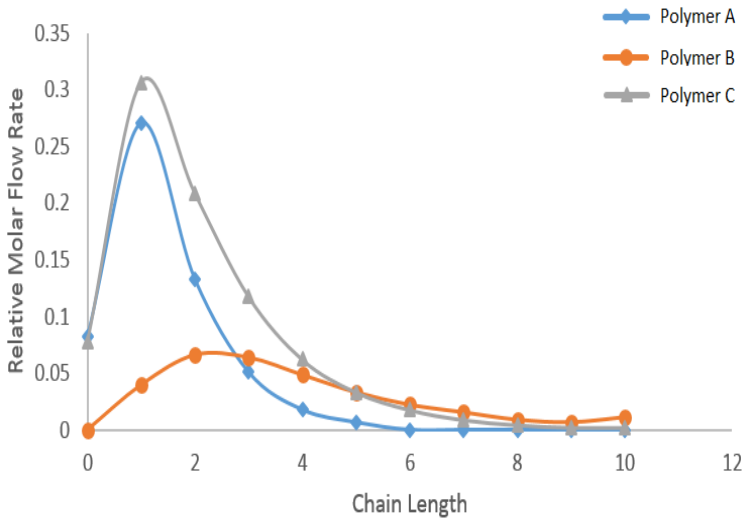

Figure 5.15. Chain Length Distribution for the CSTR Followed by a DSR

5.4.2 Stage 2 Generating Pareto Chart Between Net Sales and Capital Cost

Stage 2 focuses on generating Pareto charts between net sales (sales - operating costs) and capital cost for each reactor network, as shown in Figs. 5.16, 5.17, and 5.18. All the sales and costs are normalized with respect to the net sales of optimal DSR with $\epsilon = 0$. Here the capital cost abscissa $(1 + \epsilon)$ refers to $(1 + \epsilon) \times CC^*$, where CC^* is the minimum capital costs obtained in stage 1. For these plots, all reactor networks can eventually reach the same amount of product sales, as each network model has the same amount of provided initiator (Eqn. 5.20a). However, the single DSR case tends to consume more utility, due to dramatic temperature changes along the reactor. Therefore, the network with 4 serial CSTRs plateaus with higher net sales, as shown in Fig. 5.19. Also, the numbers below the raw material profile in Fig. 5.17 indicate the optimal number of monomer injection points at each $1 + \epsilon$ value. When $1 + \epsilon$ is below 2, 10 injection points leads to the maximum net sales. After this point, up to 15 injection points are needed for higher net sales. This finding is consistent with the trends in Table 5.8.

However, when capital cost is limited, applying more injection points would lower the production of product C, as well as the total net sales. When the capital cost is sufficiently large (production

of product C achieves its maximum), more injection points lead to higher net sales due to lower utility cost. For CSTR in series, the 4 CSTR network has the highest net sales. The CSTR followed by a DSR configuration provides the highest net sales for $\epsilon \leq 2.5$.

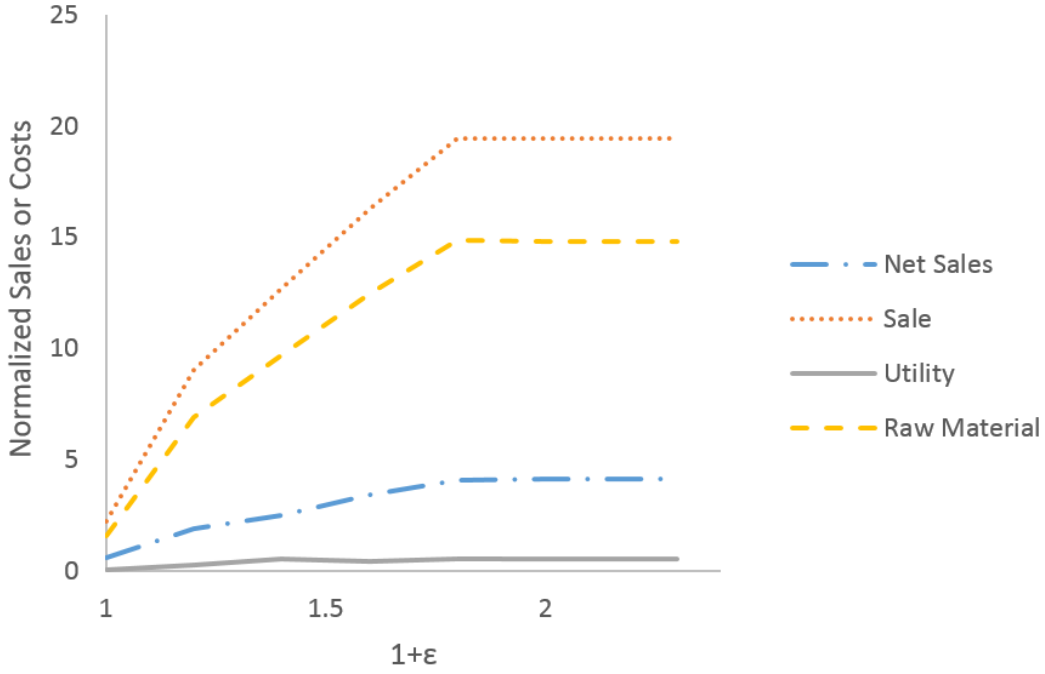

Figure 5.16. Pareto Chart for 4 CSTRs in Series

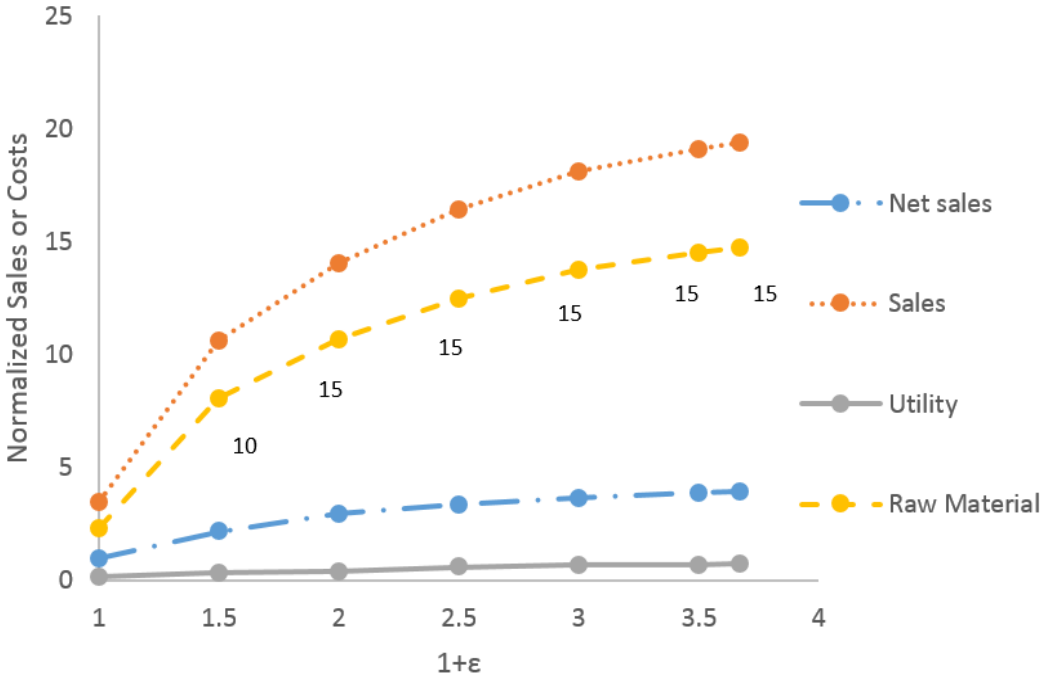

Figure 5.17. Pareto Chart for DSR

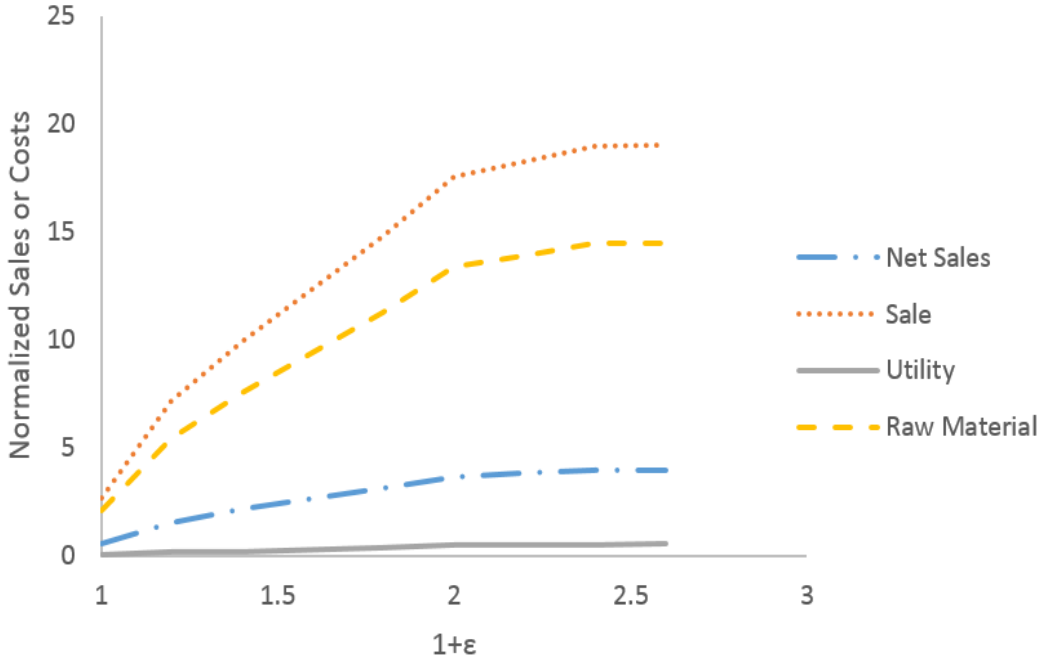

Figure 5.18. Pareto Chart for Single CSTR Followed by a DSR

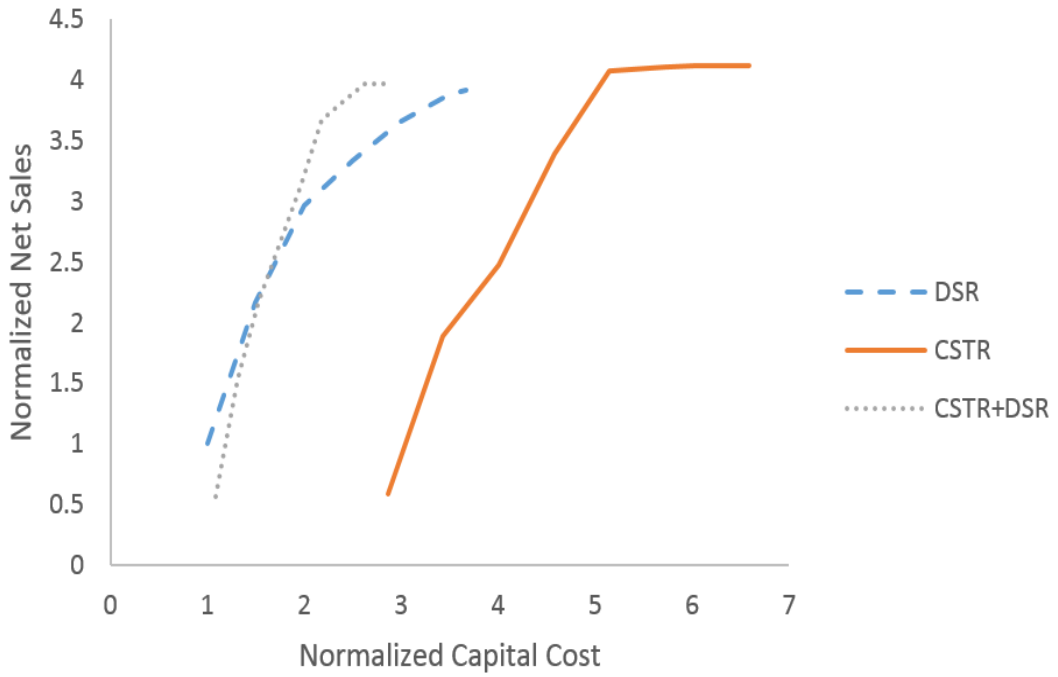

Figure 5.19. Capital Cost Versus Net Sales for Three Different Reactor Networks

5.4.3 Results Summary

Table 5.14 summarizes the relative optimal results for different reactor configurations, where values in bold are the optimal results at upper bounds. Capital cost is normalized to the optimal single DSR model. Other variables are scaled to their upper bounds. Here the DSR model has a lower capital cost because it has the highest monomer conversion (lowest weight percentage of monomers in the outlet stream) and DSR offers a digestion phase, where the weight percentage of unreacted monomer in the mixture decreases after the last monomer injection; this can be observed in Figure5.5, 5.6, and 5.7. In contrast, CSTR does not provide any digestion phase, since its reactor concentration equals its outlet concentration. If the monomer concentration in the outlet stream is low, then its concentration in the reactor is also low. And the reaction rates decrease, since they are proportional to the monomer concentration in the reactor. For this reason adding a DSR after a CSTR is more effective than adding a CSTR after a DSR; DSRs can help digest the unreacted monomers and reduce the separation unit cost, but CSTRs cannot. Moreover, the DSR alone can already produce desired polymers, so there is no need to add a CSTR behind it.

Moreover, Fig. 5.19 shows that adding a DSR after a CSTR has performance advantages over single DSR. This is due to better heat transfer and lower cooling costs, which leads to considerably better net sales. From Fig. 5.19 we see that the optimal CSTR-DSR network leads to the best trade-off between net sales and capital cost.

Table 5.14 Relative Optimal Results for Different Reactor Networks

	Single DSR			4 CSTRs in Series			CSTR + DSR		
Polymer	A	B	C	A	B	C	A	B	C
Total FR_m	0.073	0.11	0.25	0.073	0.11	0.081	0.073	0.11	0.16
FR_{ini}	0.093	0.11	0.44	0.089	0.11	0.14	0.093	0.11	0.28
FR_{cat}	$2.88 * 10^{-4}$	$3.85 * 10^{-4}$	0.037	$2.88 * 10^{-4}$	$3.85 * 10^{-4}$	0.018	$2.88 * 10^{-4}$	$3.85 * 10^{-4}$	0.024
PDI	1.22	1.15	1.20	**1.30**	1.24	1.33	**1.30**	1.26	1.40
CC	1.00			2.86			1.09		
Total V	0.084			0.076			0.025		
Total HX	2.19			2.62			2.83		
$wp_{m,N}$	0			0.44			0		

The sensitivity analysis helps us to determine the dominant product in each reactor design. For DSR, polymer B determines the reactor superstructure, such as the heat exchanger capacity and number of monomer injection points. Because polymer B uses EO as its monomer, it reacts much faster than PO. In a long DSR, fast reactions could cause run-away reaction and a large increase in adiabatic temperature. Therefore, in order to avoid safety constraint violation, monomers are added more gradually, and more cooling is required. For the CSTR case, polymer A is the dominant product. Since polymer A has the shortest chain length, its monomer feeding rates is the lowest among the three products. This would lead to a lower monomer concentration in the reactor, and slower reactions. Hence, larger reactors are needed to increase its reaction rates and its monomer conversion. For the CSTR followed by a DSR case, both polymer A and B play important roles in shaping the reactor design, because polymers B and A dominate the DSR and CSTR design, respectively.

Finally, all reactor optimization models are MINLPs, but as these models are large (as shown in Table 5.15) and highly nonlinear, MINLP solvers were not effective in solving these problems. Instead, the binary variables are systematically fixed to either 0 or 1, based on a detailed NLP-based algorithm and guided by optimal sensitivity for the binary variables. The optimization models are solved with IPOPTH in GAMS.

Table 5.15 Model Size for Different Reactor Networks

	# of Variables	# of Equality Constraints	# of Inequality Constraint
4 CSTRs in Series	2991	2949	60
DSR	51081	50832	612
CSTR + DSR	51820	51524	624

5.5 Conclusions

The focus of this study is to determine a continuous reactor network along with its operating conditions that minimizes the capital cost for multi-product rigid polyol production, where individual products are produced by the same plant in single product campaigns. Based on our previous study [85] we narrow down the reactor types to CSTRs and DSRs with multiple potential monomer injection points. Moreover, we examine three reactor networks in particular: CSTRs in series, single DSR, and a CSTR followed by a DSR. The single DSR has the lowest capital cost among the three configurations. In addition, this reactor design is dominant by polymer B. If we use this reactor network to produce another polymer which has faster kinetics than polymer B, then this new polymer product would become the dominant product and may require more injection points. For the reactor configuration with only CSTRs, at least four CSTRs are required to produce polymer that satisfies the product specifications. Its capital cost is two times larger than that of the DSR. More CSTRs may be required if we plan to use this reactor design to produce a new polymer which

has slower kinetics and larger target molecular weight than polymer A. The last configuration, a single CSTR followed by a DSR requires at least 6 monomer injection points, one for CSTR and 5 for DSR. Its relative capital cost is 9% higher than the single DSR case. However, when the normalized capital cost reaches 1.5 or higher, the CSTR followed by a DSR would have a higher annual net sales at the same capital cost level than a single DSR, because it consumes less utility. In addition, the increase in capital cost can easily be offset by the increase in net sales, since the net sales grow 4 times for the CSTR followed by a DSR network when the normalized capital cost increases from 1 to 1.5. Consequently, the optimal CSTR-DSR network leads to the best overall performance in this study.

The dynamic optimization models mentioned in Chapter 4 and 5 are able to generate optimal reactor configuration along with the optimal operation recipe. However, the model performance could degenerate when uncertainty comes into play. In the next chapter, we apply two methods: back-off and multi-scenario (MS) to analyze the impact of kinetic uncertainty on reactor network design.

Chapter 6 Reactor Network Design Under Uncertainty

The dynamic optimization models mentioned in Chapter 4 and Chapter 5 are able to generate optimal reactor configuration along with the optimal operation recipe. However, the model performance could degenerate when uncertainty comes into play. In this chapter, we apply two methods: back-off and multi-scenario (MS) strategy to analyze the impact of kinetic uncertainty on reactor network design. Back-off belongs to robust optimization approach. It shrinks the feasible region by introducing back-off terms to the inequality constraints. We adopted an iterative approach to calculate the back-off terms. For the MS method, we first find the scenarios that are worst-case violations of inequality constraints. Then, we solve the MS problem with current number of scenarios and obtain the optimal common decision profile (q). Next, we fix q and sample over the uncertainty range, and solve the equations to check for infeasible constraints. If there is no constraint violation, then stop. Else add the worst infeasible point as new scenario and go back to solve the MS problem again. Case studies are presented at the end to show the effectiveness of the these two approaches.

6.1 Literature Review

The common strategies that deal with uncertainty can be divided into two categories: the robust optimization approach and the stochastic programming approach. The robust optimization approach

allows optimal solutions to be obtained without any additional measurements, which means it does not take reactive actions and recourse variables in consideration. Hence, optimal solutions obtained by the robust optimization is more conservative. A bilevel minmax approach is a typical robust optimization formulation. The lower level problem finds the worst scenario, while the upper level finds the optimal solution based on the worst case. However, the chance for the worst case to occur is extremely low. Therefore, the bilevel formulation is often conservative. And its performance deteriorates when the most probable uncertainty level is realized by additional measurements.

Beside the bilevel formulation, there are other ways to quantify the worst scenario. Back-off method seeks the problem feasibility by adding back-off terms into the original inequality constraints to tighten the constraints and shrink the feasible region of the optimization problem. In this way, feasibility for the worst case is ensured. In this approach, quantifying and calculating the back-off terms is the key. Visser et al. encountered parametric uncertainties when dealing with an end-point optimization problem in a batch process [87]. Back-off method was introduced to handle the uncertainty in parameters. And the back-off terms were calculated by linearizing the the constraints and the time-varying state space. Diehl et al. also applied the linearized formulation along with the dual norm to derive analytical solution for the robust optimization problem. However, linearization may not result in accurate back-off terms when the problem is highly nonlinear. Galvanin et al. calculated the back-off terms from the predictions of constraint responses for given parameter distribution [88]. And then, the back-off terms are applied in the optimal design problem to ensure the optimality and feasibility of the problem. Srinivasan et al. proposed an iterative approach to obtain the back-off terms [89]. First, an initial guess is used to initialize the back-off terms, and the optimization problem with the guessed back-off terms is solved. The back-off terms are then updated by using the probability density functions of the states obtained at the optimal solution.

As mentioned before, stochastic programming approach is another common strategy to deal with uncertainty. It assumes the probability distribution of the parameter uncertainty is known and applied in order to obtain the best expected performance. In order to have a better estimation for

the probability distribution of the uncertain parameter, additional measurements and recourse variables are utilized to make the optimal trajectory more flexible. After we have a clear estimation for the uncertain parameters, reactive actions for different uncertainty levels can be applied. The biggest advantage of stochastic programming approach is that it is less conservative compared to the traditional robust optimization. However, its problem size is relatively large, since different uncertainty levels or multiple scenarios need to be considered.

Back in 1995, Ruppen et al. came up with a discretized approach to deal with uncertainty in a batch process [91]. A discrete probability distribution of the uncertain parameters is assumed. This leads to a differential algebraic optimization problem (DAE) including several model descriptions, each corresponding to a grid point in parameter space. The DAE is then transformed to an algebraic optimization problem using a time parameterization based on the method of orthogonal collocation. This idea has been extended to other fields, such as nonlinear model predictive control (NMPC). Yu et al. proposed a parallelizable advanced-step multistage NMPC [92]. It can provide a non-conservative robust control solution, which can solve two types of uncertainty: model parameters and unmeasured noise. Although stochastic programming and its applications prove it is less conservative, and more flexible, the increased problem size and computational cost is still a major concern.

In this work, multi-scenario approach is adopted to handle the uncertainty in kinetic parameters. This is done by first finding the scenarios that are worst-case violations of inequality constraints. Then, solve the MS problem with current number of scenarios and obtain the optimal common decision profile (q). Fix q and sample over the uncertainty range to find constraint violations. If there is no constraint violation, then stop. Otherwise add the worst infeasible point as a new scenario and go back to solve MS problem again. A more detailed procedure is described in next section.

6.2 Back-off Method

Back-off method is a type of robust optimization. It aims to find the worst scenario, then optimize the problem based on it. Therefore, back-off method is more conservative compared with stochastic programming. On the other hand, stochastic programming dramatically increases the model size and the computational cost. The idea behind back-off is to shrink the feasible region by introducing the back-off terms to the inequality constraints. The original problem can be formulated as Eqn. 6.1, where x and u represent the state and decision variable, respectively. θ is the uncertain parameter vector.

$$\begin{aligned} min \quad & f(u) \\ s.t. \quad & g(x,u,\theta) = 0 \\ & h(x,u,\theta) \leq 0 \end{aligned} \tag{6.1}$$

In order to ensure that all the inequality constraints can be satisfied at all levels of uncertainty, back-off terms are introduced. The problem formulation with back-off term is presented in Eqn. 6.2, where $\bar{\theta}$ denotes the uncertain parameter at nominal value, b_c stands for the positive back-off term.

$$\begin{aligned} min \quad & f(u) \\ s.t. \quad & g(x,u,\bar{\theta}) = 0 \\ & h(x,u,\bar{\theta}) + b_c \leq 0 \\ & b_c \geq 0 \end{aligned} \tag{6.2}$$

As mentioned in the previous section, when dealing with a nonlinear system, it is not ideal to apply linearization to calculate the back-off terms. First, it may lead to inaccurate back-off terms. Second, analytic solution is expensive to derive for large system. Therefore, in this work we apply an iterative method to derive the back-off terms. And the detailed procedure is described below.

- Step 1. Solve the original optimization problem in Eqn. 6.1 at nominal level. Obtain the optimal decision profiles u^*.

- Step 2. Assume the probability distributions of the uncertain parameters are known. Sample n points based on the distribution. Apply Monte Carlo simulation with decision profiles fixed to the optimal nominal values u^* to obtain the values of inequality constraints as well as the sensitivity information of the variables to uncertainties.

- Step 3. Utilize the Monte Carlo simulation results and Eqn. 6.3 to calculate the back-off terms. The value of the back-off term depends on two factors: tuning parameter η and the sample standard deviation S of the inequality constraint h. η is determined by the confidence level c, which is the probability of inequality constraint that is valid ($c = P(h(x, u, \theta) \leq 0)$. When the confidence level $c = 1$, the problem is feasible for all $\theta \in \Theta$. Larger η would results from a greater confidence level (choose $c = 0.99$, then $\eta = 3$).

$$\begin{aligned} \bar{h} &= \frac{\sum_{i=1}^{n} h_i}{n} \\ S^2 &= \frac{\sum_{n=1}^{n} (h_i - \bar{h})^2}{n-1} \\ b_c &= \eta S \end{aligned} \tag{6.3}$$

- Step 4. Solve the optimization problem in Eqn. 6.2 with the back-off terms obtained from step 3. Record the new optimal decision profiles u^{**}.

- Step 5. Update the back-off terms by performing the Monte Carlo simulation with optimal decision profiles fixed to u^{**}.

- Step 6. (Optional) Stop if the convergence criterion is reached ($|b_c^{k+1} - b_c^k| \leq \epsilon$). If not, go back to step 4 with the updated back-off terms.

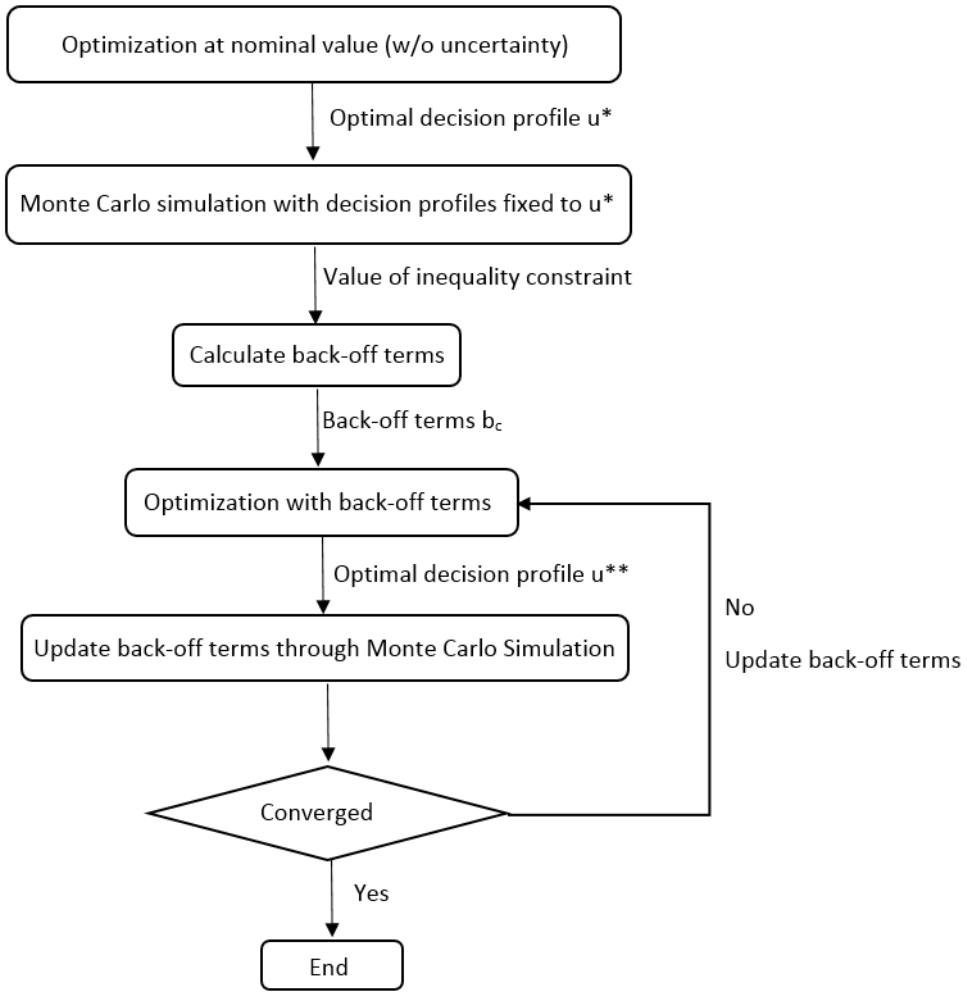

Figure 6.1. Back-off Method Flow Chart

6.3 Multi-scenario Approach

The original dynamic optimization problem without uncertainty (uncertain parameters are at the nominal values) can be summarized as follows:

$$\begin{aligned} & min \quad f(q) \\ s.t. \quad & g_i(x, q, u, \bar{\theta}) = 0, \quad i = 1..n_g \\ & h_j(x, q, u, \bar{\theta}) \leq 0, \quad j = 1..n_h \end{aligned} \tag{6.4}$$

where x represents the state variables, q denotes the decision variables that play important roles in the objective function. On the other hand, u are the decision variables that do not participate in the objective function. $\bar{\theta}$ stands for the uncertain parameters that are at the nominal value. $g_i(\cdot)$ represents the equality constraints. There are n_g equality constraints. $h_j(\cdot)$ represents the inequality constraints. And the inequality constraint's amount is n_h.

The multi-scenario formulation below applies to capital cost or other objective functions that do not depend on u.

$$\begin{aligned} & min \quad f(q) \\ s.t. \quad & g_i(x,q,u,\theta) = 0, \quad i = 1..n_g \\ & h_j(x,q,u,\theta) \leq 0, \quad j = 1..n_h \\ & \forall \theta \in \Theta \end{aligned} \tag{6.5}$$

Although q is independent of θ, x and u vary for each θ. Therefore, it is an infinite dimensional problem. Normally, θ is discretized along with x and u, leading to the formulation below:

$$\begin{aligned} & min \quad f(q) \\ s.t. \quad & g_{i,k}(x_k,q,u_k,\theta_k) = 0, \quad i = 1..n_g, k = 1..n_s \\ & h_{j,k}(x_k,q,u_k,\theta_k) \leq 0, \quad j = 1..n_h, k = 1..n_s \end{aligned} \tag{6.6}$$

where n_s is the number of scenarios. In order to figure out the sufficient level of discretization, we first assume monotonicity of Θ on inequality constraint h, then apply a two stage approach.

Monotonic assumption

Implicitly eliminate state variables and equations, assume that $\bigtriangledown_x g(x,q,u,\theta)$ is nonsingular $\forall(x,q,u,\theta)$. Then for $x(q,u,\theta)$ and $h_j(x(q,u,d),q,u,\theta) \leq 0$, $\frac{dh_j}{d\theta} = \frac{\partial h_j}{\partial \theta} + \frac{dx}{d\theta}\frac{\partial h_j}{\partial x} = \frac{\partial h_j}{\partial \theta} - \bigtriangledown_\theta g(\bigtriangledown_x g^{-1})\frac{\partial h_j}{\partial \theta}$. For $g(x,q,u,\theta) = 0$ and all fixed q,u,θ, we assume that $\frac{dh_j}{d\theta}$ is monotonic. Under these conditions,

$\hat{\theta}$ = arg max $h(x, q, u, \theta)$ is a vertex of Θ. More specifically,

$$\hat{\theta}_j^k(x) = \begin{cases} \theta_{max}^k, \dfrac{dh_j}{d\theta^k} > 0 \\ \theta_{min}^k, \dfrac{dh_j}{d\theta^k} < 0 \\ \bar{\theta}, \dfrac{dh_j}{d\theta^k} = 0 \end{cases}$$

For all inequalities $h_j \leq 0, j = 1...n_h$, we include the critical vertex $\hat{\theta}_j$ and solve the reduced MS problem:

$$\begin{aligned} & min \quad f(q) \\ s.t. \quad & g_{i,k}(x_k, q, u_k, \theta_k) = 0, \quad i = 1..n_g, k = 1..n_h \\ & h_{j,k}(x_k, q, u_k, \theta_k) \leq 0, \quad j = 1..n_h, k = 1..n_h \end{aligned} \tag{6.7}$$

Notice that $f(q)$ in formulation 6.6 $\geq f(q)$ in formulation 6.7, since x, q, and u obtained by formulation 6.6 are always feasible for formulation 6.7. On the other hand, based on the monotonicity assumption, $f(q)$ from formulation 6.7 is also feasible for problem 6.6. Therefore, $f(q)$ for formulation 6.7 is the same as in problem 6.6. Since the monotonic assumption may not always hold, a feasibility test is applied for all $j = 1..n_h$.

$$\begin{aligned} & max \quad \beta_j = h_j(x, q, u^*, \theta) \\ s.t. \quad & g_i(x, q, u^*, \theta) = 0, \quad i = 1..n_g \end{aligned} \tag{6.8}$$

where u^* is optimal solution obtained from Eqn. 6.7. If $\beta > 0$, then add the critical θ as a new scenario and solve Eqn. 6.7 again. The steps to obtain a robust and optimal reactor configuration under uncertainty are outlined below and the flowchart is presented in Fig. 6.2.

- Step 1. Solve the optimization problem in Eqn. 6.4 with uncertain parameters at the nominal value, and obtain the optimal decision profiles q^* and u^*. Record the value of each inequality

constraint $h_j(x^*, q^*, u^*, \bar{\theta})$, $j = 1...n_h$.

- Step 2. Find the scenarios that are worst-case violations of constraints. Assume the uncertain parameters affecting the inequality constraints monotonically.
  - Set $\theta = [\theta^1, \theta^2..., \theta^{n_d}]$, where n_d is total number of the uncertain parameters.
  - Set $\theta_k = [\theta^1, \theta^2..., \theta^k + \delta * \theta^k..., \theta^{n_d}]$, $k = 1...n_d$, where δ represent a small perturbation to the uncertain parameters.
  - For $k = 1...n_d$, solve $g_i(x, q^*, u^*, \theta_k) = 0$ and record the value of the inequality constraint $h_j(x, q^*, u^*, \theta_k) = h_{j,k}$
  - If $h_{j,k} - h_j(x^*, q^*, u^*, \bar{\theta}) > 0$, set $\theta_j^k = \theta_U^k$, where θ_U represents the upper range of uncertain parameter.
  - If $h_{j,k} - h_j(x^*, q^*, u^*, \bar{\theta}) < 0$, set $\theta_j^k = \theta_L^k$, where θ_L represents the lower range of uncertain parameter.
  - If $h_{j,k} - h_j(x^*, q^*, u^*, \bar{\theta}) = 0$, set $\theta_j^k = \bar{\theta}^k$, where $\bar{\theta}$ represents the nominal value of uncertain parameter.
  - In the end, we would obtain n_h number of worst cases θ. However, some worst cases might be duplicates. Hence, we use n_s to represent the number of worst scenarios, where $n_s \leq n_h$
- Step 3. Solve the MS problem with $m = 1...n_s$ and obtain the optimal solution for decision variable q^{**}.

$$\begin{aligned} & min \quad f(q) \\ s.t. \quad & g_{i,m}(x_m, q, u_m, \theta_m) = 0, \quad i = 1..n_g, m = 1...n_s \\ & h_{j,m}(x_m, q, u_m, \theta_m) \leq 0, \quad j = 1..n_h, m = 1...n_s \end{aligned} \tag{6.9}$$

- Step 4. Fix q with the optimal solution in the previous step. And conduct a Monte Carlo sampling over the uncertainty range Θ to sample n_o number of scenarios. For each new

uncertain parameter set $\theta_o, o = 1...n_o$, solve the optimization problem below to check for feasibility. If there no constraint violation, then stop. Otherwise, add the worst infeasible point as a new scenario and go back to step 3 to solve the MS problem again.

$$\begin{aligned} min \quad & f(q^{**}) + C * \sum_{j=1}^{n_h} p_j \\ s.t. \quad & g_i(x, q^{**}, u, \theta_o) = 0, \quad i = 1..n_g \\ & h_j(x, q^{**}, u, \theta_o) \leq p_j, \quad j = 1..n_h \\ & p_j \geq 0, \quad j = 1..n_h \end{aligned} \tag{6.10}$$

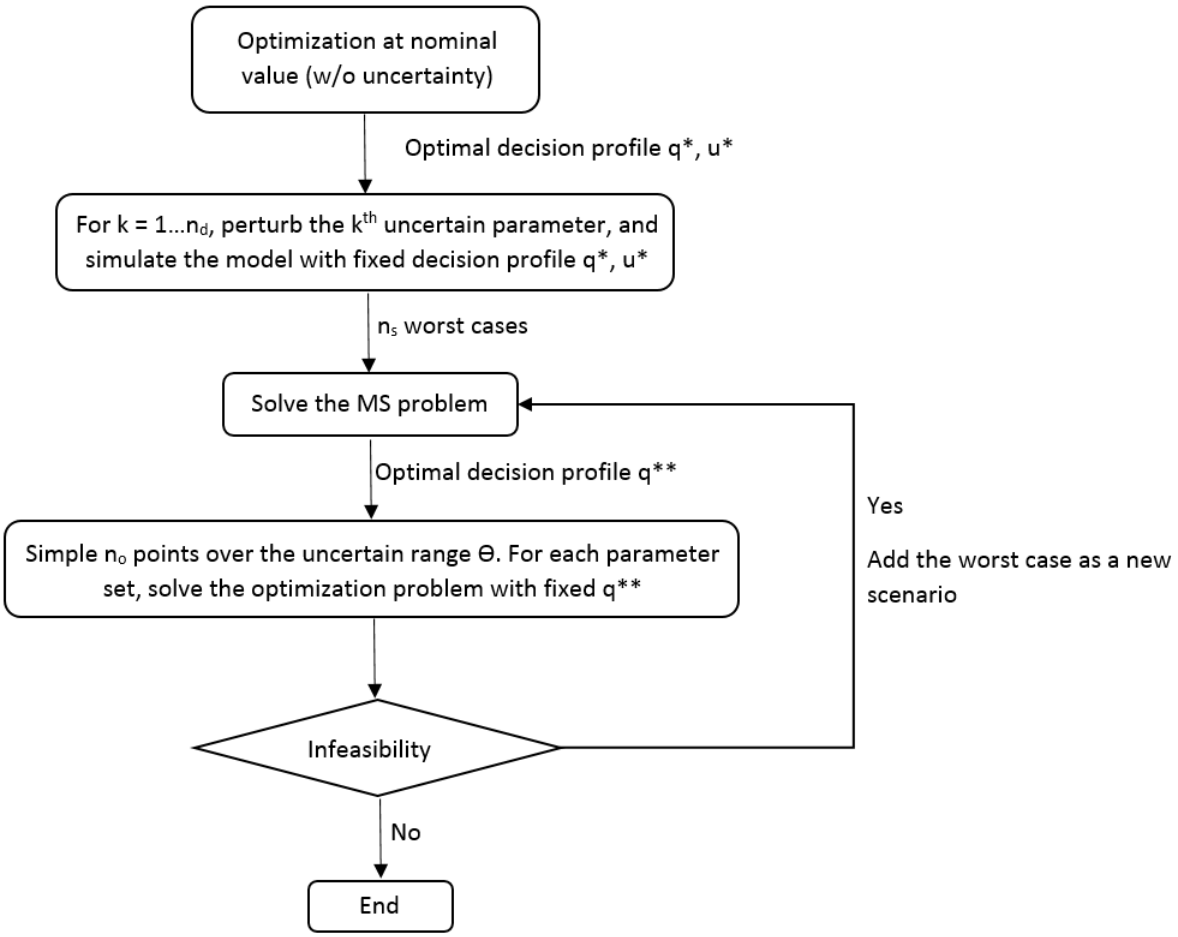

Figure 6.2. Multi-scenario Flow Chart

6.4 CSTR Configuration Design Under Uncertainty

In rigid polyol production, there exist various sources of uncertainties. In Chapter 3, we work on kinetic parameter estimation. Due to limited experimental data, the confidence ranges of the kinetic parameters are quite large. Since kinetic parameters play an important role in the model performance and accuracy, we focus on developing operating recipe for CSTR reactor structure which is applicable to produce three kinds of polymers over a wide range of kinetic parameters. All three rigid polyols follow the reactor scheme described in Table 5.2. However, each polyol is formulated by different initiator and monomer, as described in Table 5.1. In addition, Tables 5.3, and 5.4 show the kinetic parameters at nominal values for monomer PO and EO, respectively. In this study, we assume that the kinetic parameters of monomer PO are uncertain, and the uncertainty range is listed in Table 6.1, where the subscript $ini, prop, trf$ represent the initiation, propagation and transfer reaction, respectively. A stands for Arrhenius constant, Ea is the active energy.

Table 6.1 Uncertain Kinetic Parameters of PO with Corresponding Deviation

Model Parameter	Deviation	Unit
A_{ini}	ln(A) = 30 $\pm$ 1.9	$\frac{cm^3}{mol*min}$
Ea_{ini}	E = 18.6 $\pm$ 1.5	$\frac{kcal}{mol}$
A_{prop}	$\pm$ 10%	
Ea_{prop}	$\pm$ 10%	
A_{trf}	$\pm$ 10%	
Ea_{trf}	$\pm$ 10%	

The detailed model is shown in Chapter 5. It contains three main parts: 1). mass balance for initiator, monomer and growing/dormant product/unsaturated polymers, 2). energy balance for heat exchange between reactor and cooling jacket, 3). product quality and safety specifications. Since

inequality plays an important role when dealing with uncertainty, we label these specifications for convenience, where subscript p stands for polymer type $p \in A, B, C$, n is the CSTR index, l is the polymer chain length, m represents monomer, cat denotes catalyst. The superscript LB and UB represent the lower and upper bound, respectively.

- 1. An upper bound for PDI – $h_1(p) = PDI_p - PDI_p^{UB} \leq 0$.
- 2. A lower bound for production – $h_2(p) = production_p^{LB} - production_p \leq 0$
- 3. An upper bound for outlet weight percentage of monomer – $h_3(p) = WP_{m,p,N} - MAX\, mo \leq 0$.
- 4. An upper bound for outlet weight percentage of catalyst – $h_4(p) = WP_{cat,p,N} - WP_{cat,p}^{UB} \leq 0$.
- 5. An upper bound for adiabatic temperature – $h_5(p,n) = \kappa WP_{m,p,n} + T_n - T_{safety} \leq 0$.
- 6. An upper bound for heat released during the process – $h_6(p,n) = H_{p,n} - MAX\, UA_n \leq 0$.
- 7. A lower bound for molar flow rate of catalyst – $h_7(p,n) = \sum_l (F_{G_{p,n,l}} + F_{Q_{p,n,l}}) - F_{cat_{p,n}} \leq 0$,
- 8. A lower bound for OH number – $h_8(p) = OH\, num_p^{LB} - OH\, num_p \leq 0$.
- 9. An upper bound for OH number – $h_9(p) = OH\, num_p - OH\, num_p^{UB} \leq 0$.

The objective function is minimizing the capital cost and the CSTR optimization problem can be summarized as follows, where n is the index of CSTR, q stands for common decision variable (does not vary with polymer type), including reactor volume, heat exchanger capacity $MAXUA_n$, monomer injection points (binary variable β, and separation unit capacity MAX_{MO}. On the contrary, u represents decision variable that depends on polymer type. It contains reactor temperature, feeding rates of monomer, catalyst and initiator. p denotes the polymer types. There are three kinds

of polymers: A, B, and C. $g(\cdot)$ and $h(\cdot)$ represent the equality and inequality constraint, respectively. Equality constraints come from mass and energy balance. Inequality constraints result from the safety and product specifications. θ is the uncertain kinetics parameter.

$$\begin{aligned} min \quad & CC = f(q) \\ s.t. \quad & g_p(x_p(n), q(n), u_p(n), \theta_p) = 0, \quad p \in \{A, B, C\} \\ & h_p(x_p(n), q(n), u_p(n), \theta_p) \leq 0, \quad p \in \{A, B, C\} \\ & \beta_n \in \{0, 1\} \end{aligned} \tag{6.11}$$

The CSTR model at nominal value can be solved by MINLP solver sbb, and the optimal decision profile can be found in Section 5.4.1.

6.4.1 Back-off Results

The optimal CSTR structure at nominal value consists of four CSTRs in series. Only the first three CSTRs come with monomer injection points (monomer is added to the first three CSTRs). In addition, catalyst is fed to the first CSTR only. The detailed decision profile is described in Table 5.10. The decision profile is fixed to the optimal solution at nominal value, and Monte Carlo simulation is carried out with the number of trials $m = 100$. Fig. 6.3 shows the sampling points.

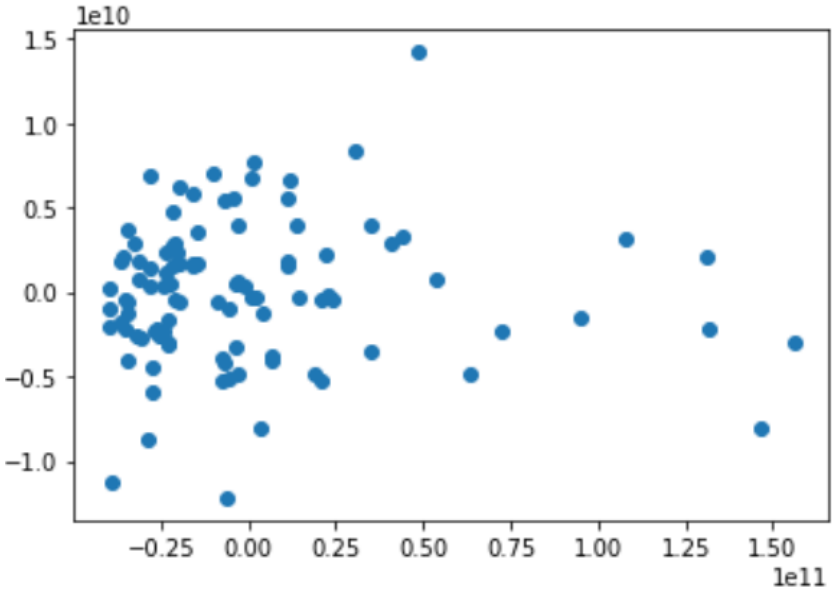

Figure 6.3. Sampling Points

The relative standard deviations S (scaled with corresponding upper or lower bound) for each inequality are listed in Table 6.2. The standard deviation for polymer B is relative small with those of polymer A and C. This is expected, since only the parameter uncertainty in PO kinetics, are considered and polymer B is based on EO kinetics.

Table 6.2 Standard Deviations of Inequality Constraints

Inequality Constraint	Polymer A	Polymer B	Polymer C
h_1	0.28	0.00	0.24
h_2	0.0024	0.00	0.0020
h_3	0.14	0.00	0.20
h_4	0.00	0.00	0.0018
$h_5(1)$	0.055	0.00052	0.15
$h_5(2)$	0.058	0.00	0.076
$h_5(3)$	0.033	0.0079	0.11
$h_5(4)$	0.0044	0.00	0.0064
$h_6(1)$	0.025	0.00029	0.077
$h_6(2)$	0.042	0.00028	0.074
$h_6(3)$	0.036	0.0073	0.11
$h_6(4)$	0.025	0.0073	0.096
$h_7(1)$	0.071	0.00	0.030
$h_7(2)$	0.066	0.0049	0.056
$h_7(3)$	0.073	0.00	0.053
$h_7(4)$	0.068	0.00	0.078
h_8	0.046	0.00	0.063
h_9	0.043	0.00	0.059

After obtaining the standard deviation, back-off terms can be calculated using $b_c = \eta * S$. And the optimization problem in Eqn. 6.2 can be solved with the back-off terms. For this study, η can only extend to 0.019, which means only 1.54% of the uncertainty range can be covered by the back-off method. We start to observe constraint violations when the uncertainty range exceeds 1.54%. There are 7 constraint violations in total. Fig. 6.4 and 6.5 shows the PDI and OH number

constraint violations, respectively. The x-axis is the uncertainty range in percentage and the y-axis is the violation percentage based on its corresponding bound. Since the lower bound for molar flow rate of catalyst is not a fixed value, the violation amount is scaled to a constant. The first constraint being violated is the PDI constraint of polymer A, its violation amount could reach 90% if 100% of the uncertainty range was covered. The PDI constraint of polymer C is violated when the uncertainty range goes to 30%. Its biggest violation amount is close to 65%. The violations for OH number are much lower compared with the ones for PDI constraint. When the uncertainty range approaches to 15%, the violation in catalyst molar flow rate constraint starts to appear.

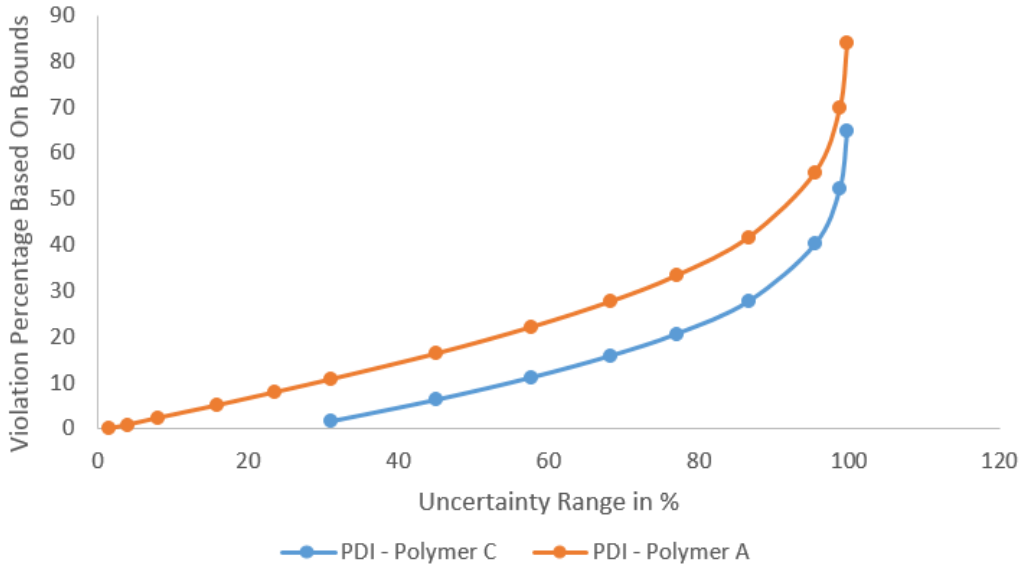

Figure 6.4. PDI Constraint Violation

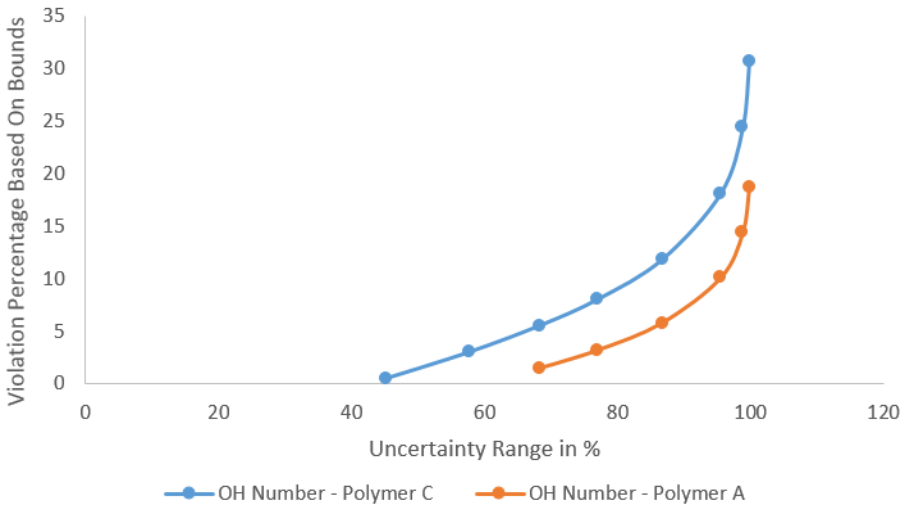

Figure 6.5. OH Number Constraint Violation

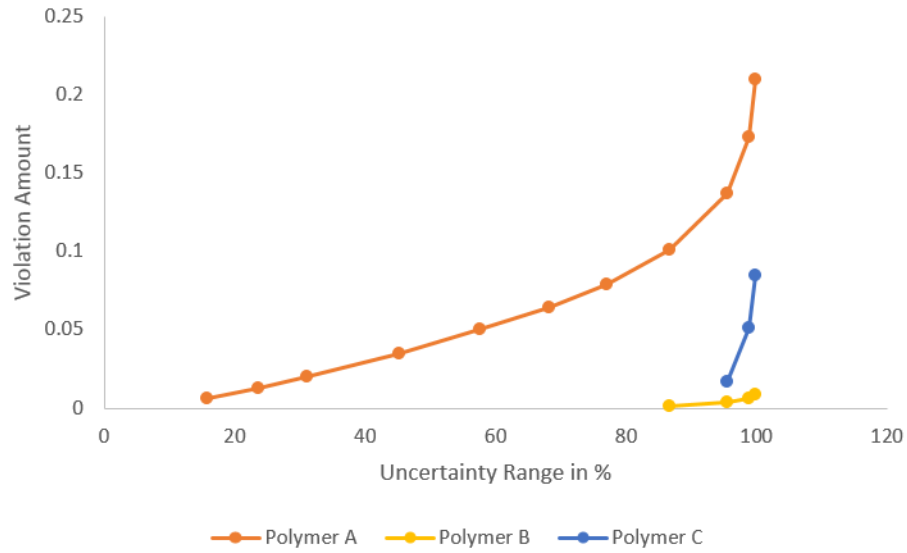

Figure 6.6. Molar Flow Rate of Catalyst Constraint Violation

Although the back-off method can only cover a small fraction of the uncertainty range, the capital cost is already 1.52 times larger than the one at nominal value. The relative optimal decision variables (scale to upper limit) are displayed in Tables 6.3 and 6.4. After applying the back-off method, the optimal values for reactor size, heat exchanger capacity, and separation unit capacity increase. In additional, the number of monomer injection points increases from 3 to 4. Therefore, the uncertainty in kinetic parameters has a strong effect on the CSTR structure design. Because of

the conservative design for the back-off method, it will not be considered for the DSR and CSTR followed by a DSR cases.

Table 6.3 Back-off Optimal Decision Profile for Common Decision Variable q

Common Decision Variable	Relative Optimal Value
V_1	0.016
V_2	0.027
V_3	0.041
V_4	0.21
HX_1	1.05
HX_2	1.02
HX_3	0.87
HX_4	0.97
SU	15910

Table 6.4 Back-off Optimal Decision Profile

Decision Variable	Polymer A	Polymer B	Polymer C
FR_{ini}	0.28	0.11	0.15
FR_{cat}	$1.00 * 10^{-3}$	$3.50 * 10^{-4}$	$2.00 * 10^{-3}$
$FR_{m,1}$	0.092	0.048	0.052
$FR_{m,2}$	0.068	0.017	0.024
$FR_{m,3}$	0.058	0.028	0.00
$FR_{m,4}$	0.025	0.020	0.0034
T_1	1.00	0.95	1.00
T_2	1.00	0.92	1.00
T_3	1.00	1.00	0.83
T_4	1.00	0.91	0.75

6.4.2 Multi-scenario Results

Step 1. Optimization at nominal value

In order to satisfy all the product and safety specifications, at least 4 CSTRs are required. And 4 CSTRs in series has the lowest capital cost according to Fig. 5.9. In addition, the optimal reactor configuration contains 3 monomer injection points (no monomer injection point for the last CSTR) and 1 catalyst injection point. The optimal decision profile is listed in Table 5.10.

Step 2. Find the scenarios that are worst-case violations of constraints

According to Table 6.1, there are 6 uncertain kinetic parameters (n_d = 6). For $k = 1...n_d$, we perturb the kth kinetic parameter with $\delta = 0.01$, and simulate the results with decision profile being fixed to the optimal results obtained from step 1. Then, evaluate the effect of the uncertain parameters on inequality constraints by calculating $\frac{dh_j}{d\theta^k}$. If it is greater than 0, then we set θ_j^k to its upper range and use $'+'$ to denote it. If it is less than 0, then we set θ_j^k to its lower range and use

$'-'$ to denote it. If it equals to 0, then we set θ_j^k to its nominal value and use $'0'$ to denote it. In the end, we would obtain a set of kinetic parameters for each inequality constraint. For this case study, there are 6 unique sets of kinetic parameters, which are displayed in Table 6.5.

Table 6.5 Worst Scenarios

Model Parameter	S1	S2	S3	S4	S5	S6
A_{ini}	+	+	-	0	+	+
A_{prop}	+	+	-	0	+	+
A_{trf}	+	+	-	0	+	+
Ea_{ini}	+	+	-	0	+	+
Ea_{prop}	+	-	-	0	-	0
Ea_{trf}	+	+	-	0	-	-

Step 3. Solve the MS problem

The multi-scenario method can cover 2.3% of the uncertainty range listed in Table 6.1. When the uncertainty range expands beyond 2.3%, we start to observe constraint violations. The first constraint that is violated is the PDI constraint for polymer A, followed by polymer C's PDI constraint. Fig. 6.7 shows the violation percentage based on corresponding upper bounds. Although PDI constraint of polymer A starts to be violated when uncertainty range expands beyond 2.3%, the violation amount is below 10% when uncertainty range reaches 30%. When the uncertainty range goes to 40%, PDI constraint for polymer C starts to be violated. Finally, when we reach 100% of the uncertainty range, the violation percentages are 41.7% and 26.5% for PDI constraint of polymer A and C, respectively.

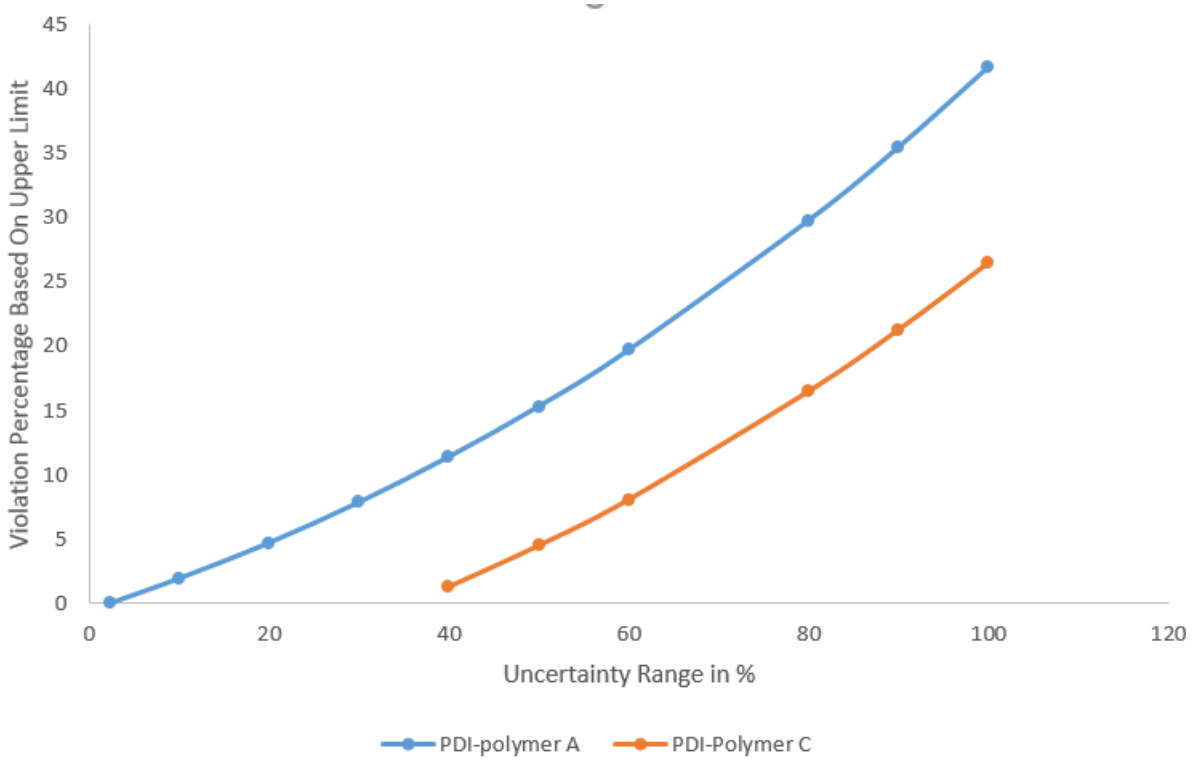

Figure 6.7. Constraint Violations

The capital cost for the multi-scenario model is 1.07 times larger than the capital cost at nominal value. It consists of 4 CSTRs, 4 monomer injection points and 1 catalyst injection point (catalyst is injected into the first CSTR only). The relative values of decision variables are displayed in Tables 6.6, 6.7, 6.8 and 6.9. These decision variables are scaled based on their upper bounds. V is the reactor volume, HX represents the heat exchanger capacity. SU stands for the capacity of the monomer separation unit. FR represent the feeding rate. T is temperature. The numeric subscript denotes the index of CSTR. The subscript ini, cat and m stands for initiator, catalyst, and monomer, respectively. If we compare the MS optimal common decision profile with the one at nominal value, it is not hard to observe that MS formulation requires larger reactor, higher capacities for heat exchanger and separation unit. This is expected, since the MS method includes multiple worst cases besides the one at nominal value. The feeding profiles of MS are close to the ones at nominal value. For polymer B, the feeding and temperature profiles do not vary with different scenarios. This is expected, since we only assume the kinetic parameters related to monomer

PO are uncertain. And polymer B is polymerized by EO, which has certain kinetics.

Table 6.6 MS Optimal Decision Profile for Common Decision Variable q

Common Decision Variable	Relative Optimal Value
V_1	0.00226
V_2	0.00414
V_3	0.00560
V_4	0.08304
HX_1	1.157
HX_2	0.320
HX_3	0.276
HX_4	0.850
SU	5810

Table 6.7 MS Optimal Decision Profile for Polymer A

Decision Variable	S1	S2	S3	S4	S5	S6
FR_{ini}	0.093	0.089	0.087	0.093	0.089	0.093
FR_{cat}	$2.59 * 10^{-4}$	$2.59 * 10^{-4}$	$2.59 * 10^{-4}$	$2.59 * 10^{-4}$	$2.59 * 10^{-4}$	$2.59 * 10^{-4}$
$FR_{m,1}$	0.029	0.029	0.029	0.027	0.029	0.029
$FR_{m,2}$	0.021	0.021	0.022	0.022	0.022	0.021
$FR_{m,3}$	0.016	0.018	0.018	0.018	0.017	0.015
$FR_{m,4}$	0.0072	0.0068	0.0066	0.0070	0.0074	0.0086
T_1	1.00	1.00	1.00	0.96	1.00	1.00
T_2	1.00	1.00	1.00	1.00	1.00	0.99
T_3	1.00	1.00	1.00	1.00	1.00	1.00
T_4	1.00	1.00	1.00	1.00	1.00	1.00

Table 6.8 MS Optimal Decision Profile for Polymer B

Decision Variable	S1	S2	S3	S4	S5	S6
FR_{ini}	0.11	0.11	0.11	0.11	0.11	0.11
FR_{cat}	$3.45 * 10^{-4}$	$3.45 * 10^{-4}$	$3.45 * 10^{-4}$	$3.45 * 10^{-4}$	$3.45 * 10^{-4}$	$3.45 * 10^{-4}$
$FR_{m,1}$	0.053	0.053	0.053	0.053	0.053	0.053
$FR_{m,2}$	0.016	0.016	0.016	0.016	0.016	0.016
$FR_{m,3}$	0.013	0.013	0.013	0.013	0.013	0.013
$FR_{m,4}$	0.030	0.030	0.030	0.030	0.030	0.030
T_1	1.00	1.00	1.00	1.00	1.00	1.00
T_2	1.00	1.00	1.00	1.00	1.00	1.00
T_3	1.00	1.00	1.00	1.00	1.00	1.00
T_4	1.00	1.00	1.00	1.00	1.00	1.00

Table 6.9 MS Optimal Decision Profile for Polymer C

Decision Variable	S1	S2	S3	S4	S5	S6
FR_{ini}	0.16	0.15	0.15	0.15	0.15	0.15
FR_{cat}	0.011	0.011	0.011	0.011	0.011	0.011
$FR_{m,1}$	0.062	0.051	0.047	0.060	0.056	0.069
$FR_{m,2}$	0.012	0.011	0.00019	0.011	0.011	0.011
$FR_{m,3}$	0.013	0.015	0.015	0.0016	0.0024	0.0008
$FR_{m,4}$	0.00	0.0004	0.017	0.0052	0.017	0.0062
T_1	0.89	0.97	0.79	0.94	0.91	0.97
T_2	1.00	1.00	0.95	0.93	0.91	0.94
T_3	0.98	1.00	0.97	0.93	1.00	0.92
T_4	0.87	0.87	0.74	0.86	0.84	0.87

Step 4. Feasibility test through Monte Carlo simulation

In order to verify the monotonic assumption, m points are sampled over the uncertainty range Θ. For each point, we exam its feasibility by solving the problem in Eqn. 6.10 with the common decision variable q fixed to the MS optimal solution. For this case study, m = 110. In order to present the sampling points in a two dimensional plot, principal component analysis (PAC) is applied to lower the uncertain vector θ from 6-dimension to 2-dimension. In Fig. 6.8, the green dots represent the new sampling points, and the red dots denote the six scenarios applied in the MS formulation from step 3. After PCA, S1, S2, S5, and S6 are very close to each other, and collapse into one point (the red dot on the left).

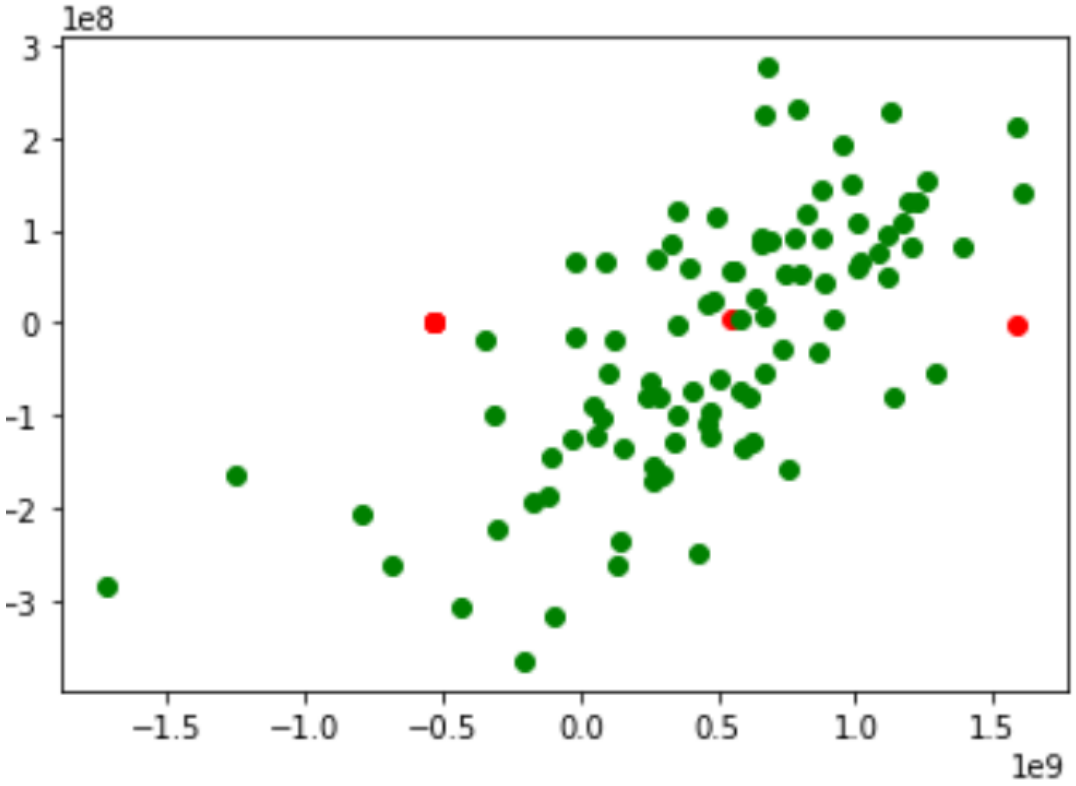

Figure 6.8. Sampling Points

For all the sampling points, the optimization problem in Eqn. 6.10 is feasible, which confirms the monotonic assumption. The box plots below show the distributions for the values of inequality constraints. Box Plot displays the summary of the set of data values having properties like min-

imum (Q1 - 1.5*IQR), first quartile (Q1), median (Q2), third quartile (Q3) and maximum (Q3 + 1.5*IQR). IQR stands for the interquartile range, which equals to Q3 - Q1. If a value is above the maximum or below the minimum, it is considered as an extreme value and denoted by a circle. In the box plot, a box is created from the first quartile to the third quartile, a horizontal line is also there which goes through the box at the median. Here x-axis denotes the polymer type, while the y-axis shows the frequency distribution.

Fig. 6.9 shows the distribution of the PDI constraint. The PDI value of Polymer A is very close to its upper bound. On the contrary, for polymer B, its PDI value is well below the upper limit.

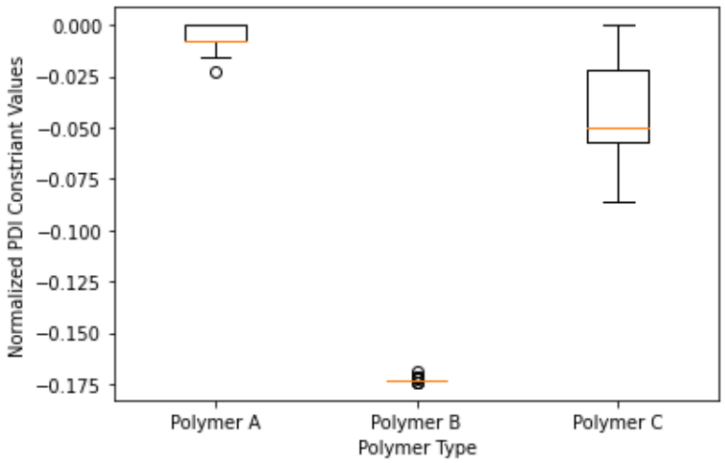

Figure 6.9. Distribution of PDI Constraint h_1

For all three polymers, the median of production constraint is near 0, which means for half of the cases, the production rate is at its lower bound. Polymer C is more flexible regarding this constraint compared with the other two polymers.

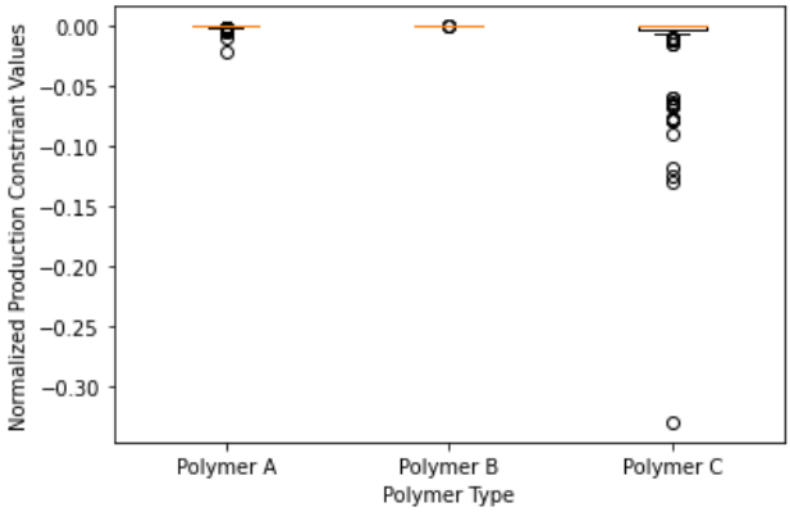

Figure 6.10. Distribution of Production Constraint h_2

For the outlet weight percentage of monomer constraint, medians of polymers A and B are near 0 (at upper bound). For most of the cases, the constraint value for polymer C is well below the upper limit.

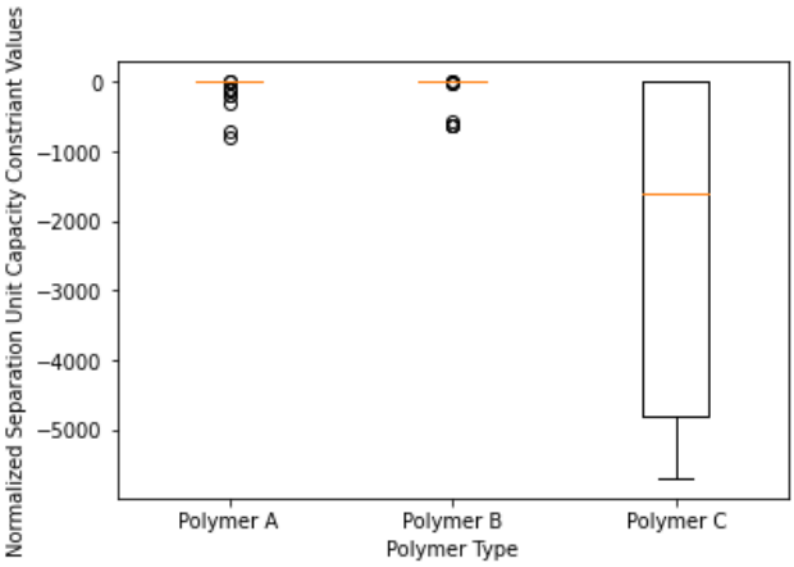

Figure 6.11. Distribution of Outlet Weight Percentage of Monomer Constraint h_3

For the outlet weight percentage of catalyst constraint, the values of polymers A and B are always at 0 (at upper bound). For half of the cases, the constraint values for polymer C are below the upper limit.

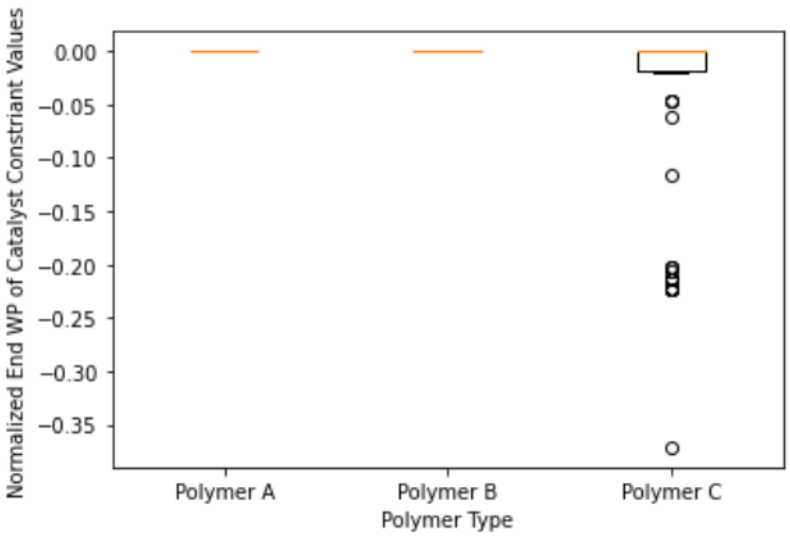

Figure 6.12. Distribution of Outlet Weight Percentage of Catalyst Constraint h_4

For the adiabatic temperature constraint, the highest values for all polymers are below 0, which means the adiabatic temperature constraint is not active.

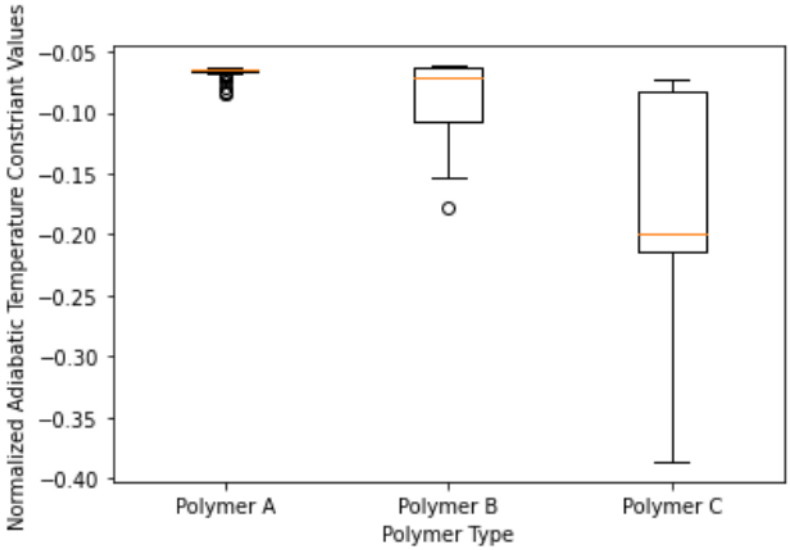

Figure 6.13. Distribution of Adiabatic Temperature Constraint h_5

For polymer B, its heat release amount is near or at the upper bound. However, the heat release amounts for polymers A and C are well below the upper bound. This is expected, since polymer B is based on EO, which would generate more heat per mole of reacted monomer.

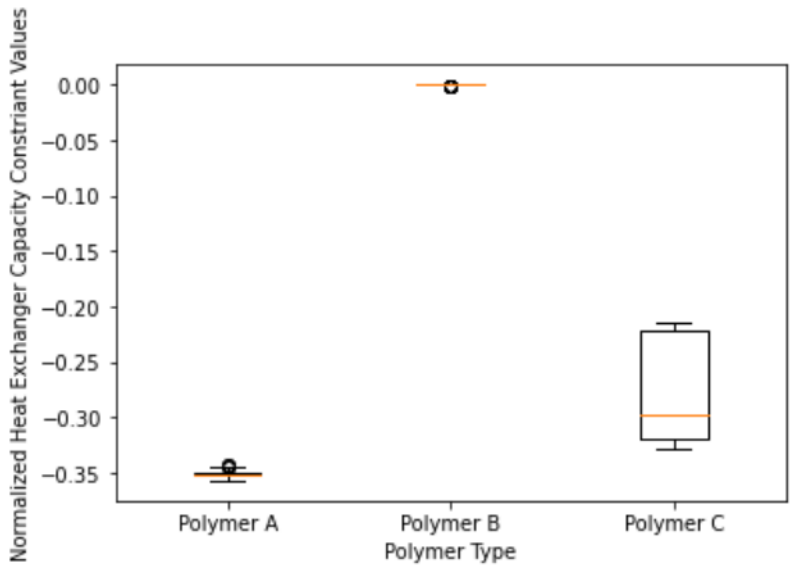

Figure 6.14. Distribution of Heat Release Constraint h_6

For polymers A and B, the catalyst molar flow rate constraint is always at its lower bound. This is not the case for Polymer C, since we have a high tolerance regarding catalyst amount in the reactor for polymer C.

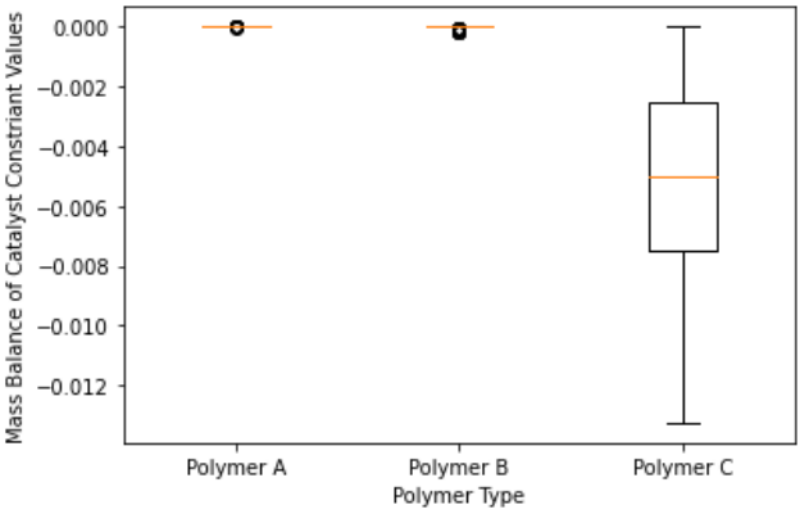

Figure 6.15. Distribution of Catalyst Molar Flow Rate Constraint h_7

Combining Figs. 6.16 and 6.17 we can tell that Polymer B tends to have an OH number close to its upper bound. On the contrary, the OH number for polymer C is close to its lower limit.

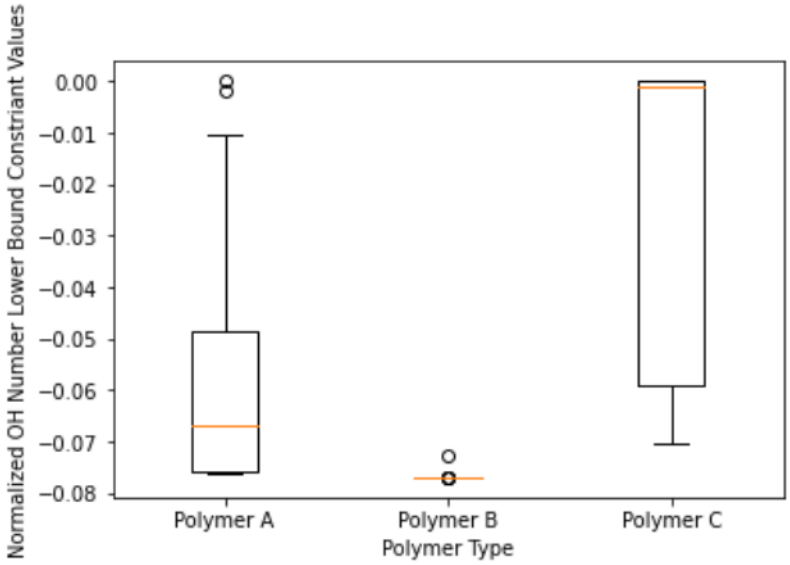

Figure 6.16. Distribution of OH Number Lower Bound Constraint h_8

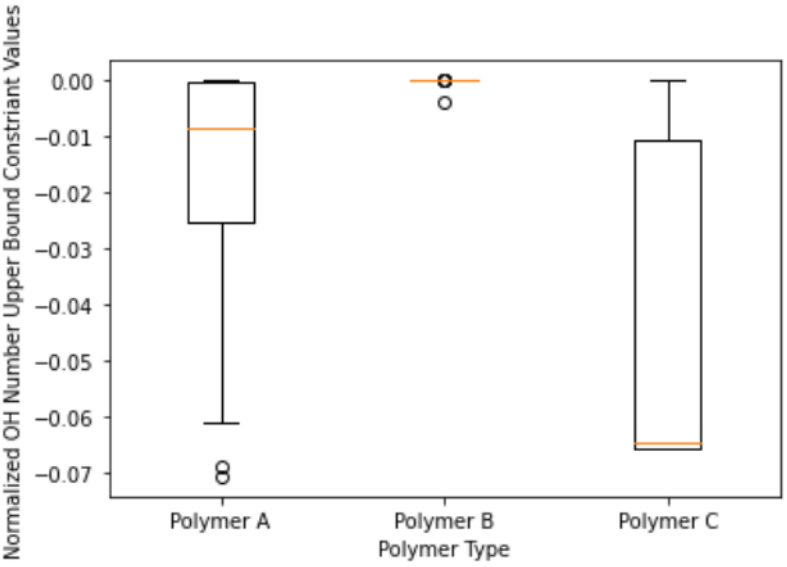

Figure 6.17. Distribution of OH Number Upper Bound Constraint h_9

6.5 DSR Configuration Design Under Uncertainty

According to Section 5.4.1, with the help of DSR, polymers with lower PDIs could be generated. Since PDI constraints are the ones that can be easily violated in the CSTR configuration design under uncertainty, we expect reactor networks contain DSR to handle a wider range of uncertainty.

In the section, we apply the MS method to two reactor designs that contain DSR: single DSR and a CSTR followed by a DSR, to examine the impact of uncertainty in kinetic parameters.

6.5.1 Single DSR

The six scenarios in Table 6.5 have been applied to the single DSR MS design. This design can cover 100% of the uncertainty range. In addition, the optimal design contains 13 monomer injection points and its optimal capital cost is 2.37 times larger than the one at nominal value. The increase in capital cost is caused by the increase in reactor volume, capacities of heat exchanger and separation unit. The relative optimal feeding rates of initiator and catalyst, as well as the optimal capacities of heat exchanger and separation unit are listed in Table 6.10. And the relative optimal monomer feeding rates and temperature profiles for these six scenarios are shown in Figs. 6.18, 6.19 and 6.20. All of these relative values are scaled to their upper bounds. The optimal profiles of polymer B do not vary with scenario, since we are only considering the parameter uncertainty in PO kinetics and polymer B is based on monomer EO, whose kinetics are certain.

Table 6.10 MS Optimal Decision Profile of Single DSR

Scenario	S1	S2	S3	S4	S5	S6
	Polymer A					
FR_{ini}	0.089	0.089	0.091	0.089	0.091	0.12
FR_{cat}	$2.58 * 10^{-4}$	$2.71 * 10^{-4}$	$2.70 * 10^{-4}$	$2.62 * 10^{-4}$	$2.78 * 10^{-4}$	$3.33 * 10^{-4}$
	Polymer B					
FR_{ini}	0.10	0.10	0.10	0.10	0.10	0.10
FR_{cat}	$3.46 * 10^{-4}$	$3.46 * 10^{-4}$	$3.46 * 10^{-4}$	$3.46 * 10^{-4}$	$3.46 * 10^{-4}$	$3.46 * 10^{-4}$
	Polymer C					
FR_{ini}	0.45	0.34	0.50	0.37	0.38	0.52
FR_{cat}	0.034	0.027	0.038	0.028	0.030	0.043
HX	13.60					
$wp_{KOH,N}$	1940					

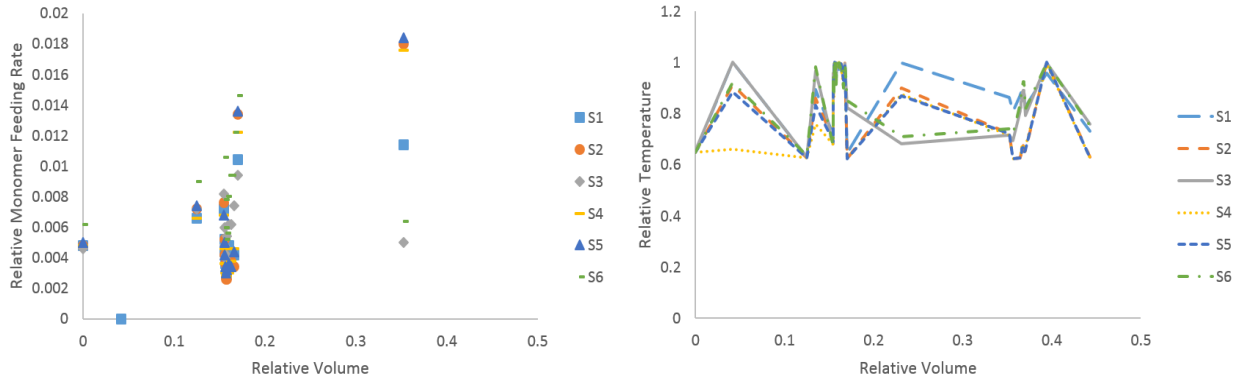

(a) Feed Profile

(b) Temperature Profile

Figure 6.18. MS Decision Profiles of Single DSR for Product A

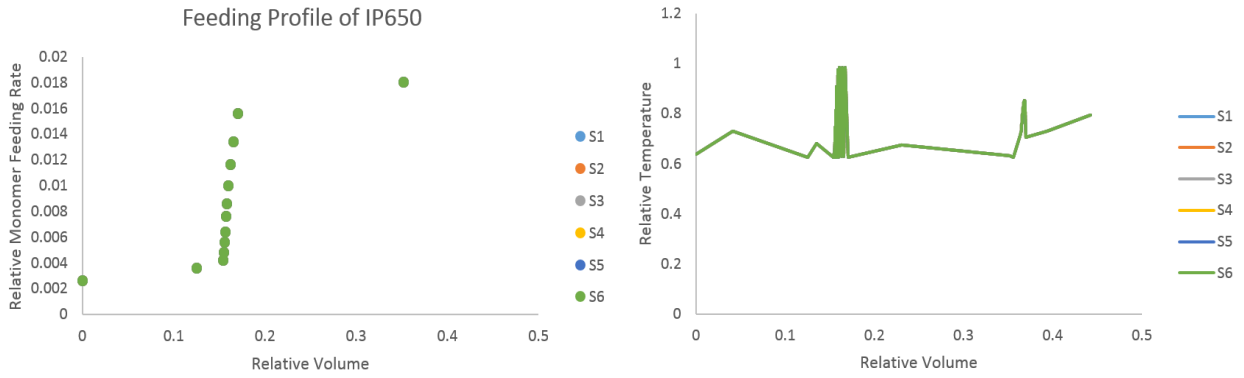

(a) Feed Profile (b) Temperature Profile

Figure 6.19. MS Decision Profiles of Single DSR for Product B

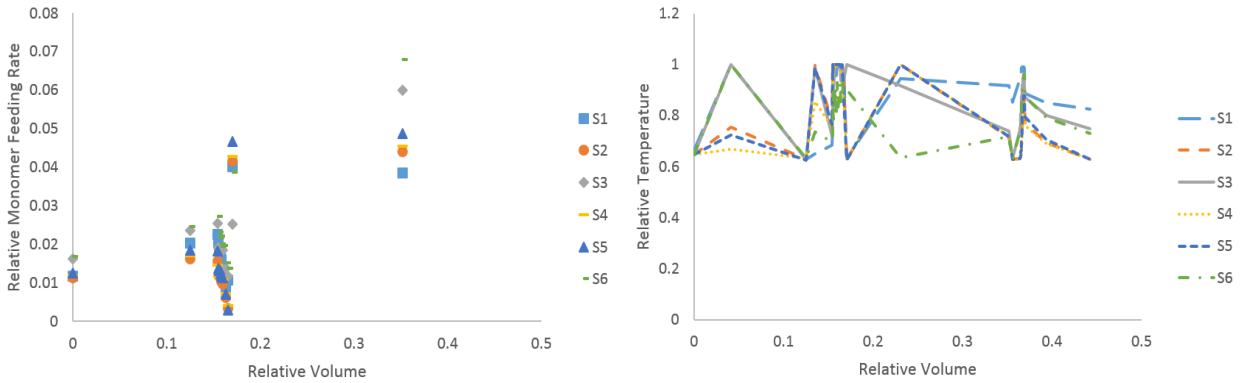

(a) Feed Profile (b) Temperature Profile

Figure 6.20. MS Decision Profiles of Single DSR for Product C

100 points are sampled to verify the MS results' feasibility. These 6-dimension kinetic parameter vectors are projected into 2-dimension using PCA and are denoted by the green dots in Fig. 6.21. The red dots represent the six scenarios applied in the MS formulation. S1, S2, S5, and S6 collapse into one point after projection (the rightmost point). The middle dot is S4, and the red dot on the left is S3.

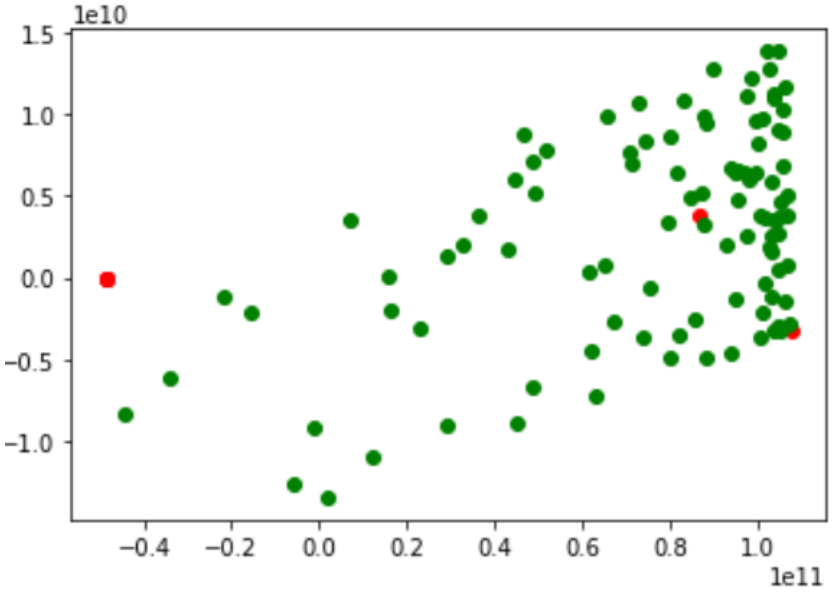

Figure 6.21. Sampling Points Projected in 2D

For all the sampling points, we obtain a feasible solution to Eqn. 6.10, which confirms the monotonic assumption. The box plots below show the value distributions of inequality constraints. Fig. 6.22 shows the distribution of the PDI constraint. For polymer A, the median of the constraint value is at zero, which implies the PDI constraint is active for the most of the time. For the other two products, the PDI constraint's medians are away from zero. This is expected, since polymer A has the lowest PDI upper limit, followed by polymer C.

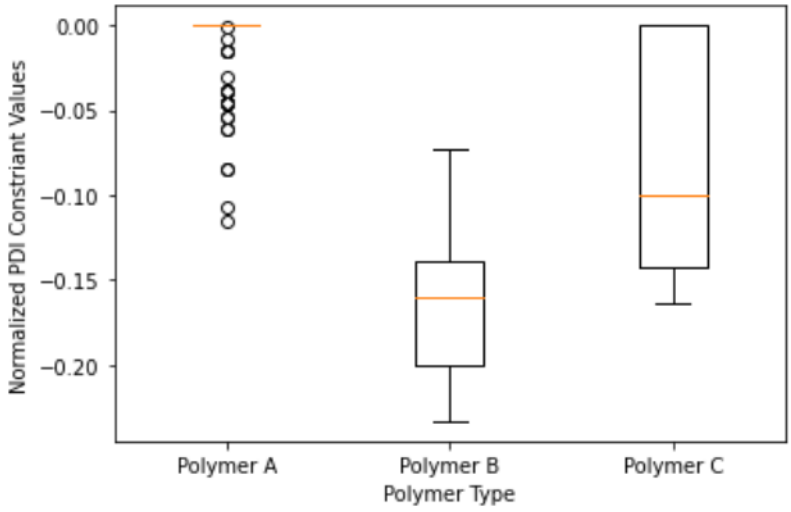

Figure 6.22. Distribution of PDI Constraint h_1

For polymers A and B, the medians of production constraint are near zero, which means for half of the cases, the production rate is at its lower bound. Polymer C is more flexible regarding this constraint compared with the other two polymers.

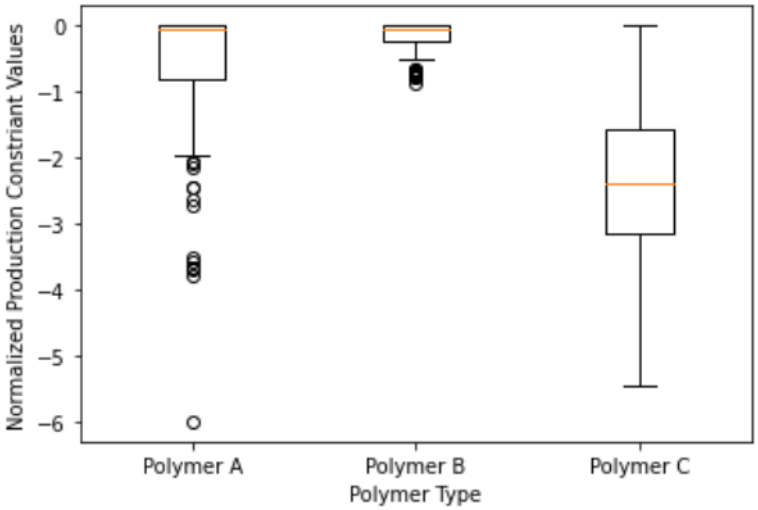

Figure 6.23. Distribution of Production Constraint h_2

For the outlet weight percentage of monomer constraint, all the medians are away from zero. Therefore, the separation unit capacity is larger enough to cover all the cases.

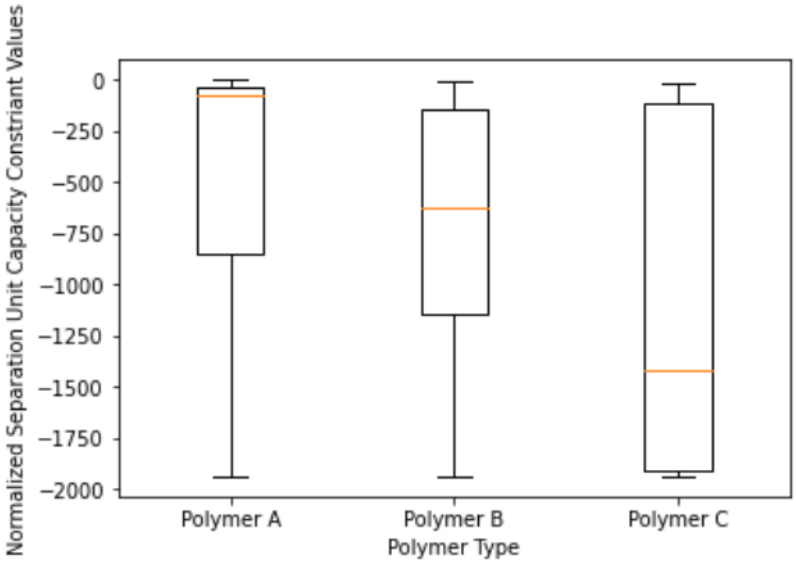

Figure 6.24. Distribution of Outlet Weight Percentage of Monomer Constraint h_3

For the outlet weight percentage of catalyst constraint, the constraint values of polymers A and

B are always zero (at upper bound). The median of polymer C is a little bit below zero. This is expected, since polymer C has a higher upper limit for this constraint.

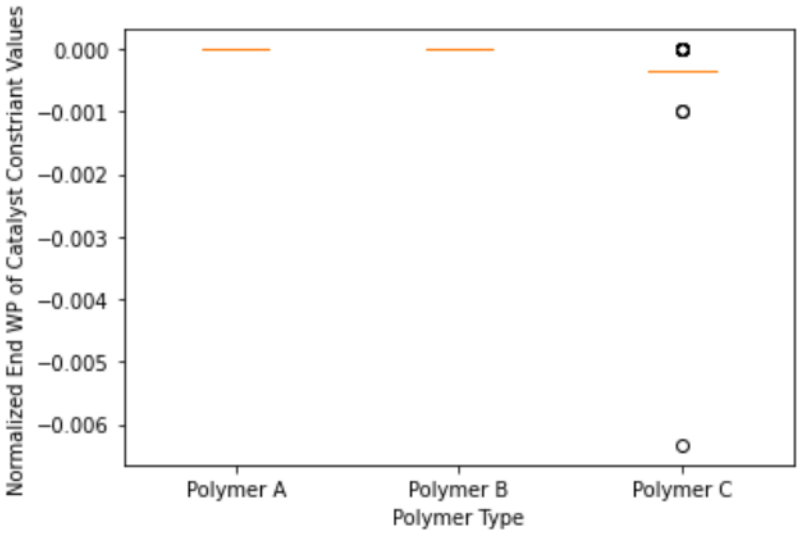

Figure 6.25. Distribution of Outlet Weight Percentage of Catalyst Constraint h_4

For the adiabatic temperature constraint, the highest constraint values for all polymers are below zero, which means the adiabatic temperature constraint is not active.

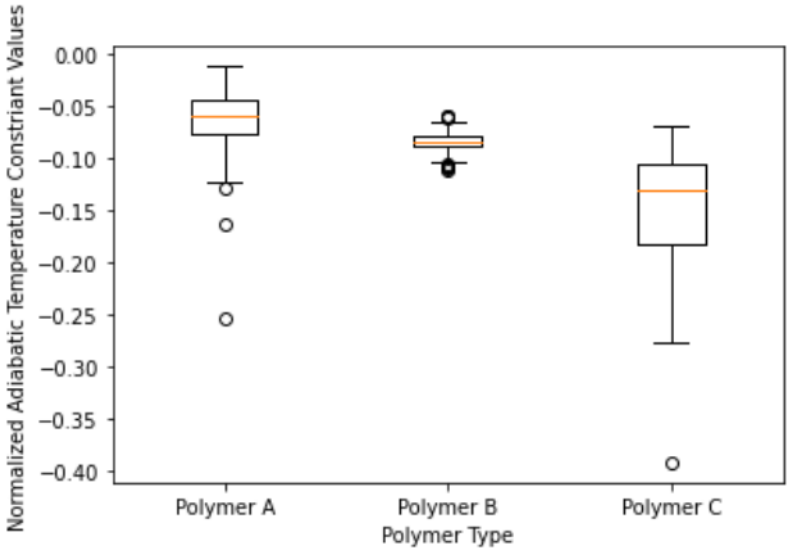

Figure 6.26. Distribution of Adiabatic Temperature Constraint h_5

According to Fig. 6.27, polymer C tends to release more heat during the reaction. This is expected since polymer C has the highest production rate.

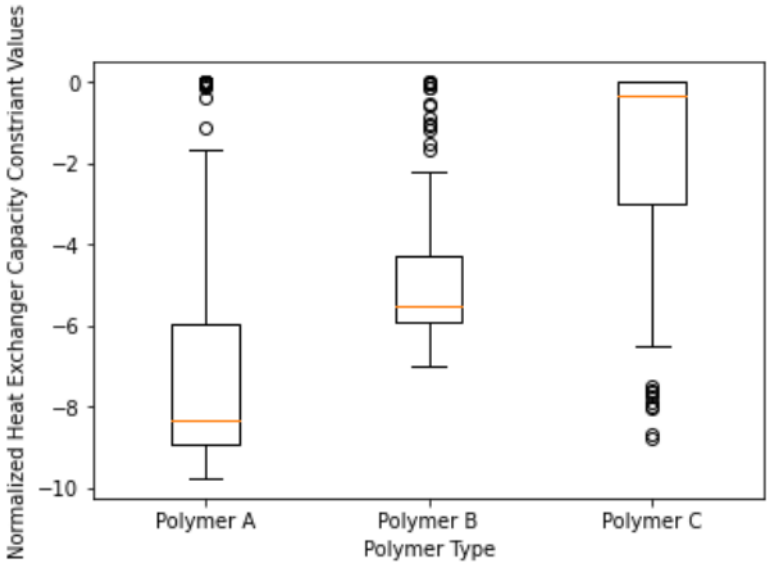

Figure 6.27. Distribution of Heat Release Constraint h_6

For polymers A and B, the catalyst molar flow rates are always at lower bounds. This is not the case for Polymer C, since we have a high tolerance regarding catalyst amount in the outlet stream for polymer C. Hence, more catalyst is fed to reactor when producing polymer C.

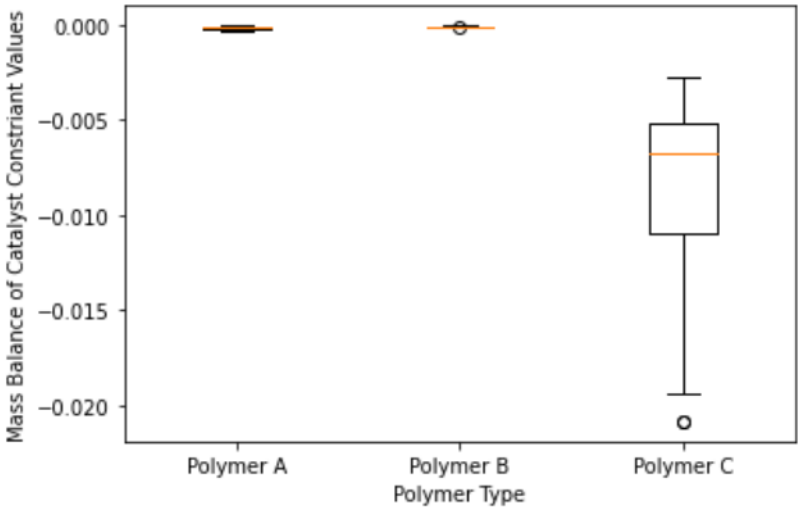

Figure 6.28. Distribution of Catalyst Molar Flow Rate Constraint h_7

Combining Figs. 6.29 and 6.30 we can find that Polymer B tends to have an OH number close to its upper bound. On the contrary, the OH numbers for polymers A and C are close to their lower limit.

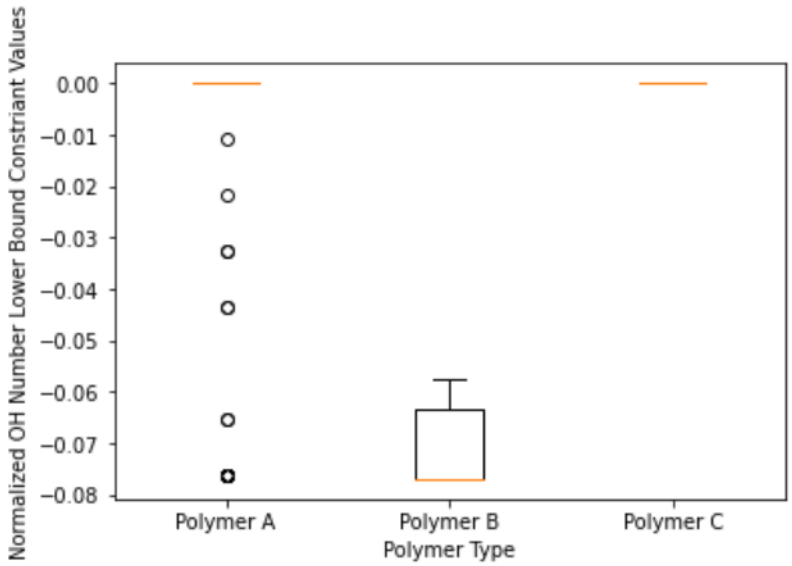

Figure 6.29. Distribution of OH Number Lower Bound Constraint h_8

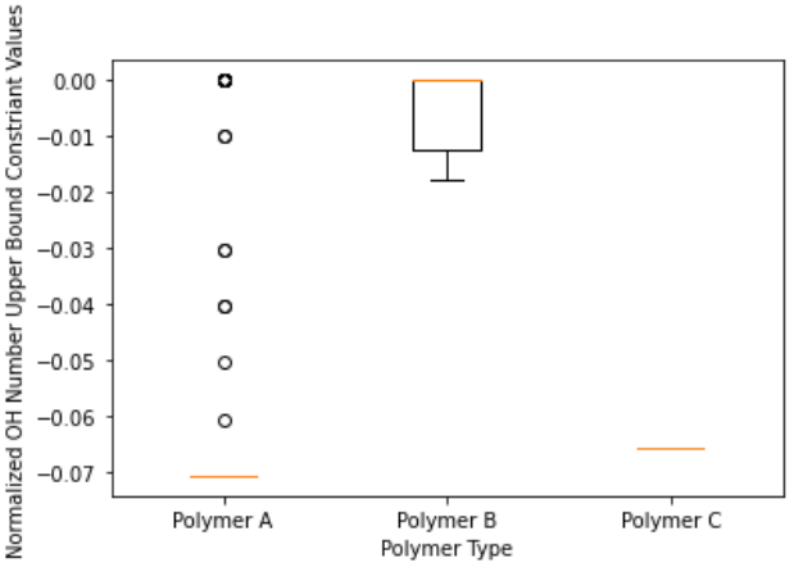

Figure 6.30. Distribution of OH Number Upper Bound Constraint h_9

6.5.2 CSTR Followed by a DSR

The MS design containing the scenarios in Table 6.5 can cover the whole uncertainty range. The optimal design contains one CSTR followed by a DSR with 5 monomer injection points and its optimal capital cost is 3.55 times higher than the one at nominal value. The increase in capital cost

is caused by the increase in reactor volume (both CSTR and DSR), capacities of heat exchanger and separation unit. The relative optimal feeding rates of monomer to the CSTR, initiator, and catalyst, as well as the optimal capacities of heat exchanger, separation unit, and CSTR volume, temperature are listed in Table 6.11. And the relative optimal monomer feeding rates to the DSR and DSR temperature profiles for these six scenarios are shown in Figs. 6.31, 6.32 and 6.33. All of these relative values are scaled to their upper bounds. The optimal profiles of polymer B do not change with scenario, since it uses EO for polymerization, and there is no uncertainty in EO kinetics.

Table 6.11 MS Optimal Decision Profile of CSTR Followed by a DSR

Scenario	S1	S2	S3	S4	S5	S6
	Polymer A					
FR_{ini}	0.087	0.087	0.22	0.082	0.22	0.14
FR_{cat}	$2.58 * 10^{-4}$	$2.58 * 10^{-4}$	$6.67 * 10^{-4}$	$2.69 * 10^{-4}$	$6.67 * 10^{-4}$	$6.67 * 10^{-4}$
FR_{mo} (CSTR)	0.039	0.016	0.17	0.029	0.17	0.092
T (CSTR)	1.00	1.00	1.00	1.00	1.00	1.00
	Polymer B					
FR_{ini}	0.091	0.091	0.091	0.091	0.091	0.091
FR_{cat}	$4.02 * 10^{-4}$	$4.02 * 10^{-4}$	$4.02 * 10^{-4}$	$4.02 * 10^{-4}$	$4.02 * 10^{-4}$	$4.02 * 10^{-4}$
FR_{mo} (CSTR)	0.081	0.081	0.081	0.081	0.081	0.081
T (CSTR)	1.00	1.00	1.00	1.00	1.00	1.00
	Polymer C					
FR_{ini}	0.40	0.51	0.51	0.35	0.51	0.52
FR_{cat}	0.030	0.038	0.041	0.027	0.041	0.045
FR_{mo} (CSTR)	0.19	0.18	0.19	0.054	0.19	0.19
T (CSTR)	1.00	1.00	1.00	1.00	1.00	1.00
HX (CSTR)	8.29					
HX (DSR)	4.40					
$wp_{KOH,N}$	0.01733					
V (CSTR)	1					

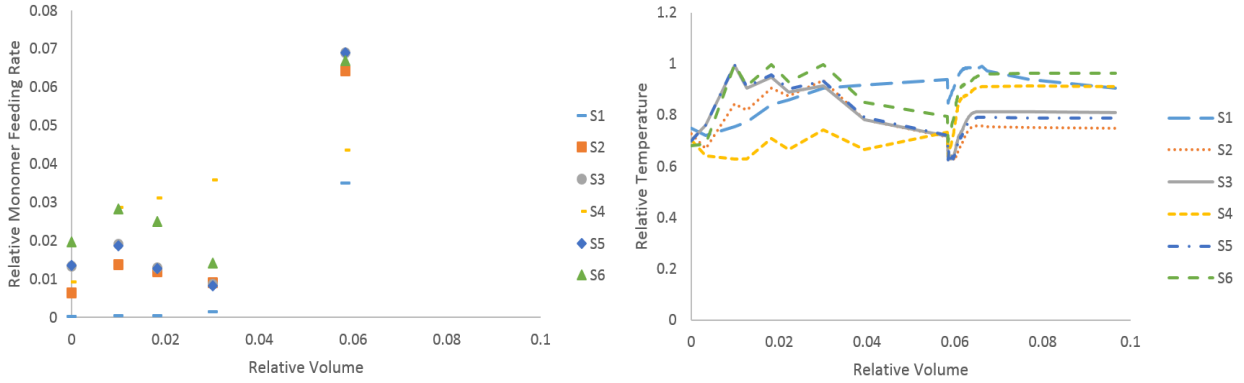

(a) Feed Profile (b) Temperature Profile

Figure 6.31. MS Decision Profiles of CSTR Followed by a DSR for Product A

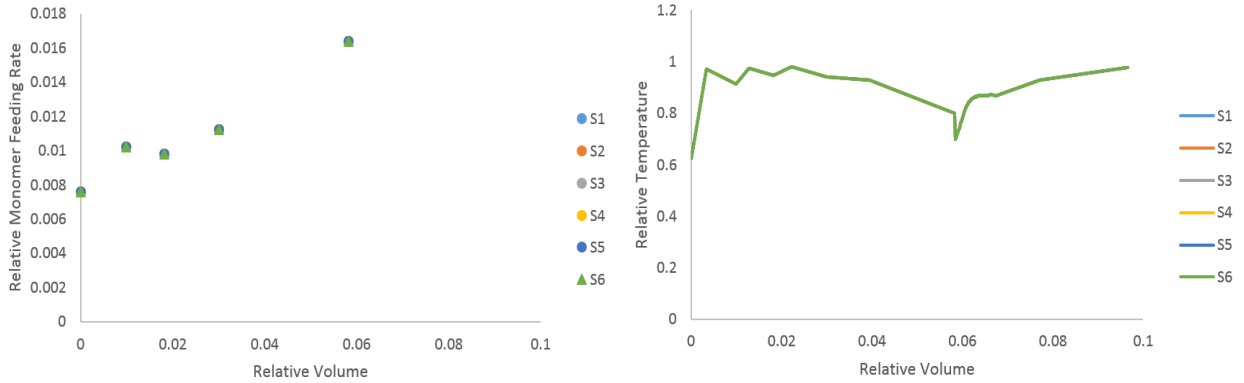

(a) Feed Profile (b) Temperature Profile

Figure 6.32. MS Decision Profiles of CSTR Followed by a DSR for Product B

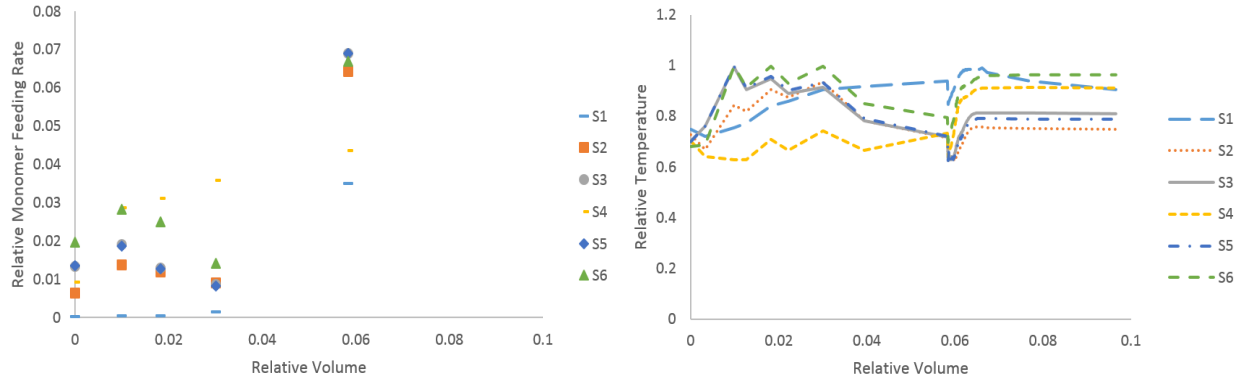

(a) Feed Profile (b) Temperature Profile

Figure 6.33. MS Decision Profiles of CSTR Followed by a DSR for Product C

We verify the feasibility of the MS design with 100 Monte Carlo samples of uncertain parameters, as shown in Fig. 6.21. For all the sampling points, we obtain a feasible solution to Eqn. 6.10, which implies the MS design should work for any point in the uncertainty range. The box plots below show the value distributions of inequality constraints. Fig. 6.34 shows the distribution of the PDI constraint. For polymers A and C, the medians of the constraint value are at zero, which implies the PDI constraint is active for the most of the time. For polymer B, the PDI constraint's median is below zero. This is expected, since polymer B has the highest PDI upper limit.

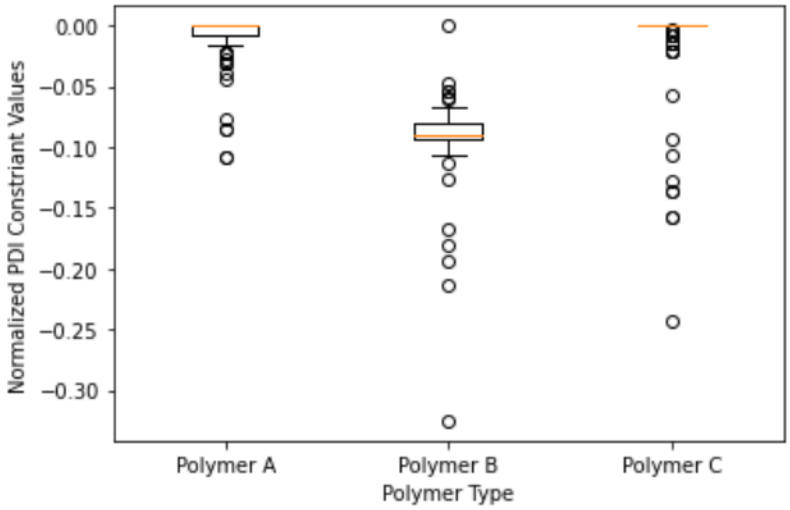

Figure 6.34. Distribution of PDI Constraint h_1

The median production rate of polymer A is the lowest, followed by polymers B and C. The outlet weight percentage of monomer constraint is always active for all three polymers, since the separation unit capacity is near zero, as shown in Table 6.11.

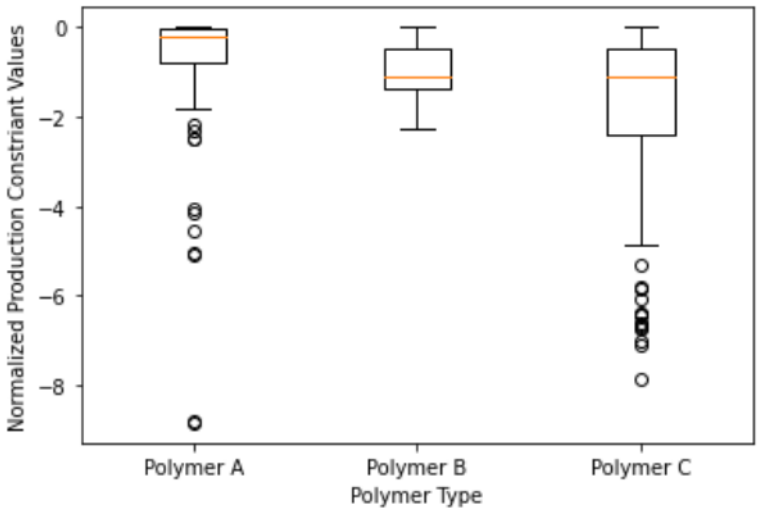

Figure 6.35. Distribution of Production Constraint h_2

For the outlet weight percentage of catalyst constraint, the constraint values of polymers A and B are always zero (at upper bound). The median of polymer C is a little bit below zero. This is expected, since polymer C has a higher upper limit for this constraint.

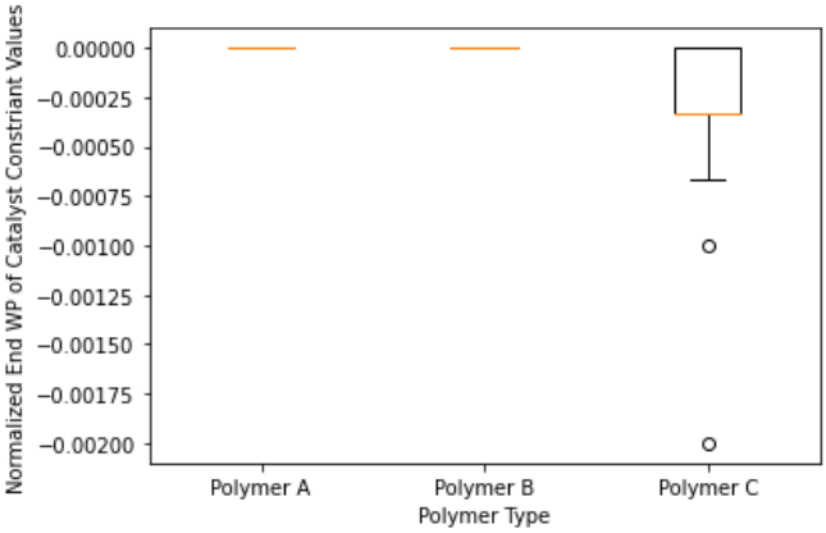

Figure 6.36. Distribution of Outlet Weight Percentage of Catalyst Constraint h_4

For the adiabatic temperature constraint, it is active in CSTR, but inactive in DSR.

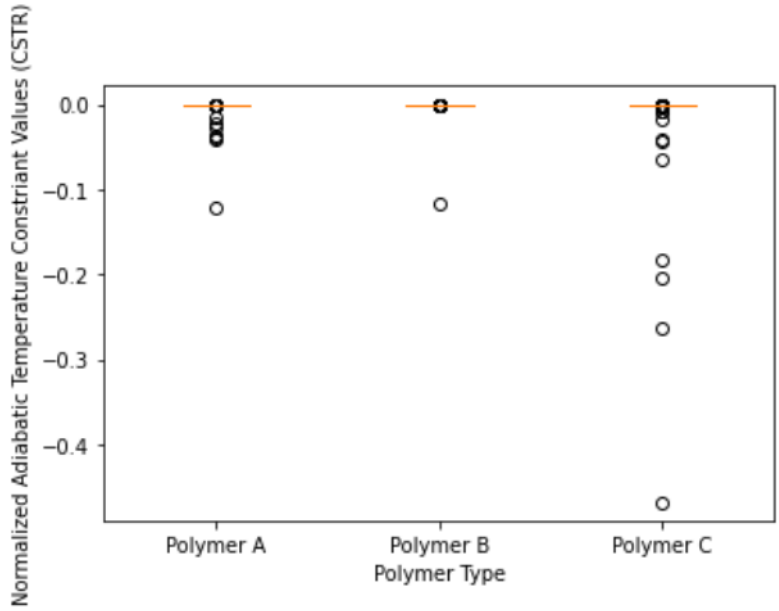

Figure 6.37. Distribution of Adiabatic Temperature Constraint in CSTR h_5

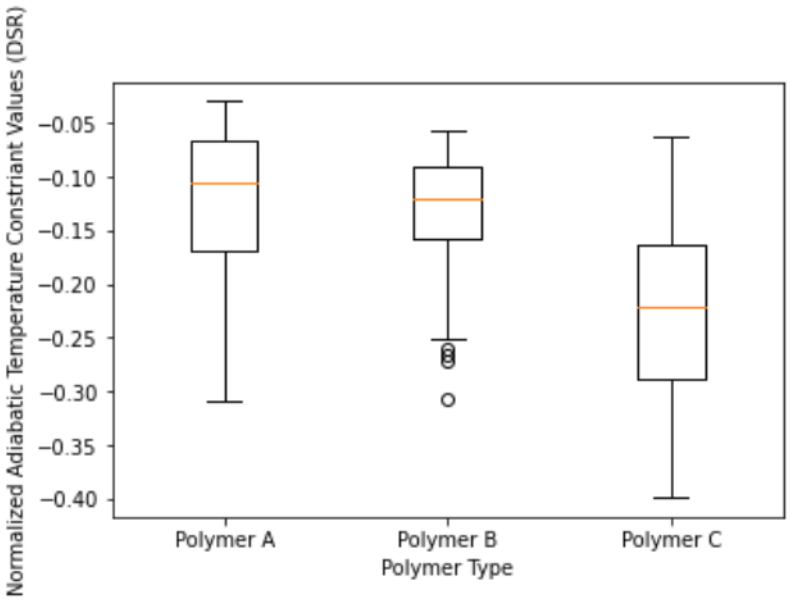

Figure 6.38. Distribution of Adiabatic Temperature Constraint in DSR h_5

According to Fig. 6.39 and 6.40, polymer B tends to release more heat during the production in both CSTR and DSR. This is expected since polymer B and C have similar production rate, and polymer B is based on EO, which would generate more heat per mole of consumption.

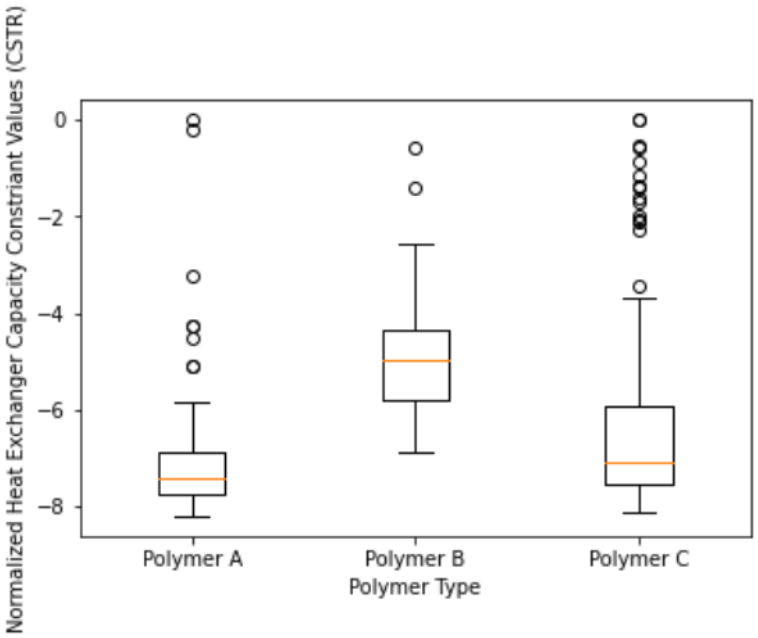

Figure 6.39. Distribution of Heat Release Constraint in CSTR h_6

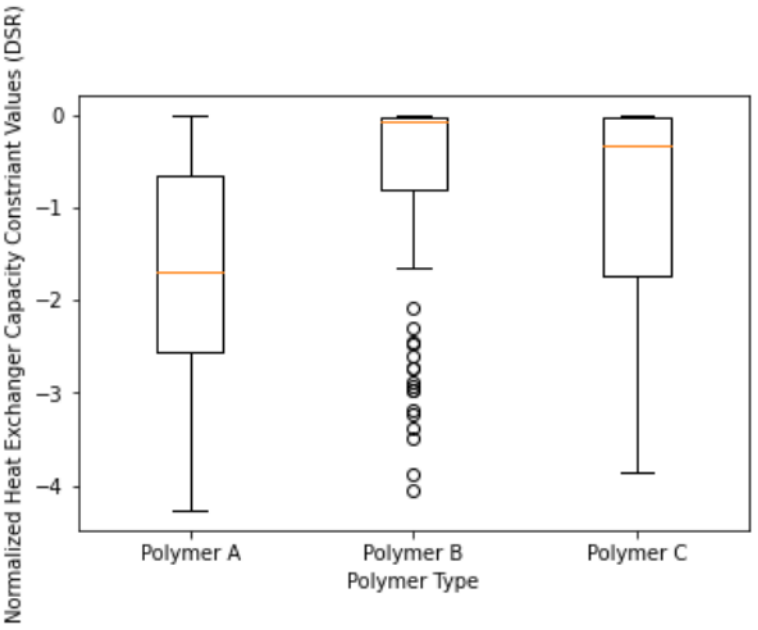

Figure 6.40. Distribution of Heat Release Constraint in DSR h_6

For polymers A and B, the catalyst molar flow rates are always active for both CSTR and DSR. This is not the case for Polymer C, since we have a high tolerance regarding catalyst amount in the outlet stream for polymer C. Hence, more catalyst can be added to the reactor when producing

polymer C.

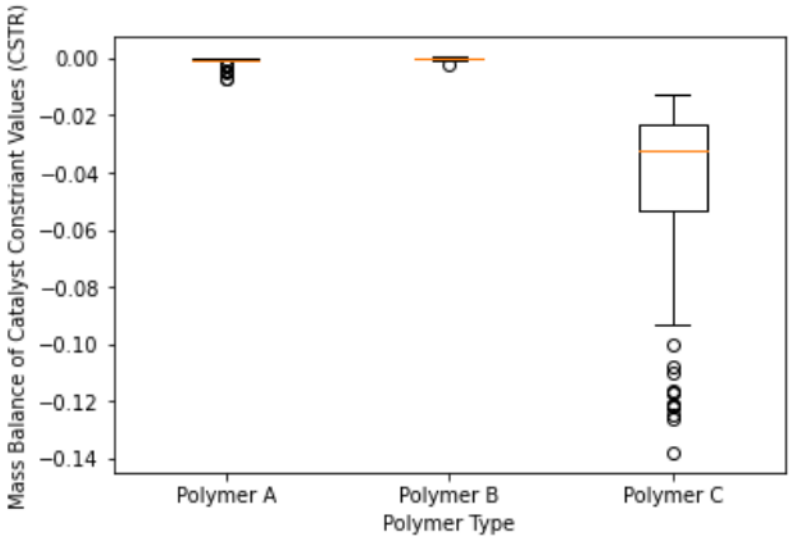

Figure 6.41. Distribution of Catalyst Molar Flow Rate Constraint in CSTR h_7

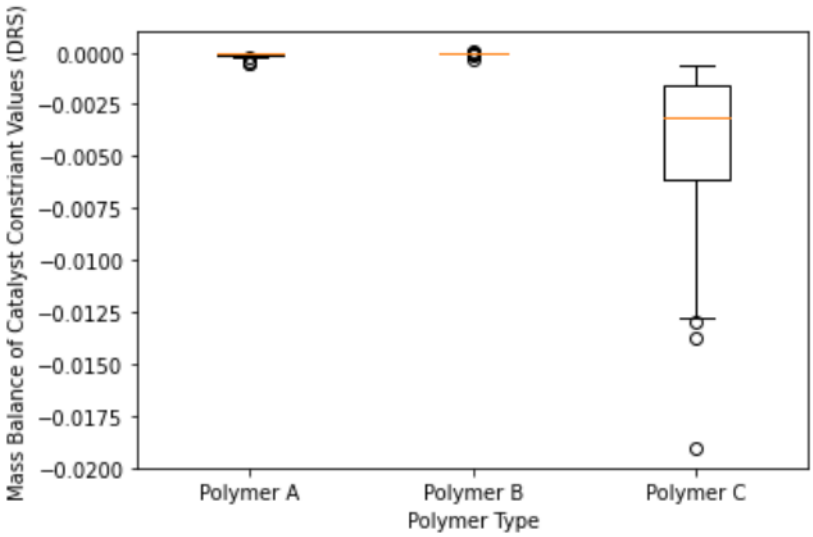

Figure 6.42. Distribution of Catalyst Molar Flow Rate Constraint in DSR h_7

Combining Fig. 6.43 and 6.44 we can tell that the OH numbers are closer to their lower bounds for all three polyol products.

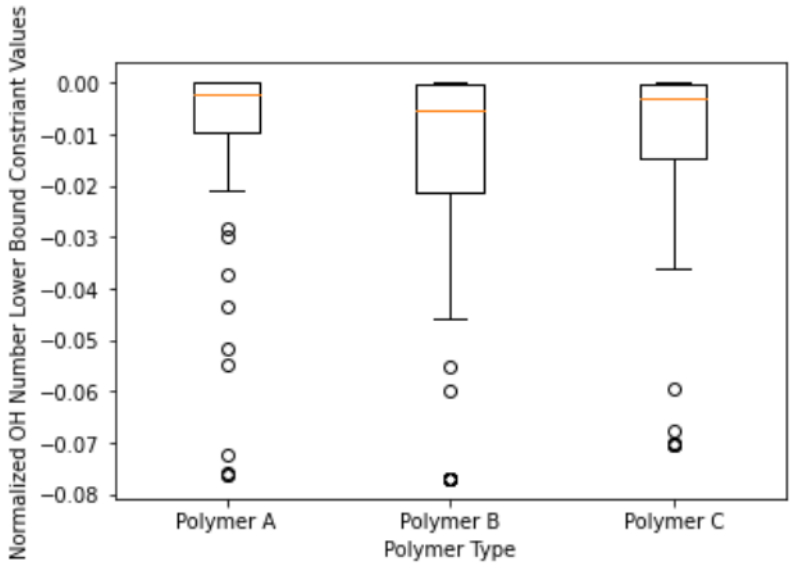

Figure 6.43. Distribution of OH Number Lower Bound Constraint h_8

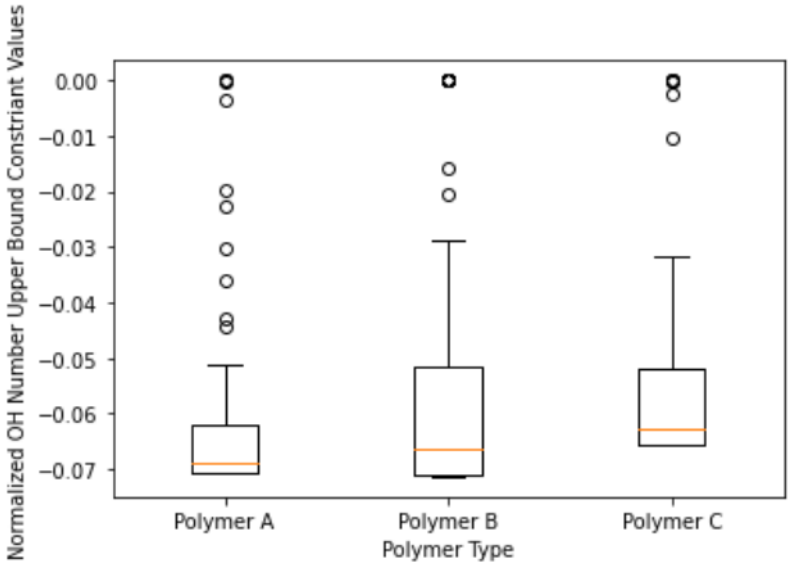

Figure 6.44. Distribution of OH Number Upper Bound Constraint h_9

6.6 Conclusions

The objective of this study is to analyze the effect of uncertainty in kinetic parameters on configuration design. In order to design a reactor network that would be feasible for any kinetic parameter set in the uncertainty range, back-off and multi-scenario method are adopted. The back-off method

is more conservative than the multi-scenario approach, since MS allows different scenario to have different operating recipe, while the common decision variables (reactor volume, injection points, capacity of heat exchanger and separation unit) are the same for all the scenarios. However, back-off method can operate without any additional measurements or resources. In order to apply MS in reality, we need to come up with a way to measure or estimate the kinetic parameters online.

When we apply the back-off method to the CSTR design, 1.54% of the uncertainty range can be covered. And 7 inequality constraints would be violated if the uncertainty range exceeded 1.54%. While the MS approach can cover 2.3% of the uncertainty range in CSTR design. And 2 inequalities would be violated when the uncertainty range exceeded 2.3%. Figs. 6.45 and 6.46 compares the violation amounts for these two different methods. The violations of MS occur after the back-off violations. And the violation amounts for MS are less than the back-off violation amounts. When the uncertainty range reaches 100%, the violation amounts of MS are half of the back-off violation amounts. In addition, according to Tables 6.3 and 6.6, the optimal reactor size, capacities of heat exchanger and monomer separation unit obtained by the back-off method are much larger. Furthermore, the optimal capital cost obtained from the back-off formulation is 1.42 times of MS optimal capital cost. All of these confirm that back-off method is more conservative than the MS approach.

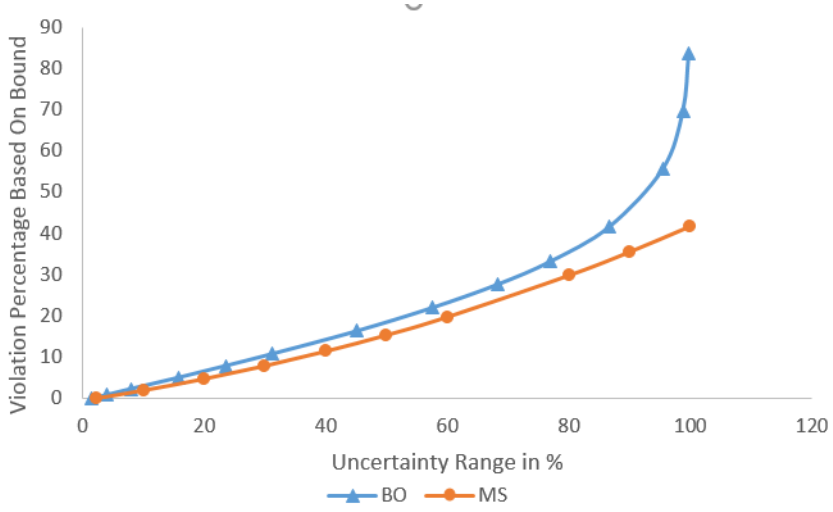

Figure 6.45. Violation Amount for PDI Constraint of Polymer A

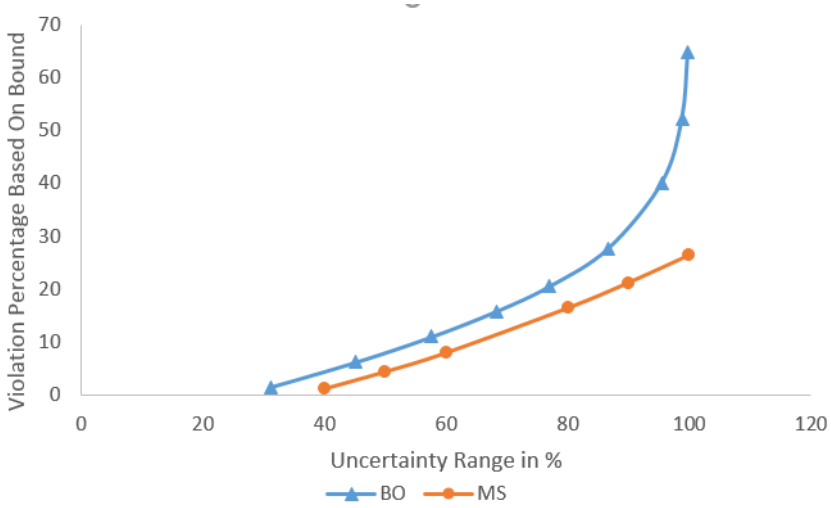

Figure 6.46. Violation Amount for PDI Constraint of Polymer C

We also apply the MS method to reactor networks that contain DSR, since DSR would result in polymers owning lower PDIs compared with CSTR, and PDI constraint is the one that is violated in the CSTR design. Both single DSR and CSTR followed by a DSR configurations can cover 100% of the uncertainty range. Table 6.12 summaries the relative optimal capital cost (scaled to the optimal capital cost of single DSR in Section 5.4.1) for each reactor network. Single DSR with 13 monomer injection points is the ideal configuration to handle uncertainty in kinetic parameters. It can cover the full uncertainty range, while it has a low relative capital cost.

Table 6.12 Relative Optimal Capital Cost for Different Reactor Networks

	CSTR (Back-off)	CSTR (MS)	DSR (MS)	CSTR + DSR (MS)
Uncertainty range can be covered	1.54%	2.30%	100.00%	100.00%
Relative optimal capital cost	4.35	3.06	2.37	3.87

Chapter 7 Conclusions

This work adopts model-based optimization, which is a classic strategy for process optimization. It has been widely used in multiple fields, including control, integration and online implement. Although nonlinear dynamic optimization problem requires high computational cost, it is valuable since it can capture detailed dynamic behavior in the process and provide more accurate solutions, especially when dealing with processes that are highly nonlinear.

The aim of this work is to design continuous reactor networks that are able to produce polymers that meet product specifications, as well as corresponding operating recipes. With the support of the advanced dynamic optimization methods, we construct detailed optimization models to estimate kinetic parameters, to design optimal reactor configurations and to adopt back-off and multi-scenario approach to deal with uncertainty in the polymerization process. This chapter summarizes the results of each chapter and recommend some future directions.

7.1 Summary and Contributions

Chapter 1 first analyzes the advantages and disadvantages of continuous process. Then, it explains the motivation behind this project, which is switching the polymer production from the existing semi-batch reactor to continuous process to lower the capital cost and to satisfy the increasing demand for rigid polyols. In addition, we introduce two important methods in reactor network design: superstructure approach and attainable region. The former one can determine the objective value, the optimal reactor network and operating conditions simultaneously. However, the optimal solution is only as rich as the proposed superstructure and the model formulations are typically

nonconvex, leading to many near-optimal solutions. Attainable region aims to find all possible outputs for all possible reactor configurations. However, attainable regions with more than two dimensions are hard to construct. At the end of this chapter, we mention two categories to deal with uncertainty: robust optimization and stochastic programming. Robust optimization is more conservative, but it does not require any additional measurement or resources.

Chapter 2 introduces the dynamic optimization approach, which is core technique that has been adopted throughout the entire thesis. It can also be applied to online applications, including predictive control, state estimation and online process identification. There are two general ways to solve a dynamic optimization problem: sequential approach and simultaneous method. Since sequential approach cannot handle path and inequality constraints directly in the sensitivity analysis, we adopt the simultaneous collocation method to discretize the continuous horizon into a finite element mesh. In this way, DAE problem is converted into NLP, which can be solved by sequential quadratic programming (SQP) method, generalized reduced gradient (GRG) method, and interior point method.

Chapter 3 aims to estimate the kinetic parameters for a polymerization process. The detailed reaction scheme, data sources as well as the dynamic optimization model formulation can be found in this chapter. In summary, there are six unknown kinetic parameters, two kinds of data sources. The optimal results obtained from these two data sources are not consistent with each other. This may be caused by the incompatibility of these two data sources. In addition, despite which data source is applied, more than half of the kinetic parameters cannot be estimated independently when the bounds for activation energies are not present. After adding the bounds for activation energies, fewer kinetic parameters have large standard deviations, but the activation energies solve to lower bounds (should probably be fixed).

Chapter 4 focuses on developing continuous reactor networks that are able to produce rigid polyols under strict product and safety specifications. Meanwhile, optimal operating conditions that would lead to the minimum capital cost are determined. In order to achieve this goal, we combine the ideas in Feinberg's works (CSTR and DSR play important roles in shaping the attainable region

boundary) and Lakshmanan's papers (solving reactor modules in an increasing manner). We first examine the reactor network with one CSTR or one DSR. Then, we enrich the reactor design by adding additional CSTR/DSR. This process is continued until there is no improvement in the objective function. In the end, five reactor networks are derived and compared. For each reactor network, the model consists of three main parts: material balance, energy balance, product and safety specifications. The results are summarized as following:

- Single CSTR: Product specifications cannot be satisfied, if only one CSTR is utilized.
- Single DSR: A DSR with 10 monomer injection pints has the lowest capital cost among the five examined reactor networks. In order to obtain the optimal injection profile, we discretize the DSR into 40 zones with equal volume and come up with an iterative approach (Fig. 4.3).
- Two CSTRs in series: The capital cost of two CSTRs in series is 2.64 times bigger than the one of DSR. Majority of the monomers are fed to the first reactor. Hence, the second reactor is functioned as a digestion system.
- CSTR followed by a DSR: The capital cost of two CSTRs in series is 1.2 times bigger than the one of DSR. Two monomer injections per DSR are enough to produce the desired rigid polyol. In the reactor configuration, the majority of the reactions occur within the CSTR. And the DSR is used to further digest the unreacted monomer in the reactor.
- DSR followed by a CSTR: As the number of monomer injection points per DSR reaches 6, the CSTR residence time drops to zero. This implies that is is not necessary to add a CSTR behind a DSR. Single DSR is enough to produce desired polymer.

Chapter 5 continues to study reactor network design. The objective to construct reactor networks that are able to produce multiple rigid polyols with product and safety constraints. Based on the results in the previous chapter, we determine to study three networks.

- Single DSR: Instead of discretizing the DSR into zones with fixed volume, we discretize the DSR into zones with different volume (volume of each zone is an independent decision

variable). In this way, optimal injection profile can be obtained without going through the iterative approach proposed in the previous chapter. The optimal result is consistent with the one in the previous chapter, that a DSR with 10 monomer injection points has the lowest capital cost. In addition, we discover that polymer B is the dominant product in DSR design due to faster kinetics.

- CSTRs in series: At least 4 CSTRs are required in order to allow all three polymers to satisfy their product specifications. The capital cost of 4 CSTRs in series is 2.86 times larger than the one of single DSR. In addition, polymer A is the dominant product in CSTR design.
- CSTR followed by a DSR: This reactor design requires at least 6 injection points in total, one for the CSTR and 5 for the DSR. Its capital cost is 1.09 times bigger than the DSR capital cost.

Chapter 5 also focuses on generating Pareto charts between new sales (sales - operating cost) and capital cost. All three reactor networks mentioned above can eventually reach the same amount of product sales, since the limitation for raw material is the same for all the cases. However, single DSR tends to consume more utility due to dramatic temperature changes in the reactor. Therefore, the network with 4 CSTRs plateaus with higher net sales. However, in order to obtain the same amount of sale, the network with 4 CSTRs requires a higher capital investment. In contrast, the CSTR followed by a DSR configuration leads to higher net sales than DSR alone.

Chapter 6 studies the effect of uncertainty in kinetic parameters on different configuration designs. In order to design a reactor network that would work for any kinetic parameter pair in the uncertainty range, back-off and multi-scenario method are adopted. For CSTR design, 1.54% of the uncertainty range can be covered by the back-off method. And 7 inequality constraints would be violated if the uncertainty range exceeds 1.54%. The MS approach can cover 2.3% of the uncertainty range. And 2 inequalities would be violated when the uncertainty range exceeds 2.3%. The back-off method is more conservative than the multi-scenario approach, since MS allows different scenarios to have different operating recipes, while the common decision variables are the same

for all the scenarios. However, back-off method can operate without any additional measurements or resources. In order to apply MS in reality, we need to come up with a way to measure or estimate the kinetic parameters online. The MS design for the single DSR and CSTR followed a DSR configurations can cover the full uncertainty range. In addition, single DSR with 13 monomer injection points has the lowest capital cost.

7.2 Recommendations for Future Work

7.2.1 Model Development of Rigid Polyol Production

The dynamic optimization models developed in Chapter 4 and 5 are able to deliver optimal reactor network and operating conditions by including the mass balance, energy balance, product and safety constraints into the model. However, in order to make them the representatives of the actual processes, we need to complete several additional tasks.

- In order to verify the models and estimate the kinetic parameters, model validation through lab-scale experiment or computational simulations is required. According to Chapter 6, small perturbation in the kinetic parameters can have a strong impact on the reactor structure and the operating recipe.

- The reactor networks developed in this work only involve polymerization with a single monomer. We could analyze how does copolmerization affect the current reactor design. Will the current reactor configuration be suitable for copolymerization process?

- More complex kinetics, such as catalyst deactivation and fouling could be considered. Since we have an upper limit for the catalyst outlet weight percentage, and a lower bound for the catalyst molar flow rate, it would be a challenge to design a reactor network that would function in the presence of catalyst deactivation. And fouling would impact the efficiency of heat transfer and the safety specification.

7.2.2 Online Optimization and Control

This work is focused on off-line reactor network and recipe design. However, with the presence of uncertainty, the model performance weakens. Back-off and MS methods are adopted to deal with the uncertainty. MS approach is less conservative, but it requires additional measurements to estimate the uncertain kinetics. Hence, in order to apply MS in reality, we need to focus on these tasks:

- Measure the reactor temperature, composition in the reactor or collect other information online to estimate the kinetic parameters.
- Generate operating recipe based on the estimated kinetics to make sure the product can meet the specifications.
- Include online state estimation and optimal control to predict the future dynamic behavior over a time horizon and address the operating conditions as needed.

7.2.3 Grade Transition

In Chapter 5, continuous reactor networks that are able to produce multiple rigid polyols are developed. However, we have not studied the grade transition, which can provide potential values in reducing the transition time as well as decreasing the off-grade product. Based on the type of product specification, two optimization approaches can be considered. One is for single-value product property targets and the other one is for specification bands.

7.2.4 Integration of Demand Forecasting, Scheduling and Real-time Optimization

Factories, plants, supply chains, and distribution systems are planned to flow perfectly and waste nothing, but everyday "surprises" ripple through these complex systems, wreaking villainous havoc. 94% of the world's waste is industrial. $446 billion of excess inventory is standard in supply chains.

The real cost of poor quality and downtime is $861 and $ 689 billion, respectively. In order to reduce the cost, we need to integrate demand, supply, scheduling and real-time optimization.

Starting from the demand forecasting, future demand can be estimated using traditional time-series model, such as ARIMA or deep learning network, including convolution and recurrent neutral networks. Based on the accurate predicting for future demand, inventory information, and grade transition, production scheduling can be addressed by formulating and solving mixed integer dynamic optimization problems. During production, NMPC can also be adopted to ensure the product meets specifications. And the inventory information can be updated based on the output of production.

Appendices

Appendix A Nomenclature

Notation

Notation used in the reactor model

A = Arrhenius constant

C = set of components in the process in Chapter 4; concentration in Chapter 5

$COMP$ = set of components in the process

C_p = heat capacity

Ea = activation energy

F = molar flow rate at the outlet stream

F^0 = molar flow rate at the inlet stream

FR = feeding rate

H_{cool} = monomer cooling

H_p = provided cooling

H_r = heat released

H_{rxn} = heat of reaction

k = rate constant

$\dot{M}$ = mass flow rate

M_n = number average molecular weight

MON = set of monomers in the process

M_w = weight average molecular weight

MW = molecular weight

$\bar{MW}$ = average molecular weight

N = set of CSTR or DSR zone

R = gas constant

PDI = polydispersity index

PR = production rate

r = reaction rate

T = temperature

T_{ad} = adiabatic temperature

T_f temperature of the feed

T_{safety} = upper bound for adiabatic temperature

V = volume

wt = weight percentage

$\dot{V}$ = volumetric flow rate

τ = residence time

ρ = density

σ = mole fraction of unalkoxylated active sites of initiator

$[\cdot]$ = concentration

Superscripts

b = solution mixture inside the reactor

m = monomer

n = index of each CSTR or each DSR zone

$*$ = value at the bound

Subscripts

c = components involved in the process

cat = catalyst

l = chain length of polymer

LB = lower bound

m = monomer

N = final CSTR or DSR zone

n = index of each CSTR or each DSR zone

p = polymer type $\in \{A, B, C\}$

rxn = reaction index $\in \{i, p, t\}$ in Chapter 4; reaction index $\in \{ini, prop, trf\}$ in Chapter 5

UB = upper bound

s = chain length of polymer

Reactions

e, exc = exchange

i, ini = initiation

p, $prop$ = propagation

t, trf = transfer

Notation used in the dynamic optimization formulation

CC = capital cost

ϵ = capital cost factor

f = cost function

g = equality constraint

h = inequality constraint

J = injection profile

K = maximum number of finite element

u = decision variable

V = DSR volume

y = algebraic state variable

z = differential state variable

$\dot{z}$ = differential equation

Ω = polynomial of order K

τ = normalized volume

Superscripts

L = lower bound

U = upper bound

Subscripts

i = index of finite element

j = index of collocation point

k = index of collocation point

N = final CSTR/DSR zone

n = index of each CSTR or each DSR zone

V_f = end of DSR

β = binary variable for monomer injection

Bibliography

[1] H. Engels, H. Pirkl, R, Albers, R. W. Albach, J.Krause, A. Hoffmann, H. Casselmann, J. Dormish, *Polyurethanes: Versatile Materials and Sustainable Problem Solvers for Today's Challenges*. Angew. Chem. Int. Ed. 2013, 52, 9422-9441.

[2] J. Grosse- Willerich, K. Wiss, K.-H. Wassmer, C. Buss, and V. Chilekar, *Process for the Continuous Production of Polyether Polyols*. BASF SE, assignee. Patent US, 09 Feb. 2017, No.0037183.

[3] L. K. E. Achenie, L. T. Biegler, *A Superstructure Based Approach to Chemical Reactor Network Synthesis*, Computers chem. Engng. 14(1): 23-40, 1990.

[4] A. C. Kokossis, C. A. Floudas, *Optimization of Complex Reactor Network – II. Nonisothermal Operation*, Chemical Engineering Science, 49(7), 1994.

[5] C. Zhang, Z. Shao, X. Chen, X. Gu, L. Feng, L. T. Biegler, *Optimal flowsheet configuration of a polymerization process with embedded molecular weight distributions*, AlChE Journal, 2016, 62(1), 131-145.

[6] D. Ming, D. Glasser, D. Hildebrandt, B. Glasser, M. Metgzer. *Attainable Region Theory: An Introduction to Choosing an Optimal Reactor*, John Wiley & Sons, Inc., New Jersey, 2016.

[7] D. M. Feinberg. *Optimal Reactor Design From a Geometric Viewpoint. Part II. Critical Sidestream Reactors*, Chemical Engineering Science, 55 2455-2479, 2000.

[8] D. M. Feinberg. *Optimal Reactor Design From a Geometric Viewpoint. Part III. Critical CFSTR*, Chemical Engineering Science, 55, 3553-3565, 2000.

[9] A. Lakshmanan, L. T. Biegler, *Synthesis of Optimal Chemical Reactor Networks*, Ind. Eng. Chem. Res. 35, 1344-1353, 1996.

[10] B. W. Bequette, *Nonlinear Control of Chemical Processes: a Review*, Industrial Engineering Chemistry Research, 30(7): 1391–1413, 1991.

[11] C. E. Garcia, D. M. Prett, M. Morari, *Model Predictive Control: Theory and Practicea Survey*, Automatica, 25(3): 335–348, 1989.

[12] M. Morari, J. H. Lee, *Model Predictive Control: Past, Present and Future*, Computers Chemical Engineering, 23(4-5): 667–682, 1999.

[13] J. B. Rawlings, *Tutorial Overview of Model Predictive Control*, Control Systems, IEEE, 20(3): 38–52, 2000.

[14] Z. Yu, L. T. Biegler, *Advanced-step Multistage Nonlinear Model Predictive Control*, IFAC-PapersOnLine, 51(20): 122-127, 2018.

[15] B. Srinivasan, S. Palanki, D. Bonvin, *Dynamic Optimization of Batch Processes I. Characterization of the Nominal Solution*, Computers Chemical Engineering, 27(1): 1–26, 2003.

[16] B. Srinivasan, D. Bonvin, E. Visser, S. Palanki, *Dynamic Optimization of Batch Processes II. Role of Measurements in Handling Uncertainty*, Computers Chemical Engineering, 27(1): 27–44, 2003.

[17] L. T. Biegler, *An Overview of Simultaneous Strategies for Dynamic Optimization*, Chemical Engineering and Processing: Process Intensification, 46(11): 1043–1053, 2007.

[18] S. Kameswaran, L. T. Biegler, *Simultaneous Dynamic Optimization Strategies: Recent Advances and Challenges*, Computers Chemical Engineering, 30(10–12): 1560–1575, 2006.

[19] T. E. Marlin and A. N. Hrymak, *Real-time Operations Optimization of Continuous Processes*, in American Institute of Chemical Engineering Symposium Series - Fifth International Conference on Chemical Process Control, 93: 85-112, 1997.

[20] J. F. Shapiro, *Challenges of Strategic Supply Chain Planning and Modeling*, Computers Chemical Engineering, 28(6-7): 855–861, 2004.

[21] I. E. Grossmann, *Enterprise-wide Optimization: A New Frontier in Process Systems Engineering*, AIChE Journal, 51(7): 1846–1857, 2005.

[22] C. A. Floudas, X. Lin, *Continuous-time Versus Discrete-time Approaches for Scheduling of Chemical Processes: a Review*, Computers Chemical Engineering, 28(11): 2109–2129, 2004.

[23] I. Harjunkoski, C. T. Maravelias, P. Bongers, P. M. Castro, S. Engell, I. E. Grossmann, J. Hooker, C. Mndez, G. Sand, J. Wassick, *Scope for Industrial Applications of Production Scheduling Models and Solution Methods*, Computers Chemical Engineering, 62: 161–193, 2014.

[24] C. T. Maravelias, C. Sung, *Integration of Production Planning and Scheduling: Overview, Challenges and Opportunities*, Computers Chemical Engineering, 33(12): 1919 – 1930, 2009.

[25] P. M. Verderame, J. A. Elia, J. Li, C. A. Floudas, *Planning and Scheduling Under Uncertainty: A Review Across Multiple Sectors*, Industrial Engineering Chemistry Research, 49(9): 3993–4017, 2010.

[26] C. A.Mendez, J. Cerda, I. E. Grossmann, I. Harjunkoski, M. Fahl, *State-of-theart Review of Optimization Methods for Short-term Scheduling of Batch Processes*, Computers Chemical Engineering, 30(6–7): 913–946, 2006.

[27] A. Ben-Tal, A. Nemirovski, *Robust Optimization – Methodology and Applications*, Math. Program, 92: 453–480, 2002.

[28] D. Bertsimas, D. B. Brown, C. Caramanis, *Theory and Applications of Robust Optimization*, Society for Industrial and Applied Mathematics, 53(3): 464–501, 2011.

[29] B. L. Gorissen and İ. Yanıkoğlu and D. Den Hertog, *A Practical Guide to Robust Optimization*,Omega, 53: 124-137, 2015.

[30] B. Srinivasan, D. Bonvin, E. Visser, S. Palanki, *Dynamic Optimization of Batch Processes: Ii. Role of Measurements in Handling Uncertainty*, Computers chemical engineering, 27(1):27–44, 2003.

[31] C. Welz, B. Srinivasan, D. Bonvin *Measurement-based Optimization of Batch Processes: Meeting Terminal Constraints On-line via Trajectory Following*, Journal of Process Control, 18(3): 375-382, 2008.

[32] G. Francois, D. Bonvin, *Chapter One - Measurement-Based Real-Time Optimization of Chemical Processes in Control and Optimisation of Process Systems*, Advances in Chemical Engineering, Academic Press, 43: 1-50, 2013.

[33] J. V. Kadam, M. Schlegel, B. Srinivasan, D. Bonvin, W. Marquardt, *Dynamic Optimization in the Presence of Uncertainty: From Off-line Nominal Solution to Measurement-based Implementation*,Journal of Process Control, 17(5): 389-398, 2007.

[34] T. H. Cormen, C. E. Leiserson, R. L. Rivest, C. Stein, *Introduction to Algorithms (2nd ed.)*, MIT Press McGraw–Hill, pp. 344, 2001

[35] M. I. Kamien, N. L. Schwartz, *Dynamic Optimization: The Calculus of Variations and Optimal Control in Economics and Management (2nd ed.)*, New York: Elsevier, pp. 261, 1991.

[36] D. E. Kirk, *Optimal Control Theory: An Introduction. Englewood Cliffs*, NJ: Prentice-Hall. pp. 94–95, 1970.

[37] R. M. Smith, M. F. Asaro, *Process Economics Program (PEP) Report 45C Polyols for Polyurethanes*, IHS Markit, 2019

[38] Y. Nie, L. T. Biegler, C. M. Villa, J. M. Wassick, *Reactor Modeling and Recipe Optimization of Ring-Opening Polymerization: Block Copolymers*, Ind. Eng. Chem. Res. 53 (18): 7434-7446, 2014.

[39] J. Shi, L. T. Biegler, I. Hamdan, *Optimization of Grade Transitions in Polyethylene Solution Polymerization Processes*, AIChE Journal, 62: 1126-1142, 2016.

[40] Y. Wang, L. T. Biegler, G. S. Ostace, R. A. Majewski, *Optimal Polymer Grade Transitions for Fluidized Bed Reactors*, Journal of Process Control, 88: 86–100, 2020.

[41] V. M. Zavala and L. T. Biegler, *The advanced-step NMPC controller: Optimality, stability and robustness*, Automatica, 45(1): 86-93, 2009.

[42] H. Jang, J. H. Lee, L. T. Biegler, *A robust NMPC scheme for semi-batch polymerization reactors*, IFAC-PapersOnLine, 49(7): 37-42, 2016.

[43] V. S. Vassiliadis, R. W.H. Sargent, C. C. Pantelides, *Solution of a Class of Multistage Dynamic Optimization Problems. 1. Problems Without Path Constraints*, Industrial Engineering Chemistry Research, 33(9): 2111–2122, 1994.

[44] V. S. Vassiliadis, R. W.H. Sargent, C. C. Pantelides, *Solution of a Class of Multistage Dynamic Optimization Problems. 2. Problems With Path Constraints*, Industrial Engineering Chemistry Research, 33(9): 2123–2133, 1994.

[45] W. F. Feehery, P. I. Barton, *Dynamic Optimization With State Variable Path Constraints*, Computers Chemical Engineering, 22(9): 1241–1256, 1998.

[46] M. Schlegel, K. Stockmann, T. Binder, and W. Marquardt, *Dynamic Optimization Using Adaptive Control Vector Parameterization*, Computers Chemical Engineering, 29(8): 1731–1751, 2005.

[47] J. E. Cuthrell, L. T. Biegler, *On the Optimization of Differential-Algebraic Process Systems*, AIChE Journal, 33(8): 1257–1270, 1987.

[48] H. G. Bock, M. Diehl, D. B. Leineweber, J. P. Schl¨oder, *A Direct Multiple Shooting Method for Real-time Optimization of Nonlinear DAE Processes*, in Nonlinear Model Predictive Control, ser. Progress in Systems and Control Theory, F. Allgower, A. Zheng, Eds. Birkhauser Basel, 26: 245-267, 2000,

[49] P. Drag, K. Styczen *A Two-Step Approach for Optimal Control of Kinetic Batch Reactor with Electroneutrality Condition*, Przeglad Elektrotechniczny, June 2012.

[50] H. G. Bock and K.-J. Plitt, *A Multiple Shooting Algorithm For Direct Solution of Optimal Control Problems*, 9th IFAC world congress, Budapest, 1984.

[51] L . T. Biegler, *Nonlinear Programming: Concepts, Algorithms, and Applications to Chemical Processes*, Society for Industrial and Applied Mathematics, Philadelphia, 2010.

[52] A. Wächter, L. T. Biegler, *On the Implementation of an Interior-point Filter Line-search Algorithm for Large-scale Nonlinear Programming*, Mathematical programming, 106(1):25–57, 2006.

[53] A. S. Drud, *CONOPT - a Large-scale GRG Code*, ORSA Journal on Computing, 6(2):207–216, 1994.

[54] A. S. Drud, *CONOPT: A GRG Code for Large Sparse Dynamic Nonlinear Optimization Problems*, Mathematical Programming, 31(2): 153–191, 1985.

[55] L. T. Birgler, emphEfficient Solution of Dynamic Optimization and NMPC Problems, Systems and Control Theory, vol 26. Birkhäuser, Basel, 2000.

[56] R. Quirynen, S. Gros, M. Diehl, *Inexact Newton-type Optimization With Iterated Sensitivities*, Society for Industrial and Applied Mathematics, 28(1): 74–95, 2018.

[57] C. G. Petra, *A Memory-distributed Quasi-Newton Solver For Nonlinear Programming Problems With a Small Number of General Constraints*, Journal of Parallel and Distributed Computing, 133: 337-348, Nov. 2019.

[58] P. Boggs and J. Tolle, *Sequential Quadratic Programming*, Acta Numerica, Vol 4: 1-51, 1995.

[59] P. E. Gill, E. Wong, *Sequential Quadratic Programming Methods*, Mathematics and its Applications, vol 154. Springer, New York, NY, 2012.

[60] A. Barclay, P. E. Gill, J. B Rosen, *SQP Methods And Their Application To Numerical Optimal Control*, 1997.

[61] J. Nocedal, S. J. Wright, *Sequential Quadratic Programming. In: Numerical Optimization*, Springer Series in Operations Research and Financial Engineering. Springer, New York, NY. 2006.

[62] P. E. Gill, W. Murray, M. A. Saunders, *SNOPT: An SQP Algorithm for Large-Scale Constrained Optimization*, Society for Industrial and Applied Mathematics, 47(1): 99-131, 2005.

[63] P. E. GILL, E. WONG, *User's Guide for SNOPT Version 7.6: Software for Large-Scale Nonlinear Programming*, Jan. 2017.

[64] P. E. GILL, *USER'S GUIDE FOR NPSOL 5.0: A FORTRAN PACKAGE FOR NONLINEAR PROGRAMMING*, June, 2001.

[65] L. S. Lasdon, R. L. Fox, M. W. Ratner, *Nonlinear Optimization Using the Generalized Reduced Gradient Method*, 1974.

[66] J. S. Arora, *Chapter 13 - More on Numerical Methods for Constrained Optimum Design in Introduction to Optimum Design (Fourth Edition)*, Academic Press, Boston, 2017.

[67] J. K. Paeng, J. S. Arora, *Dynamic Response Optimization of Mechanical Systems With Multiplier Methods*, ASME. J. Mech., Trans., and Automation, 111(1): 73–80, March 1989.

[68] B. A. Murtagh, M. A. Saunders, *Large-scale Linearly Constrained Optimization*, Mathematical Programming, 14(1): 41-72, 1978.

[69] B. A. Murtagh, M. A. Saunders, *MINOS 5.51 Usuer'S Guide*, Stanford University, 2003.

[70] J. Nocedal, S. J. Wright, *Numerical Optimization (2nd ed.)*, Springer Publishing, ISBN 0-387-30303-0, 2016.

[71] R. H. Byrd, J. Nocedal, R. A. Waltz, *Knitro: An Integrated Package for Nonlinear Optimization*, 2017

[72] H. Hofmann, *Kinetic Data Analysis and Parameter Estimation. In: Chemical Reactor Design and Technology*, NATO ASI Series (Series E: Applied Sciences), vol 110, 1986.

[73] K. C. Yeh, *Kinetic Parameter Estimation by Numerical Algorithms and Multiple Linear Regression: Theoretical*, J Pharm Sci, 66(12): 1688-91, Dec. 1977.

[74] J. Villota, D. Sebastián, A. Pavas, J. Camilo, B. Ramírez, K. Johana, R. Colorado, A. Adriana, *Modeling and Kinetic Parameter Estimation of the Enzymatic Hydrolysis Process of Lignocellulosic Materials for Glucose Production*, Industrial Engineering Chemistry Research, 59(38): 16851-16867, 2020.

[75] C. Schenk, L. T. Biegler, L. Han, J. Mustakis, *Kinetic Parameter Estimation from Spectroscopic Data for a Multi-Stage Solid–Liquid Pharmaceutical Process*, Organic Process Research Development, 25(3): 373-383, 2021.

[76] Y. Nie, L. T. Biegler, C. M. Villa, J. M. Wassick, *Reactor Modeling and Recipe Optimization of Polyether Polyol Processes: Polypropylene Glycol*, AICHE Journal, 59(7), 2013.

[77] Di Serio M, Tesser, R, Dioli A, Santacesaria E. *Kinetics of ethoxylation and propoxylation of ethylene glycol catalyzed by KOH*, Ind Eng Chem Res. 41: 5196-5206, 2002.

[78] C. Hum, C. Wang, M. Tassano *Polyether Plant Design*, Dept. of Chemical and Biomolecular Engineering, School of Engineering and Applied Science, University of Pennsylvania, April 18, 2017.

[79] V. M. Zavala, and L.T.Biegler, *Optimization-Based Strategies for the Operation of Low-Density Polyethylene Tubular Reactors: Nonlinear Model Predictive Control*, Computers and Chemical Engineering, 33: 1735-1746, 2009.

[80] B. P. Patil, E. Maia, L. Ricardez-Sandoval, *Integration of Scheduling Design, and Control of Multi-Product Chemical Processes Under Uncertainty*, AlChE Journal, 61: 2456-2470, 2015.

[81] A. Flores-Tlacuahuac and I. E. Grossmann, *Simultaneous Cyclic Scheduling and Control of a Multiproduct CSTR*, Ind. Eng. Chem. Res., 45: 6698-6712, 2006.

[82] D. Petersen, L. D. R. Beal, D. Prestwich, S. Warnick, and J. D. Hedengren, *Combined Non-cyclic Scheduling and Advanced Control for Continuous Chemical Processes*, Process, 5, 83, doi:10.3390/pr5040083, 2017.

[83] L. D. R. Beal, D. Petersen, G. Pila, B. Davis, S. Warnick and J. D. Hedengren, *Economic Benefit from Progressive Integration of Scheduling and Control for Continuous Chemical Processes*, Processes, 5, 84, doi:10.3390/pr5040084, 2017.

[84] Y. Nie, L. T. Biegler, C. M. Villa, J. M. Wassick, *Discrete Time Formulation for the Integration of Scheduling and Dynamic Optimization*, Industrial & Engineering Chemistry Research, Vol. 54(16): 4303-4315, 2015.

[85] Y. Wen, L. T. Biegler, M. P. Ochoa, L. Matthews, A. J. Ferrio, J. Weston, N. Nikbin, *Continuous Reactor Network Design for Rigid Polyol Production*, Chemical Engineering Science, 2020.

[86] K. Miettinen, *Nonlinear Multiobjective Optimization*, Springer, Berlin, 1998.

[87] E. Visser, B. Srinivasan, S. Palanki, and D. Bonvin, *A feedback-based Implementation Scheme for Batch Process Optimization*, Journal of Process Control, 10(5): 399–410, 2000.

[88] F. Galvanin, M. Barolo, F. Bezzo, and S. Macchietto, *A Backoff Strategy for Model-based Experiment Design Under Parametric Uncertainty*, AIChE journal, 56(8): 2088–2102, 2010.

[89] B. Srinivasan, D. Bonvin, E. Visser, and S. Palanki, *Dynamic Optimization of Batch Processes: II. Role of Measurements in Handling Uncertainty*. Computers & chemical engineering, 27(1): 27–44, 2003.

[90] J. Shi, L. T. Biegler, I. Hamdan, J. Wassick, *Optimization of Grade Transitions in Polyethylene Solution Polymerization Process under Uncertainty*, Computers & Chemical Engineering, 95: 260-279, 2016.

[91] D. Ruppen, C. Benthack, and D. Bonvin, *Optimization of Batch Reactor Operation under Parametric Uncertainty Computational Aspects*, Journal of Process Control, 5(4): 235–240, 1995.

[92] Z. Yu, L. T. Biegler, *Advanced-step Multistage Nonlinear Model Predictive Control: Robustness and Stability*, Journal of Process Control, 84: 192-206, 2019.